Tunisian Republic

Ministry of Higher Education and

Scientific Research

****

University of Monastir

****

National Engineering School of Monastir

****

PH.D. THESIS

Realized by:

Ahmed Komti

TO OBTAIN THE DEGREE OF DOCTOR

IN ENERGY ENGINEERING

Multiscale Modeling, Simulation, and Analysis of Airborne Particulate Pollution from Road Transportation Networks: Application to the Coastal Urban Environment of Sousse City, Tunisia.

Defended on: 27/12/2025 in front of jury composed of:

Ms. Jalila Sghaier	Professor	ENIM	President
Mr. Ahmed Bellagi	Professor Emeritus	ENIM	Reviewer
Mr. Habib Farhat	Associate Professor	ISSAT-Sousse	Reviewer
Mr. Mohammed Naceur Borjini	Professor	ENIM	Examiner
Mr. Khalifa Slimi	Professor	ENIM	Thesis Director
Mr. Salah Khardi	Professor	UGE	Co-Supervisor
Mr. Abdessalem Jbara	Assistant Professor	ISTLS	Co-Supervisor

Laboratory of Thermal and Energy Systems LR99ES31

2024 / 2025

Acknowledgements

I would like to express my deepest gratitude and sincere appreciation to all those who, directly or indirectly, supported, guided, and encouraged me throughout this challenging and rewarding doctoral journey. I am especially thankful to my thesis supervisor, **Professor Khalifa Slimi** (National Engineering School of Monastir), for his invaluable guidance, insightful feedback, and continuous support during all stages of this research.

My sincere thanks also go to my co-supervisors, **Mr. Abdessalem Jbara** (Assistant Professor at the Higher Institute of Transport and Logistics of Sousse) and **Mr. Salah Khardi** (Gustave Eiffel University), for their constant support, technical guidance, and valuable contributions throughout the entire thesis.

I would also like to sincerely thank **Ms. Najah Kechiche** for providing material resources, and for her continued support during the course of this work. My sincere thanks also go to the members of the thesis jury for the honor of evaluating this work and for their constructive feedback:

- **Professor Sghaier Jalila**, National Engineering School of Monastir
- **Professor Ahmed Bellagi**, National Engineering School of Monastir
- **Mr. Habib Farhat**, Associate Professor, Higher Institute of Applied Sciences and Technology of Sousse
- **Professor Mohamed Naceur Borjini**, National Engineering School of Monastir

I am also grateful to the entire team at the Laboratory for the Study of Thermal and Energy Systems (LESTE) at the National Engineering School of Monastir for their support, collaboration, and technical assistance during various stages of this research.

Abstract

This study addresses the pressing concern of urban air pollution driven by particulate matter (PM), a major threat to public health. The research begins by examining the dispersion of traffic emissions in Sousse, Tunisia, utilizing the SIRANE model. PM_{10} and $PM_{2.5}$ concentrations were measured at 19 model receptors positioned at the city's most congested road intersections to identify areas most affected by traffic. Three hotspots were pinpointed during peak hours, with PM_{10} concentrations of 75.1, 52.1, and 33.6 µg/m³ and $PM_{2.5}$ values of 45.1, 31.78 and 22.89 µg/m³, respectively in Area 1, Area 2 and Area 3. These hourly PM_{10} and $PM_{2.5}$ concentrations exceeded the EU standard limit fixed at 40 µg/m³ and 25 µg/m³, respectively.

Next, the GRAL (Graz Lagrangian model) micro-scale dispersion system was employed to analyze these three polluted zones during both rush and non-rush hours. The simulated PM_{10} and $PM_{2.5}$ concentrations were then compared with real-time measurements collected using PM pollutant sensors in the identified areas. The results were validated, showing an average fractional bias (FB) within the acceptable range of -0.3 to 0.3 and a normalized mean square error ($NMSE^{\frac{1}{2}}$) below 2. Additionally, the mean measurements and modeled ratio of $PM_{10}/PM_{2.5}$ are higher than 0.5, which suggests that exhaust emissions, tire, and brake wear are the main causes of PM emissions.

These insights are crucial for shaping urban planning and air quality management strategies, offering a reliable framework to combat pollution and safeguard public health in urban environments.

Résumé

Cette étude traite de la problématique urgente de la pollution atmosphérique urbaine liée aux particules (PM), considérée comme une menace majeure pour la santé publique. La recherche débute par l'analyse de la dispersion des émissions du trafic routier dans la ville de Sousse, en Tunisie, à l'aide du modèle SIRANE. Les concentrations de PM_{10} et $PM_{2.5}$ ont été mesurées à 19 récepteurs virtuels situés aux intersections routières les plus congestionnées de la ville afin d'identifier les zones les plus affectées. Trois zones critiques ont été identifiées durant les heures de pointe, avec des concentrations horaires de PM_{10} de 75,1 ; 52,1 ; et 33,6 µg/m³ et des valeurs de $PM_{2.5}$ respectives de 45,1 ; 31,78 ; et 22,89 µg/m³ dans les zones 1, 2 et 3. Ces niveaux dépassent les seuils fixés par les normes européennes, soit 40 µg/m³ pour le PM_{10} et 25 µg/m³ pour le $PM_{2.5}$.

Ensuite, le modèle GRAL (Graz Lagrangian model) a été utilisé pour simuler à l'échelle microscopique la dispersion des polluants dans ces trois zones, en conditions de pointe et hors pointe. Les concentrations simulées ont été comparées aux mesures réelles collectées via des capteurs de particules. Les résultats obtenus ont été validés, avec un biais fractionnel moyen (FB) compris entre -0,3 et 0,3, et une racine carrée de l'erreur quadratique moyenne normalisée $NMSE^{\frac{1}{2}}$ inférieure à 2. Par ailleurs, le ratio moyen $PM_{10}/PM_{2.5}$, mesuré et modélisé, supérieur à 0,5, indique que les principales sources d'émissions sont l'échappement des véhicules, l'usure des pneus et des freins.

Ces résultats apportent des éléments essentiels pour orienter l'aménagement urbain et les politiques de gestion de la qualité de l'air, en fournissant un cadre robuste pour lutter contre la pollution et protéger la santé des populations en milieu urbain.

Table of content

List of figures

List of tables

Nomenclature

Symbol	Description	Unit
C(x,y,z)	Concentration at point (x,y,z)	mass·m^{-3}
C_ext	Background concentration above canyon	mass·m^{-3}
C_street	Average concentration inside street canyon	mass·m^{-3}
dV	Control volume	m^3
dt	Time step	s
dx$_1$	Spatial increment (x_1-direction)	m
dx$_2$	Spatial increment (x_2-direction)	m
dx$_3$	Spatial increment (x_3-direction)	m
E	Dissipation rate of turbulent kinetic energy	m^2·s^{-3}
EF_B,$_{(i)}$	Brake-wear PM emission factor	g·km^{-1}·veh^{-1}
EF_H,$_{(i,j,k,l)}$	Hot exhaust PM emission factor	g·km^{-1}·veh^{-1}
EF_m	Fleet-average PM emission factor	g·km^{-1}·veh^{-1}
EF_R,$_{(i)}$	Road-surface abrasion PM emission factor	g·km^{-1}·veh^{-1}
EF_T,$_{(i)}$	Tire-wear PM emission factor	g·km^{-1}·veh^{-1}
EF$_{(i,j,k,l)}$	Total PM emission factor for vehicle class (i,j,k,l)	g·km^{-1}·veh^{-1}
H	Street/building height	m
H_s	Effective emission height	m

Symbol	Description	Unit
k	Turbulent kinetic energy	$m^2 \cdot s^{-2}$
L	Street length	m
$\mathbf{m_{(p,i)}}$	Mass of particle i	kg
P_b	Buoyancy production of turbulent kinetic energy	$m^2 \cdot s^{-3}$
P_m	Shear production of turbulent kinetic energy	$m^2 \cdot s^{-3}$
$\bar{\mathbf{p}}$	Mean pressure	Pa
$\mathbf{p_{(i,j,k,l)}}$	Share of vehicles in class (i,j,k,l)	–
Q	Emission rate (source strength)	$mass \cdot s^{-1}$
Q_H,turb	Turbulent flux at street/ABL interface	$mass \cdot time^{-1}$
Q_r	Traffic flow on road segment r	$veh \cdot h^{-1}$
R	Number of integration steps	–
ρ	Air density	$kg \cdot m^{-3}$
σ_w	Standard deviation of vertical turbulent velocity	$m \cdot s^{-1}$
σ_y	Horizontal dispersion coefficient	m
σ_z	Vertical dispersion coefficient	m
t	Time	s
t_a	Averaging time for concentration	s
$\bar{\mathbf{u}}$	Advective velocity along the street	$m \cdot s^{-1}$

Symbol	Description	Unit
$\bar{u}_i$	Mean wind velocity components (i = 1,2,3)	$m \cdot s^{-1}$
u_d	Mixing velocity (σ_w / √2π)	$m \cdot s^{-1}$
U	**Wind speed at emission height**	**$m \cdot s^{-1}$**
U_d	Mixing/transfer velocity	$m \cdot s^{-1}$
U_street	Street-level average wind speed	$m \cdot s^{-1}$
W	Street or road width	m
x	Coordinate (horizontal)	m
x_i	Spatial coordinate	m
y	Coordinate (crosswind)	m
z	Coordinate (vertical)	m
δ_{ij}	Kronecker delta	–
μ_t	Turbulent viscosity	$m^2 \cdot s^{-1}$

Acronyms

Acronym	Definition
AZR	Second-order Macroscopic Traffic Model
BCR	Building Coverage Ratio
CALPUFF	California Puff Dispersion Model
CAMx	Comprehensive Air Quality Model with Extensions
CFD	Computational Fluid Dynamics
CMAQ	Community Multiscale Air Quality Model
CMEM	Comprehensive Modal Emissions Model
CNG	Compressed Natural Gas
CONTRAM	Continuous Traffic Assignment Model
COPERT	Computer Programme to Calculate Emissions from Road Transport
CTM	Chemical Transport Model
DAE	Aerodynamic Diameter
DEM	Digital Elevation Model
DNS	Direct Numerical Simulation
DYNASMART	Dynamic Network Assignment-Simulation Model
EF	Emission Factor
EPA	Environmental Protection Agency

Acronym	Definition
EU	European Union
FLEXPART	Flexible Particle Dispersion Model
GRAMM	Graz Mesoscale Model
GRAL	Graz Lagrangian Model
HBEFA	Handbook Emission Factors for Road Transport
HC	Hydrocarbons
HYSPLIT	Hybrid Single-Particle Lagrangian Integrated Trajectory Model
ICE	Internal Combustion Engine
IVE	International Vehicle Emissions Model
LPG	Liquefied Petroleum Gas
LES	Large Eddy Simulation
LWR	Lighthill–Whitham–Richards Traffic Flow Model
MFD	Macroscopic Fundamental Diagram
MO Theory	Monin–Obukhov Similarity Theory
NDC	Nationally Determined Contribution
NO_x	Nitrogen Oxides
OD	Origin–Destination Matrix
OSPM	Operational Street Pollution Model

Acronym	Definition
PEMS	Portable Emission Measurement System
PHEM	Passenger Car & Heavy-Duty Emission Model
PinG	Plume-in-Grid
$PM_{0.1}$	Ultrafine Particulate Matter ≤ 0.1 µm
$PM_{2.5}$	Fine Particulate Matter ≤ 2.5 µm
PM_{10}	Particulate Matter ≤ 10 µm
RANS	Reynolds-Averaged Navier–Stokes
RDE	Real Driving Emissions
SCR	Selective Catalytic Reduction
SUMO	Simulation of Urban Mobility
TMC	Traffic Management Center
UTM	Universal Transverse Mercator
VERSIT+	Vehicle Emission Regression and Simulation Tool
VISSIM	Microscopic Traffic Simulator
VOC	Volatile Organic Compounds
WHO	World Health Organization
WRF-Chem	Weather Research and Forecasting model with Chemistry

General introduction

Particulate matter has detrimental effects not only on human health but also on visibility, air quality (Ewa Anioł et al., 2023), environmental ecosystems (Valentina Gluščićv et al., 2024), and both direct and indirect climate impacts. Road traffic emissions contribute significantly to particulate matter, which includes coarse particles (PM_{10}), fine particles ($PM_{2.5}$), ultrafine particles ($PM_{1.0}$), and nanoparticles. In recent years, the concentration of these particles has been steadily increasing, prompting greater concern among regulatory bodies to address and reduce ambient air pollution (Ouyang et al., 2022).

Of particular concern are fine particles, which are small enough to penetrate deeply into the respiratory system upon inhalation, posing a serious threat to human health. Research has consistently demonstrated their ability to reach the alveoli (Pratiwi et al., 2023; Yu, 2022), leading to a range of health complications. The growing focus on this issue underscores its significance as a major public health challenge, spurring further studies aimed at developing strategies to minimize its impact (Brauer et al., 2016; Penkała et al., 2024; Yadav et al., 2019; Zhang et al., 2024).

In urban areas, inhalable particulate matter is one of the primary air pollutants. Government agencies often use particulate matter levels, alongside other pollutants such as carbon monoxide (CO), ground-level ozone (O_3), sulfur dioxide (SO_2), and nitrogen dioxide (NO_2), to evaluate air quality through the Air Quality Index (AQI) (Mustafa et al., 2025). Regulations in regions such as the United Kingdom (UK), Europe, and elsewhere typically address particles sized ≤10 μm (PM_{10}) and ≤2.5 μm ($PM_{2.5}$) (Faridi et al., 2023). However, these regulations primarily emphasize mass concentration rather than the number of particles. The first regulatory move to address particle number emissions occurred with the implementation of Euro-5 and Euro-6 (EU, 2008) and more recently Euro-7 (EU, 2018) automobile emission standards. These European Union (EU) rules mandate limits on the number of solid particles, specifically those ranging from 23 to 2500 nanometers, emitted by all classes of light-duty diesel vehicles (Kumar et al., 2010).

While there is a substantial body of research on the health impacts of $PM_{2.5}$ and NO_2, there remains a scarcity of epidemiological data concerning ultrafine particles (UFPs), defined as particles with diameters smaller than 0.1 micrometers (Bergmann et al., 2022). This gap has been emphasized by Morawska et al. (2019) and Ohlwein et al. (2019), who both call for expanded monitoring and tighter regulation of UFPs to fully understand their health

consequences. In many countries, air quality is assessed using networks of fixed monitoring stations. In Tunisia, however, this infrastructure is limited, with only 30 monitoring stations located in key urban and industrial centers in the northern part of the country (Christel Bouet et al.,2019).

Despite these limitations, the seriousness of air pollution is acknowledged. A recent report by the World Bank Group (World Bank Group, 2023) estimates that environmental degradation could cost Tunisia around 6.4% of its GDP (Gross Domestic Product) by 2050. Even in nations where monitoring networks are more developed, the sparse distribution of stations hinders accurate estimation of total population exposure. This underscores the strong link between ambient air pollution and public health risks (Pavanaditya Badida et al., 2022; Qiao et al., 2021).

To address these gaps, modeling approaches are indispensable for evaluating and interpreting air pollution patterns as a complement to physical measurements. Several models are commonly employed for this purpose, including the Operational Street Pollution Model (Kakosimos et al., 2010), AMS/EPA Regulatory Model (EPA, 2004, p. 200), California Line Source Dispersion Model (Benson, 1984), Atmospheric Dispersion Modeling System-Urban (Zhong et al., 2023), and SIRANE (Soulhac et al., 2011), which are all widely used to assess air quality across various urban environments. These tools are essential for analyzing atmospheric phenomena, particularly in situations where direct measurements are either insufficient or unavailable in specific regions.

Sousse, Tunisia, located at 35°82'N, 10°63'W (Rebaï et al., 2023), is a thriving urban center with a diverse economy that includes traditional sectors such as agriculture and fishing, as well as modern industries and services. Its strategic location and forward-thinking development initiatives have made it a hub for investment and economic growth. However, the city's population growth and economic expansion have led to a significant increase in vehicle numbers, rising from around 62,324 in 2004 to 131,868 in 2018, with 52% of these vehicles being over 15 years old (Khammassi et al., 2024). During peak hours, traffic congestion in Sousse's city center is common, as key roads connect residential areas, business districts, and educational institutions. This traffic is a major source of urban air pollution.

Motivated by this issue, our study begins by simulating the dispersion of PM_{10} and $PM_{2.5}$ across Sousse using the SIRANE model, developed by the Air Impact and Risk Laboratory at "École Centrale de Lyon, France". This model was selected for its user-friendly input file creation, ability to handle unlimited source and receptor points, computational efficiency through parallel

processing, and validated performance (Soulhac et al., 2012). For instance, Elhaddaj et al. (2019) used SIRANE to model NO_x and O_3 dispersion in Agadir, Morocco, comparing simulated results with measurements from online analyzers placed near roads. previous studies (Squarcioni et al., 2025) have reinforced the SIRANE model's capability to predict pollutant concentrations, considering factors like traffic emissions, meteorological conditions, and urban topography.

In the second phase of our study, we conduct a detailed microscopic analysis of pollution hotspots identified by SIRANE, using the GRAL model (Oettl, 2015). GRAL is renowned for its high spatial resolution, often down to a few hundred meters, which is critical for accurately modeling air pollution dynamics in urban areas (Veratti et al., 2024). It also features a robust meteorological module and accounts for the influence of buildings on airflow and turbulence, addressing a limitation of SIRANE, which does not consider building geometry. GRAL has been used to predict particulate matter levels (Berchet, Zink, Oettl, et al., 2017) and has been tested in various contexts, such as evaluating traffic-related air quality in Modena, Italy (Fabbi et al., 2019), and simulating high-resolution meteorological conditions in Heidelberg (May et al., 2024). However, GRAL has its limitations, including the computational demands of high-resolution simulations, which require significant processing power and time, especially for large-scale applications. Its accuracy also depends on the quality and availability of input data, such as detailed emission inventories and urban morphology information (Berchet, Zink, Muller, et al., 2017).

Following this, we evaluate the $PM_{2.5}/PM_{10}$ ratios at hotspot locations during both rush and non-rush hours, offering diagnostic insights into the predominant emission sources, whether fine particles from combustion or coarse particles from mechanical processes such as road dust resuspension.

Such detailed emission characterizations also offer essential data for sophisticated modeling systems allowing for more precise air quality simulations. Recent advancements in urban air pollution modeling have increasingly involved combining macroscopic traffic models with microscopic emission and dispersion simulations to enhance the spatial and temporal accuracy of pollutant concentration estimates. One notable example is the study by (De Nunzio et al., 2020), which utilized macroscopic traffic inputs such as road topology and average vehicle speeds to derive detailed vehicle-level trajectories using a machine learning approach. These trajectories were then processed analyzed using a microscopic emission model, allowing for accurate pollution estimates specific to each road segment. This approach showed much better

accuracy in predicting NO_x and CO_2 emissions than traditional large-scale models like COPERT.

At the microscale, (Essamlali et al., 2025) used the SUMO (Simulation of Urban Mobility) traffic simulator to model vehicle movements and emissions at high resolution. These results were then combined with a Gaussian dispersion model to determine pollutant concentrations across different urban layouts.

However, despite advancements in urban air quality modeling, the existing literature remains largely concentrated in European and select North African cities, with no documented applications of validated dispersion modeling systems in Tunisian urban environments. This geographic gap is particularly notable given the distinct urban morphology, meteorological variability, and mixed emission profiles characteristic of coastal cities like Sousse.

Earlier research has mainly concentrated on gaseous pollutants (like NO_x and O_3) or used restricted spatial and temporal resolutions, whereas this study presents the first high-resolution (2.5 × 3.02 m) simulation of particulate matter (PM_{10} and $PM_{2.5}$) in Sousse, integrating both horizontal and vertical dispersion dynamics. Moreover, most existing studies rarely use real-world traffic flow data, typically depending on previously compiled inventories, while this study manually calculated traffic volumes to generate localized emission factors based on the COPERT methodology. In addition, unlike our research, few studies combine macroscopic models like SIRANE with microscale models such as GRAL to assess PM behavior across spatial scales, and even fewer include detailed validation, vertical decay analysis, and $PM_{2.5}/PM_{10}$ ratio diagnostics to identify emission sources and assess street-level exposure risks. The absence of spatially and temporally adaptive policy recommendations in earlier work also limits their practical application.

In contrast, this research addresses all these gaps by offering a novel, integrative framework that merges emission modeling, dual-scale dispersion simulation, and policy-relevant exposure analysis. As a result, this study represents both a methodological innovation and the first scientific contribution of its sort in Tunisia, with scalable applicability across similar MENA (Middle East and North Africa metropolitan landscapes).

The objective of this study is to enhance the understanding of how vehicular emissions contribute to air pollution, with the goal of informing urban planning and air quality management strategies. Specifically, the research develops the first inventory of PM_{10} and $PM_{2.5}$ emissions from vehicles in the central metropolitan area of Sousse, considering both peak and

off-peak traffic periods. Initially, road traffic emissions were estimated based on vehicle counts using the European Copert 5 methodology. These estimates were then incorporated into the SIRANE model to simulate dispersion patterns and to evaluate their broader impact at the city level, with a focus on identifying areas of high pollution concentration, or "hotspots."

Subsequently, these identified hotspots were subjected to a more detailed analysis using the GRAL model. The GRAL simulation results were validated by comparing them with field measurements collected at the hotspot locations. In addition, the campaign involved calculating and analyzing the $PM_{2.5}/PM_{10}$ ratios from both the measured and modeled data to gain further insights into the sources and potential health implications of the particulate matter.

This thesis is structured into three main chapters, each addressing a specific component of the research framework:

- **Chapter 1**: This chapter provides an overview of the scientific background related to urban air pollution, focusing on particulate matter (PM_{10} and $PM_{2.5}$). It synthesizes key findings from international and regional studies, discusses emission sources, atmospheric dispersion processes, and health impacts, and reviews the main modeling approaches used globally. Particular attention is devoted to traffic-related emissions and the application of dispersion models such as COPERT, SIRANE, and GRAL in urban environments.
- **Chapter 2**: This chapter describes the study area, methodological design, and data collection framework. It details the integration of traffic data and emission estimation using the COPERT model, followed by dispersion modeling with SIRANE and GRAL. The section also outlines the spatial configuration of virtual receptors, the experimental validation setup, and the statistical metrics used to evaluate model performance and accuracy.
- **Chapter 3**: This chapter presents and interprets the results of the modeling and experimental analyses. It includes the emission characterization, spatial and temporal distribution of particulate concentrations, model validation, and diagnostic evaluation using $PM_{2.5}/PM_{10}$ ratios. The discussion connects the results to broader urban air quality contexts and concludes with the practical and policy implications of the findings, highlighting strategies for emission reduction, sustainable urban design, and public health protection.

CHAPTER 1

STATE OF THE ART

I. Introduction

Air pollution in urban areas is a growing global concern, primarily driven by the rapid expansion of motorized transportation and dense urbanization. Among the most harmful pollutants, particulate matter (PM) – including PM_{10}, $PM_{2.5}$, and ultrafine particles – poses significant risks to public health, environmental integrity, and climate systems. Road traffic has emerged as a major contributor to this pollution, emitting a complex mixture of exhaust and non-exhaust particles, particularly in regions with aging vehicle fleets and limited regulatory oversight.

Tunisia, and specifically the city of Sousse, exemplifies many of the challenges faced by urban centers in developing regions: increasing vehicle numbers, outdated infrastructure, and insufficient air quality monitoring. These factors have led to rising levels of particulate pollution, the effects of which are often underestimated due to a lack of high-resolution data and validated simulation tools.

This chapter presents a comprehensive overview of the current scientific understanding of atmospheric particulate matter, focusing on its sources, classifications, chemical composition, and dispersion mechanisms. It also reviews the health impacts of vehicular emissions, regulatory standards, and modeling frameworks used to simulate air pollution in urban environments. By analyzing both international literature and the specific context of North Africa, this chapter establishes a critical foundation for the modeling and validation methodologies developed in subsequent sections of the thesis.

II. Atmospheric Particulate Pollution

Atmospheric particles, also known as atmospheric aerosols, are solid or liquid particles suspended in the air, and their concentration levels represent one of the most commonly used indicators for assessing air pollution, but also a key parameter for understanding its impacts on human health, climate, and ecosystems. Standards for atmospheric particles vary between countries and international organizations. In fact, 94% of European countries have at least one standard for each pollutant, while only 36% of African countries have the same (Kutlar Joss et al., 2017). Many countries maintain limits that exceed the WHO's revised guidelines, which have been strengthened to address the health risks associated with air pollution. This situation raises concerns about public health and the effectiveness of current air quality regulations (Yevgen Nazarenko et al.,2021).

II-1. Characteristics

Atmospheric particles are a mixture of solid and liquid particles, composed of organic and inorganic substances and biological entities. This composition depends heavily on where the particles are collected, their sources, and their size (H. Estuardo-Moreno et al., 2022; Regina M.B.O. Duarte et al.,2020).

Particles can be classified according to their DAE, and a distinction can be made between particles with a diameter of less than 10 µm (PM_{10}), 2.5 µm ($PM_{2.5}$), also known as fine particles, and 0.1 µm ($PM_{0.1}$), known as ultrafine particles. A distinction can also be made according to how the particles are formed.

Primary aerosols are particles emitted into the atmosphere from a natural or anthropogenic source, without undergoing any physical and/or chemical changes during their time in the atmosphere (the characteristics of these PM particles remain identical from the moment they are emitted until they are sampled).

Secondary aerosols are formed in the atmosphere after the transformation of a primary particle or by gas-particle conversion with various compounds such as sulfur or nitrogen oxides.

II-2. Classification

The field of aerosol particle sizing spans multiple orders of magnitude. A widely employed classification relies on aerodynamic properties, captured via aerodynamic diameter to describe particle-size distributions.

This approach is essential for understanding transport, fate, deposition in the respiratory tract, and links to particle composition and emission sources (Peng et al., 2021).

$$D_{ae} = D_g \,.\, k \,.\, \sqrt{\frac{\rho_P}{\rho_0}} \qquad \text{(I.1)}$$

To characterize particles in aerodynamic terms, the equivalent aerodynamic diameter (D_{ae}) is defined as the diameter of a spherical particle (density = 1 g/cm³) that shares the same settling velocity as the real particle (Payne et al., 2023).

where D_g is geometric diameter, ρ_P is particle density, ρ_0 is reference density, and k is the shape factor (unity for spheres).

Different aerosol instruments may report different sizing metrics—mobility diameter, vacuum aerodynamic diameter, volume-equivalent diameter, etc. depending on their measurement principle and application, with the method's sizing definition always explicitly specified.

Atmospheric particulate matter (PM) spans a wide size range and is commonly classified into coarse, fine, and ultrafine fractions based on aerodynamic diameter (D_{ae}). As shown in Figure 1, these size distributions are typically bimodal, consisting of fine-mode particles (mainly D_{ae}<2.5 μm) and coarse-mode particles (D_{ae}>2.5 μm).

The coarse fraction, ranging from 2.5 to 10 μm, arises from mechanical processes such as wind-blown dust, unpaved roads, agricultural activities, and the evaporation of sea spray, as well as biological sources like pollen, fungal spores, and insect fragments. These particles tend to settle rapidly due to gravitational sedimentation, except under windy conditions where they can be re-suspended (Zeb et al., 2022).

In contrast, fine particles—with D_{ae}<2.5 μm—are primarily generated by combustion processes (e.g., fossil fuels, biomass burning) and gas-to-particle conversion. This category is further subdivided into two modes: the accumulation mode (0.1–2.5 μm) and the nucleation (or Aitken) mode (< 0.1 μm).

Accumulation-mode particles often result from coagulation of smaller particles or condensation of vapors onto existing particles. Their atmospheric lifetime is relatively long, as neither dry deposition nor wet scavenging is efficient in this size range. This leads to particle build-up until removal by precipitation occurs. Due to their high surface area, accumulation-mode particles play a critical role in heterogeneous atmospheric chemistry and gas-particle interactions (Xausa et al., 2018).

The nucleation mode, often referred to as ultrafine particles or $PM_{0.1}$, encompasses particles formed by gas-to-particle conversion during new particle formation (NPF) events or from hot vapor condensation during combustion. Despite contributing little to total particle mass, they dominate by number and can act as nuclei for further growth into the accumulation size range. Their atmospheric residence time is short—ranging from minutes to hours—due to rapid coagulation with larger particles or surface impaction (Bin Zhao, 2024; Bulatovic et al., 2021).

Air quality studies classify atmospheric aerosols by aerodynamic diameter because particle size governs their transport, deposition, and health relevance. Total suspended particles (TSP) encompass nearly the full atmospheric particle spectrum, while PM_{10} includes both fine and coarse particles capable of penetrating the thoracic region. $PM_{2.5}$ represents the fine fraction dominated by combustion and secondary aerosols, and PM_1 further isolates submicron particles typically originating from soot and diesel exhaust. The coarse sub-fraction $PM_{2.5–10}$ identifies mechanically generated particles such as dust, bioaerosols, and road debris.

These size fractions are also reflected in Figure 1, which shows the mass distribution of aerosol modes across aerodynamic diameters and highlights regulatory classifications used in air quality management (US EPA, 2021).

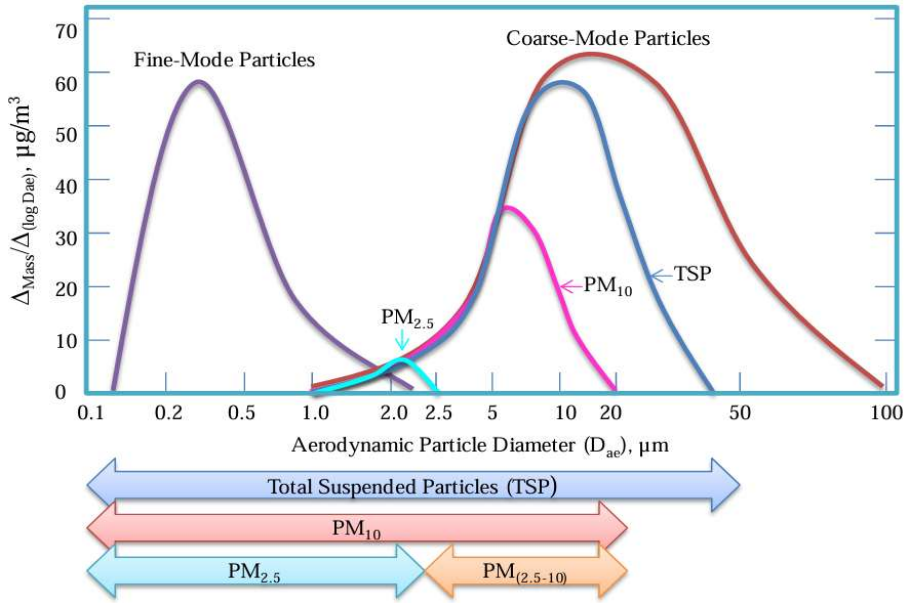

Figure 1 : Representative Particle Size Spectrum of Ambient Airborne Particulate Matter (US EPA, 1996)

II-3. Origin

The physical and chemical characteristics of atmospheric particles have been extensively investigated due to their significant implications for environmental processes and public health. These particles, commonly referred to as $PM_{2.5}$ and PM_{10}—representing particulate matter with aerodynamic diameters smaller than 2.5 and 10 µm, respectively—originate from a wide range of natural and anthropogenic sources.

II-3-1. Overview of Primary and Secondary Formation

As illustrated in Figure 2, primary particulate matter is directly emitted from sources such as road traffic, maritime activities, energy production, agriculture, residential heating, forest fires, volcanic eruptions, and sea spray, contributing components including metals, carbon black, ions, and organic compounds. Natural sources such as soil erosion, biomass burning, and volcanic activity also play a role, particularly at regional scales. In urban environments, however, a substantial fraction of fine particulate matter is of anthropogenic origin, with road transport being a dominant contributor.

Vehicle emissions release both primary particles and gaseous precursors, including volatile organic compounds (VOCs), which undergo atmospheric chemical transformations such as oxidation and photochemical reactions, leading to the formation of secondary pollutants (e.g., secondary organic aerosols and oxidized hydrocarbons) (Minhan Park et al., 2018; Véronique Ghersi et al., 2012).

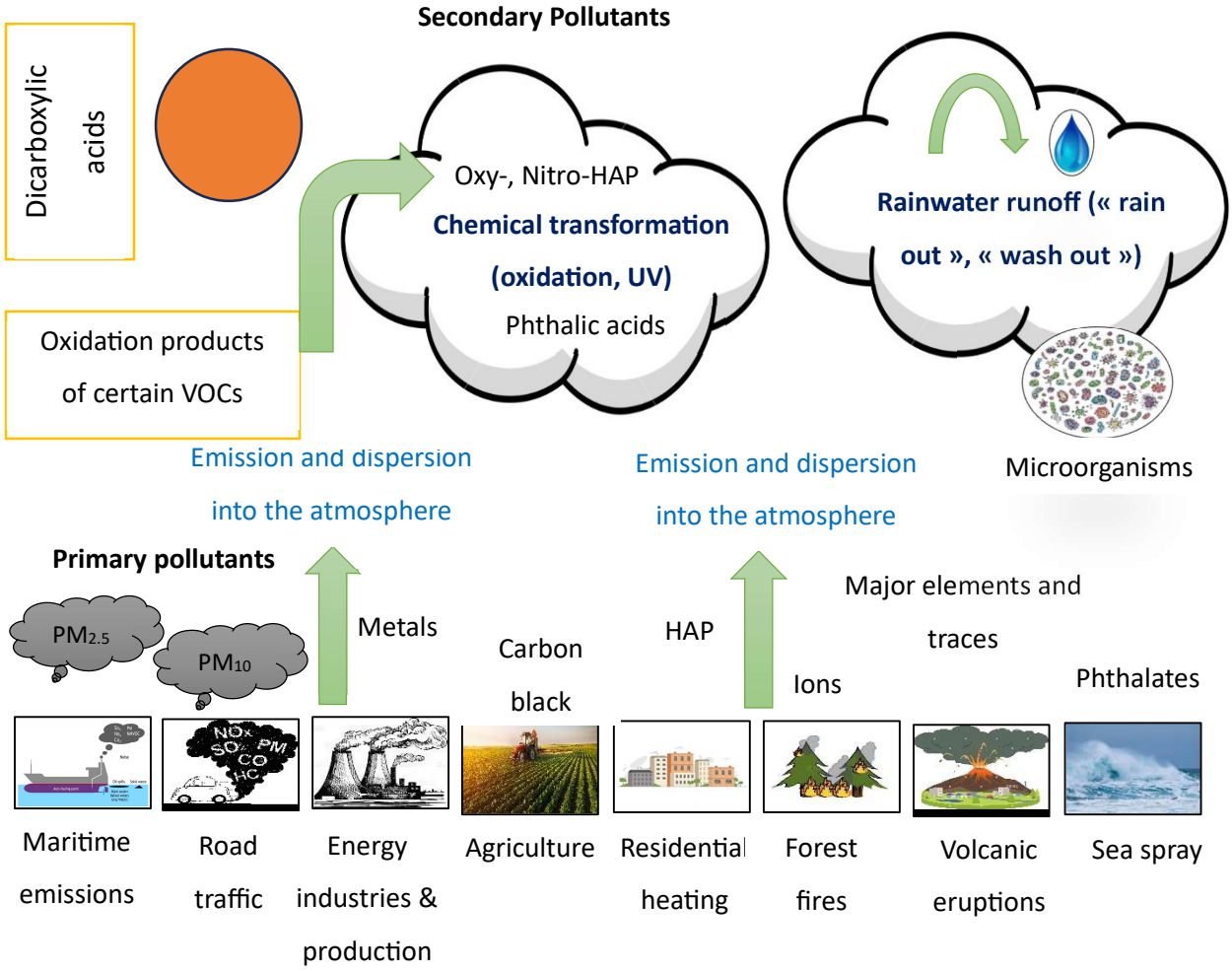

Figure 2 : Sources of $PM_{2.5}$ and PM_{10} as well as primary and secondary compounds (PAHs: polycyclic aromatic hydrocarbons, VOCs: volatile organic compounds) (Cochard, M. 2022)

II-3-2. Global Distribution of Natural and Anthropogenic Contributions

On a global scale, natural sources remain the largest contributors, accounting for about 89 % of total particulate mass, compared with 11 % from anthropogenic activities (Delmas et al., 2007). Major natural sources include crustal dust, sea salts, volcanic ash, plant debris, and biogenic sulfates, whereas anthropogenic contributions are primarily associated with industrial processes, vehicle traffic, energy production, and agricultural operations (Mohammadi-Zadeh et al., 2017). However, this global balance varies significantly by region. In heavily urbanized

or industrialized areas, anthropogenic emissions frequently exceed natural inputs, resulting in elevated $PM_{2.5}$ levels and severe air-quality degradation (Hong-gil Lee et al., 2021).

As shown in Table 1, these sources differ not only in magnitude but also in chemical composition. Natural emissions largely consist of mineral dust and sea-salt particles, whereas anthropogenic sources emit carbonaceous and metal-rich aerosols. Both types influence atmospheric radiative forcing, cloud microphysics, and human health. Fine and ultrafine fractions—especially $PM_{2.5}$—can penetrate deep into the respiratory tract, increasing risks of cardiovascular and pulmonary diseases (Minhan Park et al., 2018; Véronique Ghersi et al., 2012).

Table 1: Estimation of the Contribution of Sources to Global Emissions of Atmospheric Particles (Delmas et al. 2007)

Origins	**Sources**	**Flow (Mt.an-1)**	
		Average estimate	**Estimates Min. et Max**
Natural	Crustal dust	1500	1000-3000
	Sea salts	1300	1000-10000
	Plant debris	50	26-80
	Volcanic ash	30	4-10000
	Biogenic sulfates	90	80-150
	Volcanic sulfates	12	5-60
	Secondary organic aerosols	55	40-200
	Nitrates	22	15-50
	Total	**3059**	**2170-23540**
Anthropogenic	Soot	20	5-20
	Industrial dust	100	40-130
	Vegetation fires	80	60-160
	Anthropogenic sulfates	140	170-250
	Anthropogenic nitrates	36	26-65
	Organic aerosols	10	0.5-25
	Total	**386**	**301.5-650**

II-3-3. Chemical Composition and Fractional Structure

The size and composition of PM are closely linked to their origin and are influenced by photochemical and meteorological conditions (Petra Pokorná et al., 2022).

Larger particles (PM_{10}) generally stem from mechanical processes like abrasion and erosion, while finer fractions ($PM_{2.5}$, $PM_{0.1}$) arise mainly from combustion and industrial activities (John Tatarko et al., 2020; Xiaoliang Luo et al., 2024).

The finest particles, particularly $PM_{2.5}$ and $PM_{0.1}$, tend to contain the most toxic chemical species (Guangzhi Wang et al., 2021).

Atmospheric PM is chemically heterogeneous, consisting of three principal fractions: Carbonaceous fraction, Inorganic fraction, and Organic fraction.

Atmospheric particles exhibit a complex and heterogeneous composition, broadly categorized into carbonaceous, inorganic, and organic fractions.

The carbonaceous fraction primarily consists of elemental carbon (EC), often referred to as carbon black, and inorganic carbon forms such as carbonates.

The inorganic component encompasses a variety of ions and trace elements, including heavy metals and major mineral constituents, which can originate from both natural sources like soil dust and anthropogenic emissions such as industrial processes.

The organic fraction includes biological elements such as plants and microorganisms, but also organic compounds such as PAHs, n-alkanes, dioxins, furans, and quinones.

Certain compounds such as endocrine disruptors such as phthalates or bisphenols (H.M. ten Brink et al.,2008; Luca Ferrero et al.,2019; Ru-Jin Huang et al., 2022; Tareq Hussein et al.,2022), as well as the biological fraction (Nur Amanina Ramli et al.,2020), have been little studied to date.

Several studies have reported that toxicity varies depending on the composition of the particles and the season in which they were collected (Nora Kováts et al.,2020; Przemysław Furman et al.,2021).

- **The carbon fraction**

More specifically, the carbon fraction is found in several forms in PM. Elemental carbon (EC) is produced by combustion processes and is commonly known as carbon soot or black carbon.

This EC forms the carbon skeleton of combustion aerosols, onto which other elements and molecules can be adsorbed. Organic carbon (OC) comprises all organic compounds and biological entities.

The carbonaceous fraction of particulate matter originates from both natural and anthropogenic sources, reflecting a diverse and complex array of emission pathways. Naturally, biological sources such as vegetation, fungal spores, and marine organisms contribute to organic carbon (OC) in the atmosphere (Fei Xie et al., 2023; Xin Zhang et al., 2020).

However, anthropogenic activities, particularly combustion processes, are significant contributors to both elemental carbon (EC) and OC. These processes emit carbonaceous particles in varying proportions depending on the combustion conditions, such as temperature and oxygen availability and the type of fuel used, including wood, coal, gasoline, diesel, and heavy fuel oil.

The ratio of OC to EC is often used as an indicator to infer emission sources, with higher OC/EC ratios typically associated with biomass burning and lower ratios linked to fossil fuel combustion (Estela D. Vicente et al., 2023).

In addition to primary emissions, secondary organic carbon forms in the atmosphere through chemical and physical transformations of precursor gases, particularly volatile organic compounds (VOCs). These reactions lead to the generation of secondary compounds, including dicarboxylic acids and other oxidation products, which contribute to the organic fraction of particulate matter, as illustrated in Figure 1.

- **The inorganic fraction**

The inorganic fraction includes water-soluble ions and major and trace elements. The most abundant species are chloride anions Cl-, nitrate anions NO3-, sulfate anions SO42-, and cations sodium Na+, potassium K+, ammonium NH4+, calcium Ca2+, and magnesium Mg2+. These particles are mainly of natural origin (marine and crustal), but also of primary anthropogenic origin (fertilizers, salt-rich raw materials, etc.). Some of these molecules, NO3-, SO42-, and NH4+, are characteristic of secondary aerosol formation.

Wind plays an important role in the suspension and transport of particles, particularly PM_{10} and $PM_{2.5}$. Wind-induced resuspension occurs when particles that have settled on surfaces are returned to the atmosphere, contributing to air pollution. This phenomenon is particularly significant in urban environments and areas affected by wind erosion (J. Cobiac Linda et al.,2022).

Major and trace elements can have both natural and anthropogenic origins, with those resulting from soil erosion typically representing the natural component, as they are commonly found in the Earth's crust in the form of aluminosilicates such as (Al, Ca, Si, Mg, Fe, Ti, K, etc.). Similarly, elements associated with sea salt aerosols are identical to the major species present in seawater (Cl-, Na+, SO42-, Mg2+, etc.).

Anthropogenic elements can come from road traffic emissions, as friction between brake pads and discs releases particles rich in metals such as copper, iron, zinc, and barium (Yuki Okazaki et al.,2024), but tire abrasion on road surfaces is also a significant source of anthropogenic pollution, releasing harmful particles such as zinc, cadmium, and synthetic polymers into the environment (Neelesh Agrawal et al.,2021) and resuspending dust accumulated on roads. This dust, which accumulates over time, contains fuel residues, heavy metals, and various other pollutants that have been deposited on the road surface by vehicles (Yago Alonso Cipoli et al., 2024).

The metallurgical industry, particularly steel production, is a significant contributor to the emission of both major and trace elements, including Fe, Ca, Mn, Cu, Zn, and Al (Antoaneta Ene et al., 2024). It should be noted that the same element can come from both natural and anthropogenic sources, which can complicate the accurate identification of its origin.

Other human activities can lead to the emission of certain elements, such as the combustion of various fuels and waste, which plays a major role in the emission of heavy metals and other toxic substances into the environment. This phenomenon is particularly pronounced in coal combustion, waste incineration, and heavy fuel oil burning (Lixin Zheng et al., 2024)

- **The organic fraction**

The organic fraction consists of various families of compounds. Among these, alkanes come from vehicular, industrial, and biogenic emissions. The lightest alkanes can exist in a gaseous state, while the heaviest ones occur in solid form (Fadel et al., 2021).

Polycyclic aromatic hydrocarbons are compounds formed from several benzene rings and are known for their toxicity. The origin of these PAHs is largely anthropogenic, with most coming from vehicle exhaust, gas combustion, residential heating, incineration, smoke, and industrial processes. Other organic compounds such as hopanes are pentacyclic hydrocarbons that can be found in automotive lubricants and are therefore considered reliable markers of road traffic emissions.

Phthalates are synthetic compounds used as plasticizers to enhance the flexibility of plastic materials and are easily released into the environment due to their weak intermolecular bonds (Lu et al., 2020). They are predominantly found near waste incineration sites and have been recognized as endocrine disruptors for over a decade (Habert et al., 2009).

Dioxins (polychlorinated dibenzo-p-dioxins or PCDDs), furans (polychlorinated dibenzofurans or PCDFs) and polychlorinated biphenyls (PCBs) are large families of semi-volatile chlorinated compounds that are persistent in the environment. PCDDs and PCDFs are most often produced by vehicle emissions and industrial processes, but also by the incineration of waste at very high temperatures.

PCBs are not natural substances. These compounds have the property of being electrical insulators and non-flammable. They were therefore used extensively in electrical transformers before their high toxicity was discovered. Although their production and use are now banned, they continue to persist in the environment (Bruckmann et al., 2013).

II-4. Energy Sources and ICE Emissions

Energy production and consumption patterns strongly influence atmospheric particulate and gaseous emissions. Primary energy sources are typically categorized into fossil fuels (coal, crude oil, natural gas), nuclear fuels (uranium, thorium), and renewable resources (solar, wind, hydroelectric, geothermal, and biomass). Among these, fossil fuels continue to dominate the global transportation sector, generating most of the associated air pollutants released through internal combustion engines (ICEs).

- **Emission Pathways and Pollutant Formation**

In road transport, ICEs convert the chemical energy of fuel into mechanical work through combustion, but this process inevitably produces both exhaust and non-exhaust emissions. Exhaust gases primarily include CO_2, NO_x, CO, unburned hydrocarbons, and particulate matter, while non-exhaust particles arise from mechanical wear processes such as brake, tire, and road-surface abrasion (Lamani et al., 2024).

The quantity and composition of emissions depend on fuel type, engine calibration, operating conditions, and ambient factors such as temperature and humidity (Talbi, 2017).

Figure 3 illustrates the principal emission pathways in road transport, highlighting the contributions of exhaust, evaporative, and mechanical sources.

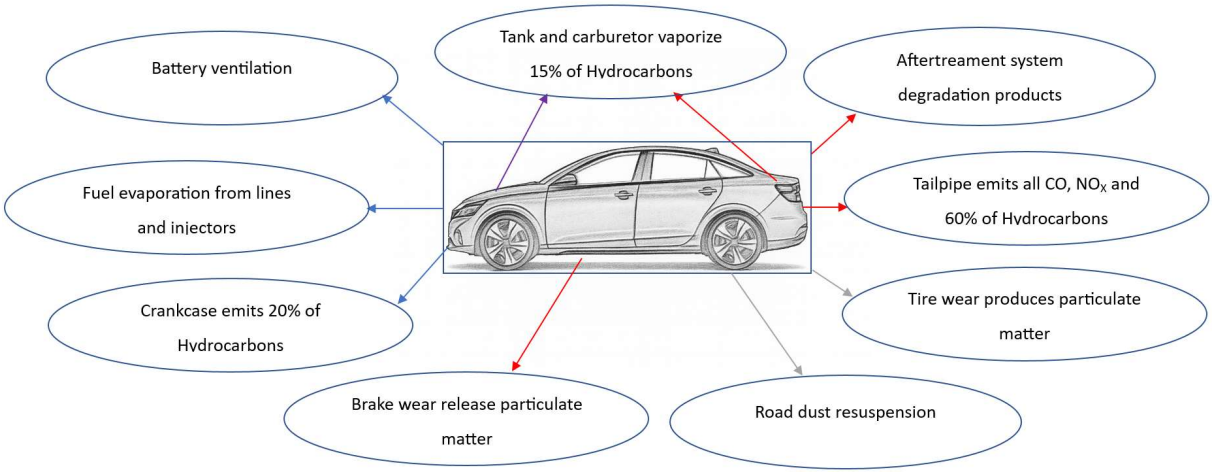

Figure 3 : Emission Pathways and Air Pollutant Sources in Road Transportation Vehicles (Red = Exhaust | Blue = Evaporative | Gray = Mechanical Wear | Purple = Combined Evaporative & Exhaust) (Adeyanju & Manohar, 2017)

The volume and composition of these emissions are influenced by factors such as fuel type, driving conditions, and surrounding environmental parameters (Lamani et al., 2024). A typical internal combustion engine consists of two main structural components: the engine block and the cylinder head. The engine block, which forms the lower portion of the engine, houses the crankshaft, pistons, connecting rods, oil pump, and, in overhead valve (OHV) engines, the camshaft. Positioned above the block, the cylinder head contains the intake and exhaust valves and, in overhead camshaft (OHC) configurations, includes the camshaft(s) as well. This architecture remains a standard in engine design, although modern implementations increasingly incorporate advanced materials and systems to enhance efficiency and reduce emissions (Dovhopolova et al., 2020). This structural configuration is visually depicted in Figure 4.

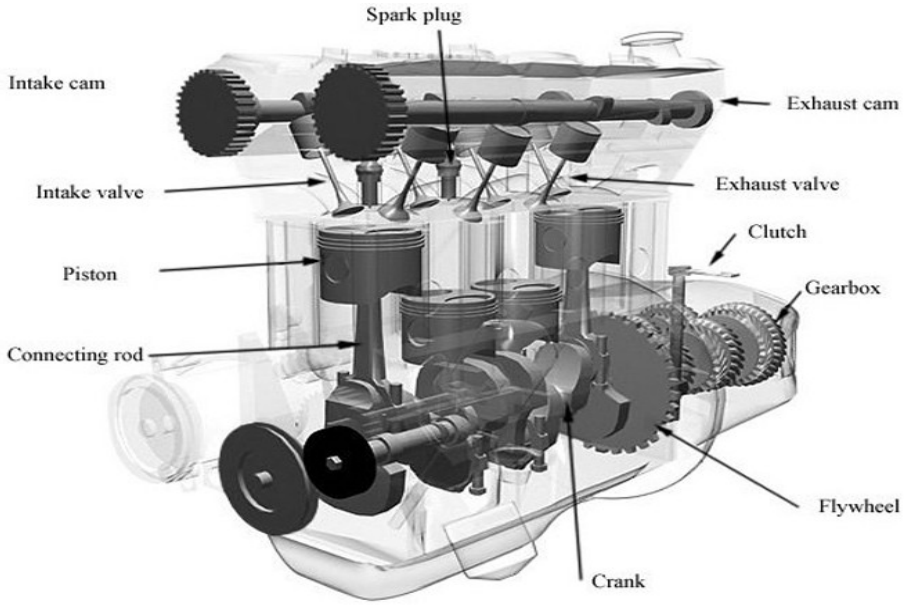

Figure 4 : Schematic Diagram of an Internal Combustion Engine Converting Liquid Fuel into Mechanical Energy (Timothy, 2003)

- **Advances in Combustion and Fuel Technologies**

Recent advances in engine design and fuel innovation have sought to minimize emissions while improving efficiency.

Approaches such as advanced combustion control, variable valve timing (VVT), split injection, and lean-burn operation reduce fuel consumption and lower NO_x emissions, particularly under part-load conditions (Qiang et al., 2024).

Computational fluid dynamics (CFD) studies of n-butanol/diesel blends demonstrate that optimizing intake-valve-closing (IVC) timing can increase brake thermal efficiency by up to 8 % while decreasing particulate output (Lamani et al., 2024).

Alternative and hybrid energy solutions are also gaining traction. Renewable diesel (e.g., Neste MY or HVO) offers reduced emissions and comparable engine performance in small turbocharged engines designed for urban mobility (Ornella Chiavola et al., 2024). Similarly, hydrogen-assisted combustion strategies improve thermal efficiency and substantially reduce NO_x at low loads (Y. Li et al., 2024).

Structurally, the ICE retains its fundamental configuration—an engine block and cylinder head—but incorporates advanced materials and electromechanical subsystems such as optimized valve drives or electromagnetic actuators, enhancing both fuel economy and

emission control (Xinyu Fan, 2025). These refinements illustrate the ongoing technological evolution of conventional powertrains toward greater environmental compatibility.

Despite these improvements, internal combustion engines remain the principal source of urban air pollution, especially in densely populated regions with high vehicle density. Their emissions contribute significantly to ambient $PM_{2.5}$, ozone precursors, and greenhouse gases.

Lifecycle assessments show that electric vehicles (EVs) generally yield lower CO_2 emissions than ICE vehicles, although benefits depend on electricity-grid carbon intensity and climatic conditions affecting battery performance (Shahbaz et al., 2015). Moreover, portable emission-monitoring systems such as PEMS are increasingly applied to validate real-world heavy-duty engine emissions, though accurate calibration against ambient particulate backgrounds remains essential for reliable measurements.

While this section has outlined the global emission processes and mitigation pathways, the specific national context—including Tunisia's vehicle fleet composition, energy mix, and policy-driven emission-reduction strategies—is discussed in Section VI, which details the country's transport-sector contribution (30.8 % of CO_2 emissions in 2022) and its projected evolution under various mitigation scenarios (Wissem, 2025).

II-5. Atmospheric Dispersion Mechanism of Particulate Pollution

The dispersion and removal of atmospheric particles are governed by a multifaceted interaction between meteorological parameters, such as atmospheric pressure, wind patterns, temperature, humidity, and solar radiation, and the physical and chemical characteristics of the particles themselves.

Wind is pivotal in both horizontal and vertical transport: it disperses particles over vast areas and enhances dry deposition by increasing mechanical turbulence, especially for larger particles (>1 μm). However, excessive wind may also cause resuspension, extending particle lifetime in the atmosphere. Atmospheric pressure gradients generate wind flows, while high-pressure systems tend to suppress vertical mixing, trapping pollutants near the surface.

Atmospheric stability, shaped by temperature gradients and surface heat flux, regulates vertical dispersion: stable conditions (e.g., winter nights) inhibit mixing, while unstable conditions promote it, as confirmed by regional studies such as in Baghdad (Imad Khraibet Rashid Al-Khuwaylidee et al., 2024).Temperature influences both dispersion and removal pathways by modifying boundary layer height, photochemistry, and particle reactivity. Elevated temperatures increase secondary aerosol formation from gases like NOx and VOCs, as well as

alter phase behavior and solubility—key to wet and dry removal processes (Hernández-Ramírez et al., 2024).

Humidity plays a central role in wet deposition: hygroscopic particles (e.g., sulfates, nitrates) grow in high-RH environments, becoming efficient cloud condensation nuclei (CCN) and increasing the likelihood of in-cloud or below-cloud scavenging. This is especially relevant during precipitation events, which can significantly reduce particle concentrations. Seasonal rainfall variability, driven by shifts in sea surface temperatures and atmospheric circulation (e.g., in Ethiopia), modulates this scavenging efficiency and thus influences regional air quality (Mulualem Abera Waza et al., 2025).

Solar radiation further influences aerosol chemistry, not only initiating photolysis but also aiding in the formation of fine particles ($PM_{2.5}$), which alter the composition and optical behavior of the atmosphere. These effects are particularly visible during smog episodes in urban environments.

Crucially, particle size remains the most decisive factor in determining atmospheric fate: ultrafine particles (<0.1 μm) are removed by diffusion, accumulation-mode particles (0.1–1 μm) persist due to inefficient removal mechanisms, and coarse particles (>1 μm) are more readily removed through gravitational settling.

Recent instrument-based studies highlight that even the smallest atmospheric particles show varying behavior based on their chemical composition, necessitating context-specific calibration to measure and predict their atmospheric life cycle accurately (Li et al., 2025). The fate of atmospheric particles, therefore, reflects a dynamic balance between physical dispersion, chemical transformation, and environmental removal, all modulated by interdependent meteorological and particle-specific factors

III. Health Consequences of Vehicular Emissions

Air pollution from road traffic is now recognized as a major contributor to public health burdens in urban environments worldwide. Several studies have shown that individuals living near high-traffic areas are more likely to suffer from chronic respiratory conditions, cardiovascular diseases, and even neurodevelopmental disorders in children. Populations most affected include children, the elderly, and individuals with pre-existing conditions, whose vulnerability to pollution-related complications is significantly elevated.

Notably, the World Health Organization (Ambient (outdoor) air pollution, 2021) and the Lancet Commission (The Lancet Commission on Pollution and Health, 2017) have emphasized that long-term exposure to vehicle emissions increases the risk of stroke, lung cancer, and ischemic heart disease. Short-term exposure to high levels of traffic pollutants, particularly during rush hours, can also trigger acute symptoms such as coughing, wheezing, and hospital admissions due to asthma or heart-related complications.

Additionally, the interaction between various pollutants including nitrogen dioxide, carbon monoxide, ozone, and volatile organic compounds can amplify their combined effects, compounding health risks during periods of intense traffic.

Vehicle-emitted air pollutants pose serious public health risks. Among the most concerning is nitrogen dioxide (NO_2), primarily produced by diesel engines. Exposure to NO_2 has been linked to reduced lung function, aggravated asthma, and increased susceptibility to respiratory infections, particularly in children (Ambient (outdoor) air pollution, 2021). Carbon monoxide (CO), another byproduct of incomplete combustion, limits the blood's ability to transport oxygen, leading to symptoms ranging from headaches and fatigue to, in extreme cases, neurological damage or death, especially in individuals with cardiovascular conditions (US EPA, 2022.).

Volatile organic compounds (VOCs), including benzene, toluene, ethylbenzene, and xylene (collectively referred to as BTEX), are emitted from fuel evaporation and exhaust. These compounds can irritate the eyes, nose, and throat and, in prolonged exposures, cause liver and kidney damage, as well as cancer (Stewart, 2021).

Ozone (O_3), a secondary pollutant formed through reactions between NOx and VOCs under sunlight, is known to trigger respiratory issues, reduce lung function, and exacerbate conditions like bronchitis and asthma, particularly during high-temperature periods (Europe’s Air Quality Status 2023).

Finally, particulate matter, specifically PM_{10} and $PM_{2.5}$, represents a major health concern due to its ability to penetrate deep into the respiratory system. These fine particles, originating from fuel combustion, brake and tire wear, and road dust resuspension, are associated with cardiovascular disease, reduced pulmonary function, and increased mortality (Christine, 2023).

Figure 5 illustrates the various non-exhaust sources of particulate matter (PM) emitted by road vehicles, including brake wear, tyre wear, road wear, and dust resuspension. These sources produce a range of particle sizes: PM_{10}, $PM_{2.5}$, and PM_1 ,each capable of penetrating different

depths of the human respiratory tract. While PM_{10} tends to deposit in the upper airways (mouth, nose, bronchi), $PM_{2.5}$ and PM_1 reach deeper into the lungs and bloodstream, where they can contribute to respiratory, cardiovascular, and systemic health effects.

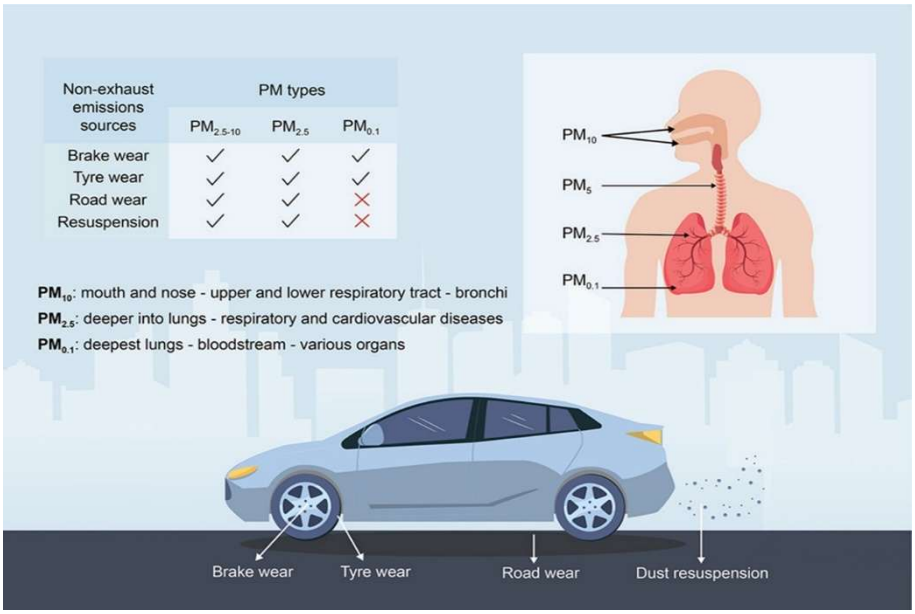

Figure 5 : Overview of Air Pollutant Types and their effects on human organs (Non-Exhaust Emissions, 2018)

Road traffic remains a major contributor to urban particulate pollution, emitting substantial amounts of fine particles ($PM_{2.5}$) and ultrafine particles (UFPs, <100 nm), both of which have profound implications for human health.

These particles stem from vehicle exhaust, brake and tire abrasion, and resuspended road dust. $PM_{2.5}$ penetrates deep into the lungs, reaching alveoli and entering systemic circulation, where it induces inflammation, oxidative stress, and endothelial dysfunction—key mechanisms in the development of cardiovascular diseases such as hypertension, myocardial infarction, and stroke (Vinay Kumar et al., 2025).

Although lighter in mass, UFPs are particularly harmful; (Dada et al., 2025) showed that these nanoparticles can cross pulmonary barriers, enter the bloodstream, and provoke systemic inflammation with possible neurological effects.

In North Africa, a 2024 geo-epidemiological study covering 12 French-speaking African countries including Algeria, Morocco, and Tunisia, reported population-weighted annual $PM_{2.5}$ concentrations ranging from 1.8 µg/m³ (Morocco) up to 65.0 µg/m³ (Cameroon), significantly surpassing the WHO guideline of 5 µg/m³. The study estimated 136,457 deaths in 2019 were attributable to ambient $PM_{2.5}$ exposure, of which 40.8% were ischemic heart disease, 38.5%

stroke, 13.2% lower respiratory infections, and 7.5% chronic obstructive pulmonary disease (Capitanio et al., 2024).

Vulnerable groups; children, elderly, and socioeconomically disadvantaged populations living near traffic corridors bear a disproportionate share of these health risks.

Further support comes from natural experiments during the COVID-19 pandemic. (Belis et al., 2025) documented that traffic reductions in the Western Balkans led to significant drops in $PM_{2.5}$ and NO_2 levels, accompanied by measurable decreases in all-cause mortality. This clear relationship between vehicular emissions and health outcomes demonstrates the potential for rapid public health improvements through targeted interventions.

In conclusion, urban air pollution, particularly that caused by road traffic includes numerous families of particulate and gaseous compounds that are well documented as toxic to human health.

The strong association between elevated $PM_{2.5}$ levels and increased rates of cardiovascular and respiratory diseases, along with premature mortality, highlights the critical public health threat posed by traffic-related air pollution.

IV. Environmental Regulations and Standards

IV -1. Emissions regulations

The regulation of vehicle emissions plays a key role in reducing air pollution caused by road transport. Since the adoption of Euro 1 in 1992, the European Union has steadily tightened emission limits for major pollutants, including carbon monoxide (CO), nitrogen oxides (NO_x), particulate matter (PM), and hydrocarbons (HC).

These increasingly strict standards have driven the development and adoption of advanced emission control technologies such as catalytic converters, particulate filters, and selective catalytic reduction (SCR) systems. As shown in Figure 6, these regulatory milestones have translated into substantial emission reductions: between Euro 3 and Euro 7, NO_x emissions from light-duty vehicles fell by 84%, PM by 96%, and CO by 82%. For heavy-duty vehicles, the decline is even more pronounced, with NO_x emissions reduced by 99%, CO by 97%, and PM by 95% between Euro I and Euro VII.

This visualization highlights the effectiveness of the Euro standards in drastically reducing vehicular pollutants over time. The upcoming Euro 7 regulation, scheduled to take effect in 2025 for passenger cars and 2027 for heavy-duty vehicles, goes further by targeting non-exhaust

emissions such as brake and tire wear, while requiring long-term durability of emission control systems. This marks a regulatory shift from laboratory compliance to real-world emissions monitoring, supported by tools like Real Driving Emissions (RDE) tests (Global Leader in Petroleum Additives, 2024).

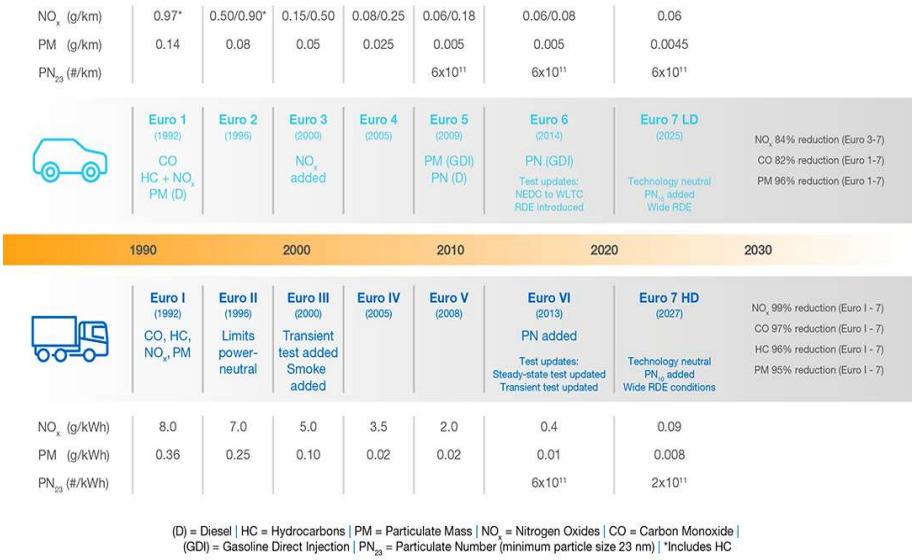

Figure 6 : Evolution of Euro emission limits for light- and heavy-duty vehicles (1992–2027). Source: (Afton Chemical to Present at 2024 Responsible Care® and Sustainability Conference, s. d.)

IV -2. Surveillance and control regulations

While global and European efforts to reduce vehicle emissions have advanced considerably through regulations such as the Euro standards, Tunisia, like many North African countries—still lacks a comprehensive legal framework to regulate tailpipe emissions from its vehicle fleet. Unlike Morocco, which enforced Euro 6 b standards for all new vehicles as of January 2023.

Tunisia does not mandate compliance with Euro emission standards, opting instead to emphasize fuel quality and general technical inspections. Its vehicle inspection system, overseen by organizations such as SGS Tunisia, involves routine checks for safety and emissions; however, these inspections mainly assess visible smoke and do not incorporate advanced diagnostic tools such as On-Board Diagnostics (OBD), Real Driving Emissions (RDE) protocols, or In-Service Conformity (ISC), which are standard practices within the European Union.

Moreover, a significant portion of Tunisia's vehicle fleet consists of older, imported cars, many of which do not meet even Euro 4 emission thresholds, contributing to elevated levels of NO_x

and particulate matter (PM) in urban areas such as Tunis and Sfax. Compounding this is the lack of a national air quality monitoring infrastructure akin to Europe's AASQA networks, though regional studies have confirmed that the transport sector is a dominant contributor to ambient air pollution.

According to the International Council on Clean Transportation (ICCT), over 60% of used vehicles exported to African countries fail to meet minimal emissions and safety standards, a trend clearly evident in Tunisia's aging fleet. Fuel quality, though regulated, still lags behind Euro-standard ultra-low sulfur diesel (10 ppm), limiting the efficiency of any imported vehicles equipped with particulate filters.

In contrast, South Africa implemented Euro 2-level controls in 2006 and Morocco now serves as a regional model with fuel-policy alignment and emissions regulation. To close this gap, Tunisia must not only adopt Euro-aligned emissions standards but also strengthen institutional capacity for emissions testing, enforce fleet renewal policies, and integrate transport-related air quality indicators into national environmental strategies, a crucial step toward addressing growing public health risks linked to vehicular pollution (Naré & Kamakaté, 2017).

V. Overview of Available Studies

V-1. State of Knowledge at the International Level (Europe, Asia, North America)

A substantial body of research from Europe, Asia, and North America has greatly advanced understanding of urban particulate pollution, particularly the sources, behavior, and health impacts of PM_{10} and $PM_{2.5}$ in densely populated environments. These studies employ a combination of empirical monitoring and advanced dispersion modeling to analyze pollutant dynamics and to inform emission-control strategies. Collectively, they reveal both the shared challenges and methodological innovations in assessing and mitigating particulate pollution. The findings emphasize the necessity of context-specific modeling frameworks that incorporate local emission patterns, meteorological conditions, street geometry, and population exposure characteristics.

Globally, disparities in $PM_{2.5}$ exposure remain evident, as illustrated in Figure 7, which shows pronounced differences in pollution intensity and associated health risks between regions. In Europe, extensive research efforts have quantified particulate emissions using standardized models and inventories such as COPERT for emission estimation and SIRANE or GRAL for urban dispersion analysis.

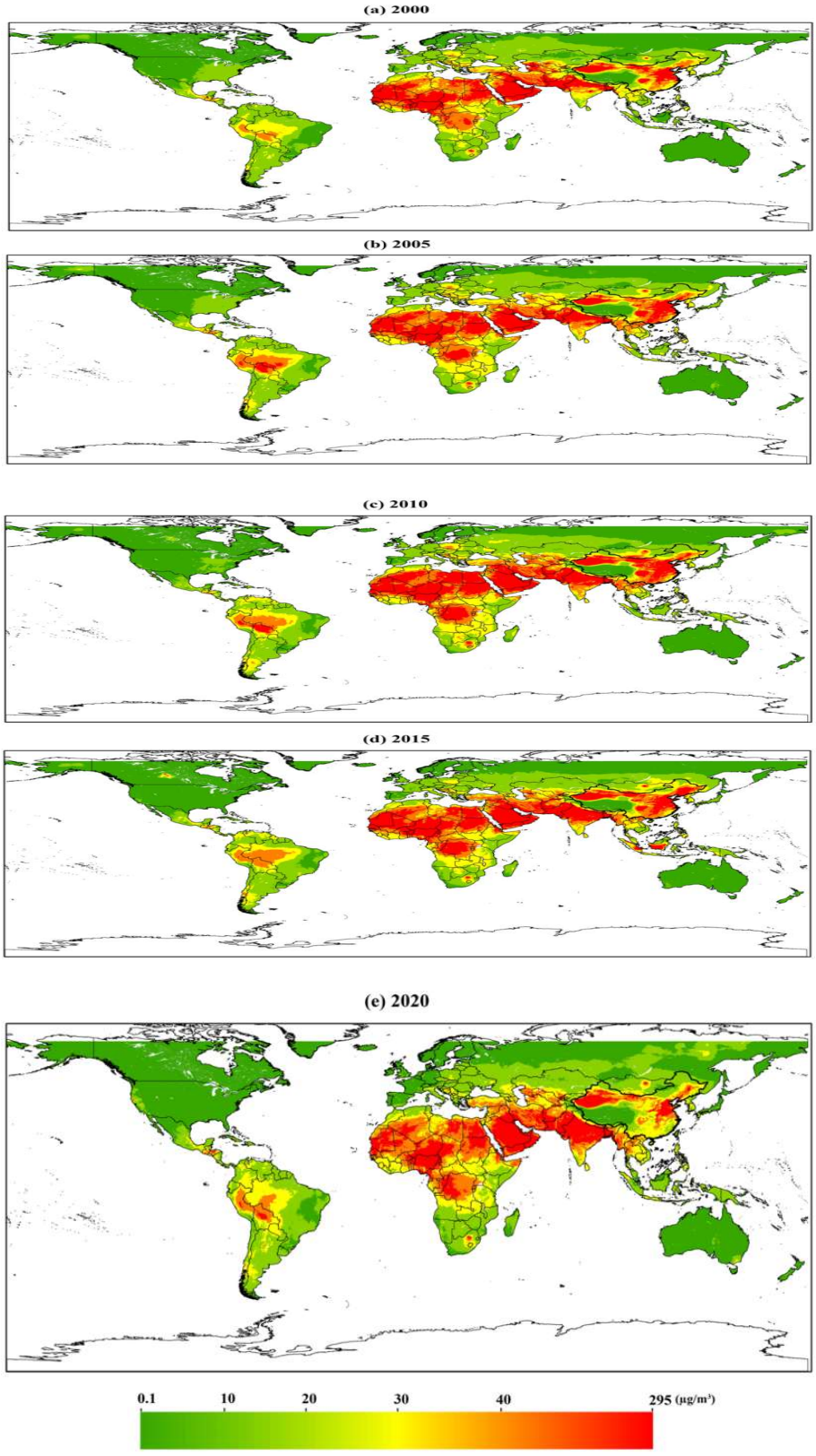

Figure 7 : Global $PM_{2.5}$ concentration trends in 1,312 cities between 2000 and 2020 (Qin Zhou et al., 2023)

In Europe, extensive research efforts have quantified particulate emissions using standardized models and inventories such as COPERT for emission estimation and SIRANE or GRAL for urban dispersion analysis. The European Environment Agency (EEA, 2023) consistently identifies road traffic as the dominant source of $PM_{2.5}$ in cities characterized by dense street canyons and high diesel-vehicle prevalence. Studies in France (Soulhac et al., 2011) and Switzerland (May et al., 2023) validated the GRAMM/GRAL system, demonstrating that GRAL's building-resolving microscale simulations accurately reproduce both spatial gradients and temporal variability of concentrations observed across urban monitoring networks such as those in Heidelberg.

In Asia, empirical observations and modeling studies highlight severe urban pollution episodes driven by rapid industrialization and traffic growth. Measurements in Delhi and Imphal, for instance, frequently report PM_{10} levels exceeding 100 $\mu g\ m^{-3}$ during rush hours, with $PM_{2.5}/PM_{10}$ ratios above 0.6, indicating strong dominance of combustion-derived aerosols. Similar conditions are observed in major Chinese megacities, where dispersion models such as AERMOD and CALPUFF are widely applied, though they often lack detailed representation of urban morphology compared with microscale models like GRAL (Pan Lu et al., 2023).

In North America, particularly in the United States and Canada, decades of regulatory monitoring and data availability have enabled advanced hybrid modeling approaches that integrate emissions, meteorology, and exposure assessment. The U.S. Environmental Protection Agency (EPA) promotes the use of the CMAQ and AERMOD models coupled with GIS-based analysis tools to evaluate exposure at neighborhood scales. Studies in Los Angeles and New York reveal how urban geometry and traffic intensity create localized pollution hotspots. Research by Alex A. Karner et al. (2010) and Knobel et al. (2023) highlights that populations living near major roadways face disproportionately high exposure to fine particulates, underlining environmental-justice disparities linked to socioeconomic status and spatial proximity to emission sources.

V-2. Research in North Africa and the Tunisian context

Compared to the extensive air quality research conducted in Europe, North America, and Asia, studies focusing on North Africa particularly Tunisia; remain relatively scarce but are steadily growing in response to increasing urbanization and associated environmental pressures. Across the region, ambient particulate matter (PM_{10} and $PM_{2.5}$) pollution is driven by both anthropogenic and natural sources, including vehicular traffic, industrial emissions, biomass burning, construction activities, and transboundary Saharan dust.

In Algeria, research has shown that traffic congestion and poorly maintained vehicles significantly elevate PM_{10} and $PM_{2.5}$ levels in urban areas, such as Algiers and Oran (Belarbi et al., 2020).

Modeling approaches such as neural networks have also been used to forecast daily PM concentrations based on historical air quality and meteorological data (Hamza Abderrahim et al., 2016). Similarly, In Morocco, studies in Fès reveal that seasonal Saharan dust intrusions contribute significantly to PM_{10} spikes, underscoring the need for air quality models to incorporate transboundary dust effects (Deabji et al., 2024).

In Tunisia, air quality concerns are increasingly significant, particularly in urban centers like Tunis, Sfax, and Sousse, where PM_{10} levels are often elevated near road intersections, industrial areas, and densely built environments. National data from the ANPE (National Agency for Environmental Protection) confirm that PM_{10} frequently exceeds the WHO daily guideline of 45 $\mu g/m^3$. For instance, (Euchi & Dahech, 2019) investigated the relationship between PM_{10} spikes and respiratory health in Sfax, revealing that brief periods of elevated PM_{10} concentrations led to sharp increases (up to 270%) in hospital admissions for respiratory conditions, using combined data from environmental monitoring and healthcare facilities.

Tunisian researchers have begun integrating emission estimation tools like COPERT and simplified dispersion models such as SIRANE to simulate PM behavior, however, these tools are often constrained by their lack of resolution or simplification of urban form. Recent research conducted across North Africa and specifically within Tunisia has contributed to a growing understanding of urban air pollution dynamics, particularly concerning PM_{10} and $PM_{2.5}$ levels.

Therefore, (Bouchlaghem & Nsom, 2012) examined the influence of Saharan dust intrusions on PM_{10} concentrations across multiple Tunisian cities, including Tunis, Sfax, and Sousse, demonstrating how regional meteorological patterns can exacerbate urban particulate levels. Similarly, (Cheberli et al., 2025) investigated indoor air quality in childcare centers in Megrine, Tunisia, revealing significant $PM_{2.5}$ exposures linked to both outdoor infiltration and indoor sources.

These studies underscore the combined impact of natural and anthropogenic factors, including traffic, urban design, and regional dust transport on air quality in Tunisian urban settings.

Despite this progress, the body of research remains underdeveloped compared to international standards, with limited studies linking pollution levels to public health outcomes, such as respiratory illnesses or cytotoxic effects. Furthermore, monitoring networks are sparse and

often not designed for high-resolution urban diagnosis, especially for $PM_{2.5}$. Closing these gaps is essential for developing locally adapted, evidence-based mitigation strategies.

VI. Description of the Tunisian Vehicle Fleet

VI-1. Fleet Composition by Vehicle Type and Energy Source

Tunisia's vehicle fleet, as of December 31, 2024, comprises approximately 2.7 million registered vehicles, with a dominant presence of internal combustion engine (ICE) vehicles. As illustrated in Figure 8 (a), private passenger cars make up the largest share of the fleet, accounting for 65%, confirming the findings of the "Land Transport Technical Agency" (ATTT) (WMC_HS_AUTO_2025, p. 40). Utility vans (21%) represent the next largest categories, while agricultural tractors (4%), mixed-use cars (6%) and other vehicle types, including two-wheelers, hold a relatively minor portion of the total stock.

It is worth noting that although motorcycles are not represented in the chart, they experienced a significant surge in registrations in 2024 from 1,740 in 2023 to over 10,000, likely driven by increasing demand for affordable urban mobility.

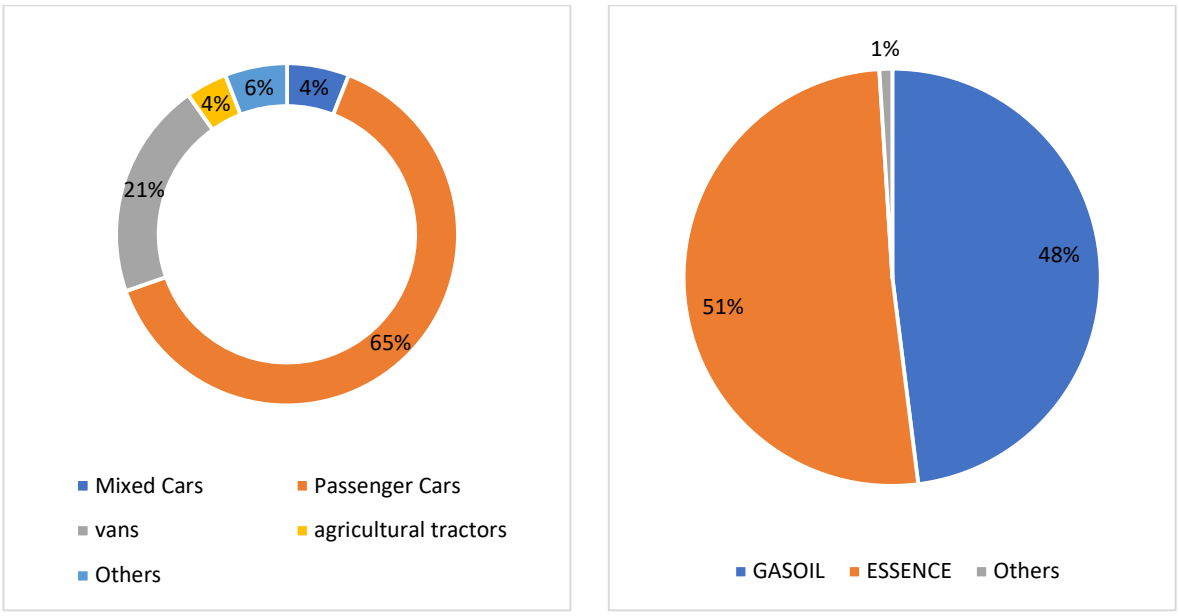

(a) (b)

Figure 8 : Distribution of the vehicle fleet by (a) vehicle type and (b) fuel type (WMC_HS_AUTO_2025, pp. 47–51)

In terms of fuel type, Figure 8 (b) shows that the fleet remains almost evenly split between gasoline (ESSENCE) and diesel (GASOIL) engines, at 51% and 48% respectively, while alternative fuel vehicles (including hybrids, electrics, and others) comprise just 1%. This

minimal share underscores the early stage of Tunisia's transition toward cleaner transport technologies.

In 2024, only 386 electric vehicles were officially registered, illustrating the marginal status of electric mobility in the national context. In contrast, hybrid vehicles have begun to gain modest traction, with Toyota leading the segment. The brand reported that 30% of its sales in Tunisia during 2024 were hybrid vehicles, and it commands an estimated 75% of the national hybrid vehicle market (WMC_HS_AUTO_2025, pp. 47–51).

The primary drivers behind the slow adoption of clean vehicle technologies appear to be related to purchase cost, limited infrastructure, and consumer skepticism; however, the presence of hybrid, electric, and even hydrogen-ready models from leading manufacturers such as Toyota, MG, and BYD signals the emergence of a diversified vehicle offering. The evolution of this trend will depend largely on how effectively the structural and policy barriers to adoption are addressed in the coming years.

VI-2. Age and Condition of the Vehicle Fleet

An additional challenge facing Tunisia's transport sector is the aging condition of its vehicle fleet. The majority of circulating vehicles, especially those entering the country via the second-hand market, are over a decade old and do not meet the latest environmental or safety standards. As shown in Figure 9, nearly half (48%) of the national fleet is more than 15 years old, while only 16% is under 5 years of age, highlighting the significant aging of the vehicle stock.

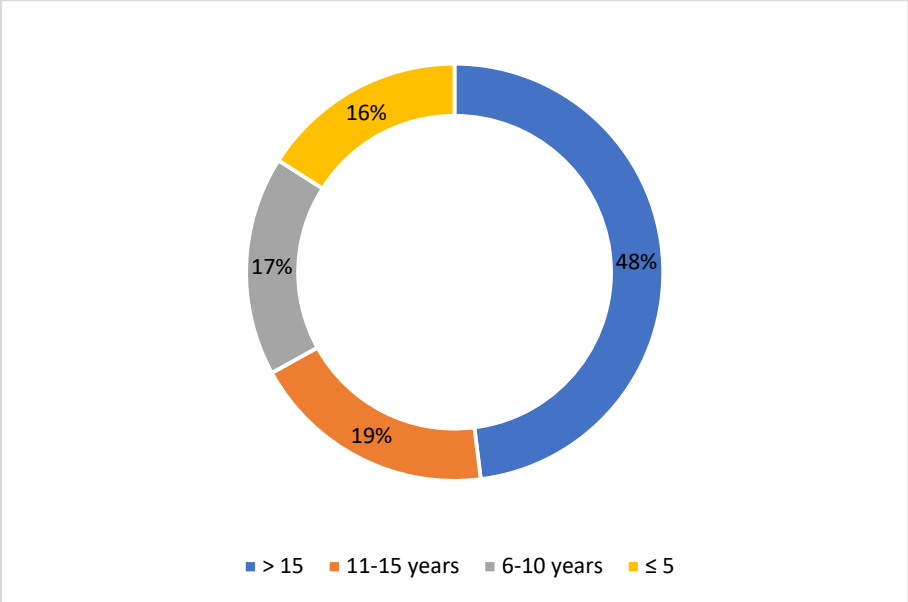

Figure 9 : Age Distribution of the Vehicle Fleet as of December 31, 2024 (WMC_HS_AUTO_2025, pp. 47–51)

The used vehicle market is highly active, with an estimated 300,000 units changing ownership annually, many of which are imported from international markets outside the authorized dealership network and are later re-registered for use within the country. This phenomenon, known as the “parallel market”, has grown significantly in recent years, increasing its share of total registrations from 21% in 2022 to 28% in 2024 (WMC_HS_AUTO_2025, p. 13).

Beyond the private sector, the public transportation fleet, particularly buses, reflects a state of structural degradation. In the Greater Tunis region, the “Tunis Transport Company” (TRANSTU) operates a fleet of 1,247 buses, of which only 650 are currently operational. The operational availability of the fleet has deteriorated sharply, falling from 87% in 2010 to a mere 7% by 2015 (WMC_HS_AUTO_2025, p. 26). This has greatly compromised service reliability and diminished public confidence in the transport system. A 2023 consumer satisfaction study revealed that while over 70% of daily commuters use buses, only 12.8% report satisfaction with the service received.

The causes of this degradation are both systemic and operational. A lack of sustained investment in infrastructure, outdated fleet management, poor maintenance regimes, and insufficient digitalization have contributed to the fleet’s obsolescence. Moreover, inefficiencies in regulation and the absence of robust public-private partnerships have slowed reform progress.

Strategic recommendations from national studies have called for legal reform, increased investment, and integration of digital solutions in order to modernize the national transport ecosystem (WMC_HS_AUTO_2025, p. 26). Until such changes are implemented, the aging fleet will continue to pose safety, environmental, and economic risks.

VI-3. Energy Transition and Infrastructure for Sustainable Mobility

Tunisia’s efforts to transition toward sustainable mobility are progressing gradually, framed within a broader strategy led by the National Agency for Energy Management (ANME). Recognizing that the transport sector contributes approximately 26% of national greenhouse gas (GHG) emissions and accounts for nearly 36% of final energy consumption, the government has begun to implement policy and infrastructural measures aimed at reducing fossil fuel dependency and promoting alternative mobility solutions (WMC_HS_AUTO_2025, p. 43). While these efforts are promising, the transition remains constrained by economic, technical, and behavioral challenges.

As of the end of 2024, the national charging infrastructure for electric vehicles remains embryonic but expanding, with 140 charging points established, including 83 open to the public.

These are distributed unequally across the territory, as illustrated in the figure 10, which highlights the regional deployment of public charging stations concentrated in major urban centers such as “Grand Tunis” (5 stations), “Nabeul” (3), “Sousse” (2), “Sfax” (2), “Monastir” (1), “Mednine” (1), and “Gabes” (1), with Grand Tunis leading in total installations.

The limited number of direct current (DC) fast-charging stations, compared to alternating current (AC) installations, restricts rapid deployment and discourages long-distance electric travel (WMC_HS_AUTO_2025, pp. 31–33). Nevertheless, national targets have been set: 5,000 electric vehicles and 60 public charging points by 2026, scaling up to 50,000 electric vehicles and 5,000 charging stations by 2030.

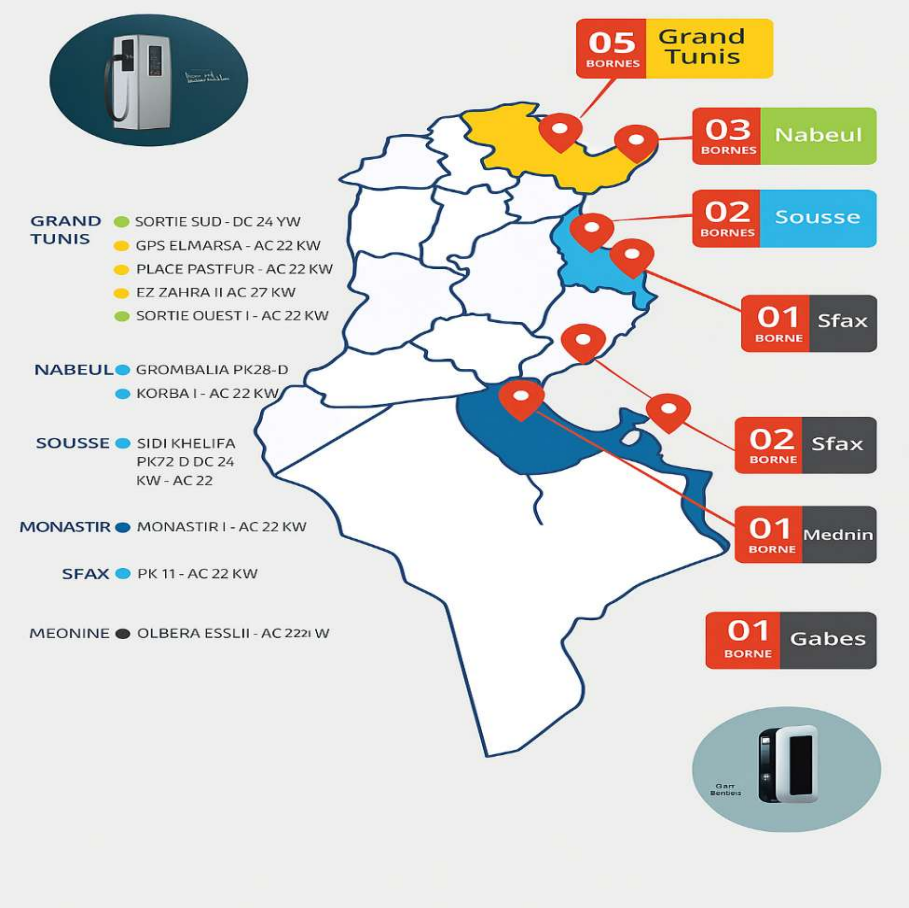

Figure 10 : Distribution of EV Charging Stations Across Tunisia (WMC_HS_AUTO_2025, pp. 47–51)

From a regulatory and fiscal standpoint, Tunisia has enacted multiple incentives to support adoption. These include the elimination of customs duties on electric vehicles, reductions of VAT from 19% to 7% on both vehicles and domestic chargers (Wallbox units), and tax deductions amounting to approximately 30,000 TND for mid-range electric models. Despite these policies, the market response has remained modest.

According to a recent Emrhod Consulting survey, only 14% of consumers expressed willingness to purchase an electric vehicle, while 47% favored traditional thermal models. High initial costs remain the primary barrier, cited by 49% of respondents as the most influential factor in decision-making (WMC_HS_AUTO_2025, p. 44).

The transition also intersects with challenges in energy policy. Currently, less than 4% of Tunisia's electricity comes from renewable sources. This diminishes the environmental advantages of electric vehicles, as relying on a carbon-intensive electricity grid may simply transfer emissions from vehicle tailpipes to power generation sources, rather than eliminating them.

The government's goal to increase the share of renewables to 30% by 2030 is crucial if electric mobility is to serve its intended environmental function (WMC_HS_AUTO_2025, p. 50).

An additional aspect of the transition involves the development of human capital and professional competencies. Electric vehicles require significantly less maintenance due to their mechanical simplicity, raising concerns about job displacement in traditional automotive repair sectors. Stakeholders such as the "National Trade Association for Automotive Mechanics " have emphasized the need to retrain workers in high-voltage systems, battery diagnostics, and embedded electronics. Training initiatives supported by international cooperation, including those implemented in Bizerte, Sfax, and Zaghouan, are early responses to this structural shift (WMC_HS_AUTO_2025, p. 44). However, such programs remain limited in scope, and broader reforms in vocational education will be needed to align workforce skills with the technological demands of the new mobility landscape.

Ultimately, Tunisia's shift toward a low-emission transport sector reflects a convergence of global environmental imperatives and domestic socioeconomic needs. While foundational policies are in place, the realization of sustainable mobility will depend on the integration of energy reform, infrastructure investment, industrial strategy, and public engagement within a coherent national roadmap. The urgency of this transition is heightened by both climate commitments and the need to modernize the national transport system to better serve citizens and support economic resilience.

VII. Modeling Frameworks

VII-1. Road Traffic Models

Accurate modeling of vehicular traffic is essential for estimating urban air pollution levels and understanding pollutant dispersion dynamics. Traffic simulation methods vary in complexity, spatial resolution, and temporal granularity. They are broadly categorized into static, dynamic, and aggregated dynamic models, each offering distinct advantages for different scales of urban analysis.

VII-1-1. Static Models

Static models estimate average traffic conditions using demographic data, land use information, and household travel surveys. These models typically follow a four-step structure:

- Trip Generation based on residential and employment densities
- Trip Distribution assigning trips across zones using gravity or entropy models
- Modal Split dividing travel demand by mode (e.g., car, transit)
- Route Assignment using speed–flow curves to allocate trips to the network

The resulting Origin–Destination (OD) matrix is used with road capacities and speeds to compute average flows. Tools like PTV Visum operationalize this framework effectively (Fellendorf & Vortisch, 2000).

However, static models assume equilibrium conditions and are therefore unable to simulate congestion or time-varying traffic behavior, limiting their applicability in studies requiring temporal resolution or localized exposure analysis (Fabien Leurent et al., 2023).

VII-1-2. Dynamic Models

Dynamic models account for time-dependent traffic behaviors and simulate vehicle interactions more realistically. They offer improved accuracy in estimating the spatial and temporal variability of traffic patterns. These models are subdivided into three primary types:

❖ **Macroscopic Dynamic Models**

Macroscopic models treat traffic flow analogously to fluid dynamics using the Lighthill–Whitham–Richards (LWR) framework. They relate traffic density, speed, and flow through a fundamental diagram.
Notable models include:

- METACOR (Diakaki et al., 2000)
- Cell Transmission Model (CTM) (Daganzo, 1994)

These models capture network-level dynamics efficiently. The Macroscopic Fundamental Diagram (MFD) concept has further enabled district-scale analysis of congestion propagation and traffic performance (Geroliminis & Sun, 2011).

❖ **Microscopic Dynamic Models**

Microscopic models simulate the behavior of individual vehicles, including acceleration, braking, car-following, and lane-changing. Tools like VISSIM (Fellendorf & Vortisch, 2010) and SUMO (Eclipse SUMO - Simulation of Urban MObility, s. d.) generate high-resolution vehicle trajectories over time.

Microscopic models are particularly recommended for studies that demand high temporal and spatial resolution, such as evaluating traffic conditions at pollution hotspots or during peak hours. They are particularly effective for modeling street-level traffic phenomena at intersections, roundabouts, and signalized corridors, areas often associated with peak pollution exposure.

❖ **Mesoscopic Models**

Mesoscopic models offer a compromise by simulating vehicle groups or platoons with statistical rules. While individual vehicle behavior is not resolved, these models still represent congestion patterns and routing decisions.

Key examples include:

- CONTRAM (Taylor, 2003)
- DYNASMART (Mahmassani et al., 2005)

Mesoscopic models are computationally efficient and are often used in hybrid systems where they provide network-wide inputs to more detailed microscopic submodels.

VII-1-3. Aggregated Dynamic Models (MFD-Based)

Aggregated models use Macroscopic Fundamental Diagrams to represent average speed and flow as a function of vehicle accumulation within an area. These models offer a computationally light method for evaluating traffic at the neighborhood or district level.

They are well-suited for assessing large-scale interventions like congestion pricing or low-emission zones (Geroliminis & Daganzo, 2008).

Table 2 presents a classification of traffic simulation models along with representative examples for each category, providing a structured overview, though it is not exhaustive. For a more comprehensive review of traffic modeling approaches, including their respective advantages and limitations, readers are referred to the work of (Bochenina et al., 2025).

Table 2 : Classification of Traffic Simulation Models

Models		**Solving method**	**Application domain**	**Results**	**Example**
Static		O/D matrix	Urban area	Average quantity of vehicles	VISSIM (Fellendorf & Vortisch, 2000)
Aggregated dynamic		Relation flow density	Several neighbourhoods	Average speed, congestion	(Geroliminis & Daganzo, 2008).
Dynamic	Macroscopic	First order (LWR)	Neighbourhood	Density & speed of vehicles	(Diakaki et al., 2000)
		Second order (AZR)	Highway		
	Mesoscopic	Aggregate flows Traffic details	Neighbourhood	Vehicle trajectory	(Taylor, 2003)
	Microscopic	Macroscopic Lagrangian	Urban network	Location, speed, acceleration per second	VISSIM (Fellendorf & Vortisch, 2010)
		Car following			

VII-2. Emission Factors Models

A wide range of tools exists for compiling on-road transportation emissions inventories, generally calculated by multiplying emission factors (EFs) with activity data across vehicle classes. These EFs are typically obtained via chassis or engine dynamometer tests within specific driving cycles, which simulate real-world urban, rural, or highway conditions.
Traffic emissions are commonly categorized as:

- **Fuel-Based Models** use national fuel statistics and fleet data to estimate emissions at broad scales, as outlined in the IPCC Emission Factor Database (The Standard for Calculating Emissions in Road Transport - INFRAS, 2022)

- **Fleet-Average Models** (e.g., NAEI in the UK, IVE tool) apply fixed EFs per vehicle category and annual mileage, suitable for national/regional inventories.

- **Speed-Dependent Models**, such as COPERT 5.6, estimate emissions as a function of average link speed and incorporate exhaust, evaporative, tyre/brake wear, and road abrasion (COPERT |Calculations of Emissions from Road Transport, s. d.).

- **Traffic Scenario-Specific Models** like HBEFA 4.2 offer differentiated emission factors based on traffic states (e.g., free flow, stop-go), vehicle types, and road classes, ideal for street-level modeling (HBEFA - Handbook Emission Factors for Road Transport, s. d.).

- **Traffic-Variable Models** adjust emission factors (EFs) based on real-time traffic characteristics such as vehicle density, queue lengths, and intersection signal conditions. For example, in Florence, high-resolution traffic sensor data were used to empirically derive relationships between CO_2 emission factors and local traffic flow, revealing significantly higher emissions during congested conditions compared to free-flow periods (Nikolaos Tsanakas et al., 2020)

- **Kinematic Regression** such models, including VERSIT+ LD, derive emission factors using regression analysis on real-world driving-cycle metrics (e.g., average speed, number of stops, acceleration/deceleration profiles). The latest version, VERSIT+ LD18, employs multiple linear regression to establish empirical relationships between pollutant emission rates (e.g., CO_2, NO_x, PM) and instantaneous kinematic variables from measured vehicle trajectories. Developed under the ARTEMIS EU project, this tool calculates emission factors for light-duty vehicles as a function of detailed driving-cycle parameters and supports fine-scale emission estimations across various traffic conditions. VERSIT+ has therefore become a preferred choice for linking microscopic traffic simulation outputs (e.g. vehicle speed and acceleration) with high-resolution emission inventories. (Grote et al., 2016).

- **Instantaneous Modal Models** (e.g., PHEM and CMEM) simulate emissions at fine temporal resolution (~1-second), linking engine operation modes (idle, acceleration, cruising) to emissions. They can be coupled with microscopic traffic simulators like VISSIM or SUMO (Zallinger et al., 2008).

VII-3. Air Quality Models

Air quality models estimate pollutant concentrations and deposition fluxes across different sites and timeframes by solving equations that describe atmospheric transport, chemistry, and physical transformations from emission sources to receptors. These methods vary in required inputs and spatial–temporal resolution.

1. Box Models

These models assume pollutants are uniformly mixed within a defined zone. Emissions undergo chemical/physical changes and exchange in and out. While not used operationally, box models are ideal for investigating specific mechanisms (e.g., single airshed behavior, Shaw et al., 2023), controlled experiments like smog chambers, or deriving annual deposition averages relevant to water contamination studies.

2. Gaussian Models

Focusing on individual or a few sources, these models often assume Gaussian distributions under steady meteorological conditions. Gaussian plume models (Csanady et al., 1973) estimate concentrations up to ~50 km with hourly averages, handling simple deposition and first-order chemistry. Gaussian puff models release discrete "puffs" to account for variable winds and complex chemistry, albeit at higher computational cost.

Hybrid plume-puff models enhance simulation accuracy under low-wind conditions by integrating multiple dispersion approaches, as reflected in recent EPA AERMOD updates that propose improved options for modeling in such scenarios (Guideline on Air Quality Models; Enhancements to the AERMOD Dispersion Modeling System, 2023).

Adaptations exist to include simple building effects via modified dispersion coefficients, but complex recirculation at street intersections requires specialized street-canyon models. In-addition, Operational Street canyon models such as OSPM and SIRANE have shown strong capabilities in simulating pollutant dispersion in urban environments.

The OSPM (Operational Street Pollution Model) remains one of the most robust tools in this category; a 2012 validation campaign across 12 monitoring sites confirmed its reliability in predicting concentrations of NO_2 and particulate matter under real-world street conditions (Robert Oleniacz et al., 2023).

On the other hand, SIRANE offers a different modeling framework by representing each street as a simplified box and resolving the advective balance at intersections. It accounts for a long-

street advection, turbulent exchanges with the atmosphere, and pollutant transport across intersections, while deploying Gaussian plume formulations to simulate dispersion above roof level (Soulhac et al., 2011, 2012). These models are widely used due to their balance between physical realism and computational efficiency in complex urban geometries.

3. Lagrangian Trajectory Models

These models track air parcels through time along wind trajectories. Advanced implementations include numerical particle and grid-based models such as HYSPLIT**,** FLEXPART, and CALPUFF. Particle-based methods effectively simulate both flat and complex terrains by simulating turbulent diffusion alongside advection. Grid-based Lagrangian models support non-linear chemistry but may struggle with conditions like land-sea breezes and wind shear (Tian et al., 2024)

4. Eulerian Models

Eulerian frameworks divide the atmosphere into a 3D grid, iteratively solving conservation equations for pollutants and meteorology. Chemical transport models (CTMs), such as Polair3D, CHIMERE, CMAQ, and CAMx—use meteorological inputs from separate models. Online CTMs (e.g., WRF-Chem) couple meteorology and chemistry, capturing feedbacks like PM effects on cloud formation. These models are scalable from urban to global domains and can include plume-in-grid (PinG) approaches that embed Lagrangian puffs within Eulerian grids (Karamchandani et al., 2009; Y. Kim et al., 2014) .

5. Computational Fluid Dynamic Models (CFD)

CFD techniques include DNS**,** LES, and RANS, each varying in turbulence handling:

- DNS offers full Navier–Stokes solutions but is computationally impractical for environmental scales.
- LES resolves large eddies explicitly and parameterizes small ones; capable but still resource-intensive.
- RANS applies time-averaged equations with turbulence closures, offering a practical balance for urban flows. Models like Code_Saturne and MISKAM now integrate chemical reactions (Gousseau et al., 2012.) highlight RANS vs. LES tradeoffs in urban settings (Robert Oleniacz et al., 2023).

Table 3 : Classification of Air Quality Models

Models	Application domain	Solution method	Examples
Chemical Transport Models (CTM)	Urban to global (from 1 km to several 100 km resolution)	Some Lagrangian models	Flexpart, Hysplit AUSTAL2000
		Eulerian models	Polair3D, CMAQ, WRF-Chem, CAMx CHIMERE
		Plume-in-Grid models	PinG , CMAQ-Urban
Gaussian Models	Local impact (up to 1 km)	Gaussian models & some Lagrangian	Polyphemus, ADMS, SIRANE, AERMOD
		Street-canyon models	SIRANE, OSPM
Computational Fluid Dynamics models (CFD)	Complex environment Local scale (up to 10 km)	RANS	Code_Saturne, MISKAM
	Research (turbulence)	LES	FAST3D-CT (Patnaik et al., 2006)

The theoretical models described above form the scientific foundation for modern air-quality simulation systems. In practice, these mathematical frameworks are implemented through specialized software platforms that integrate emission data, meteorological fields, and urban geometries within GIS-based computational environments. Such tools enable multi-scale analysis—from regional transport to street-level dispersion—and support real-time visualization, scenario testing, and policy evaluation. The following section presents a comparative overview of the most widely used simulation tools and modeling platforms, highlighting their core functionalities, spatial resolutions, and application domains in environmental management.

VII-4. Integrated Modeling Platforms and Software Tools

An atmospheric dispersion model can be broadly defined as a computational system that integrates physical, chemical, dynamical, and radiative processes to simulate the distribution and behavior of air pollutants in the atmosphere (Jacobson, 2002). These models allow

researchers and planners to forecast the impact of changing meteorological or emission conditions, facilitating rapid scenario testing and optimized pollution mitigation strategies (Huzzat et al., 2025). Simulation techniques can be categorized as analog or digital, with digital models being dominant due to their high computational speed, flexibility, and compatibility with modern systems (El-Harbawi, 2013). Today, such models have become essential tools in environmental science, engineering, and public health applications, offering critical insight into the behavior of complex atmospheric systems.

Most modern dispersion models are implemented as desktop or GIS-integrated software tools, many of which support batch processing, real-time coupling with meteorological models like WRF, and 3D visualization capabilities (El-Harbawi, 2013). In cases where precise emission data are unavailable, it is standard practice to assume worst-case emission scenarios to ensure conservative estimates, such as using maximum allowable stack emissions or peak-hour traffic loads (US EPA, 2016). It is also essential to define receptor points, i.e., locations where pollutant concentrations will be estimated and analyzed.

Different models are selected based on scale and application: Eulerian models like CMAQ, CAMx, and ADMS-Urban are well suited for regional or urban air quality forecasting and regulatory analysis (Gao et al., 2024). Gaussian models, originally developed in the 1970s, remain widely used for local-scale impact assessments due to their simplicity and computational efficiency (Jephcote & Gulliver, 2025). For simulating long-range pollutant transport, Lagrangian models such as HYSPLIT and SILAM are preferred, as they provide accurate trajectory and plume simulations over complex or extended terrains (S. Kim et al., 2009). Table 4 provides a summary description of most widely used air quality modelling software with their applications and web addresses.

Table 4 : Comparative Summary of Air Quality Modelling Tools with GIS Integration and Use Cases

Software Name	Establishment	GIS	Applications	Website
APPH Aidair	Aidair, University of Geneva	yes	Decision support for urban air quality	http://ecolu-info.unige.ch/recherche/eureka/AIDAIR/
AUSTAL View, CALPUFF View, etc.	Air Dispersion Modelling Inc.	Yes	Road and transport dispersion modelling	www.air-dispersion-model.com
AirQUIS	NILU (Norway)	Yes	Urban air quality management	http://www.nilu.no/airquis/
AJ Design Software	AJ Design Software	No	Atmospheric dispersion algorithms	http://www.ajdesigner.com/phpdispersion/point_space_equation.php
ALOHA	NOAA (USA)	Yes	Accidental release of heavy gases	http://archive.orr.noaa.gov/cameo/aloha.html
ARIA	ARIA Technologies	Yes	General air dispersion modelling	http://www.aria.fr/english/software_systems.php
ATM-PRO	ATM-PRO	Yes	Pollution and human health risk assessment	www.atmpro.be
BEE-Line Software	BEE-Line Software	Yes	Dispersion modelling	http://www.beeline-software.com/
BREEZE	Trinity Consultants	Yes	Air quality, meteorology, regulatory tools	http://www.breeze-software.com/
ADMS (Urban, Roads, etc.)	CERC (UK)	Yes	Road traffic, industrial emissions modelling	http://www.cerc.co.uk/environmental-software.html
DISPER, DESCAR	Canarina Algoritmos Numéricos	Yes	Water and air pollution analysis	http://www.canarina.com/airpollutiondispersion.htm
CAPARS	AlphaTRAC, Inc.	Yes	Atmospheric dispersion	http://www.alphatrac.com/
OSPM	National Environmental Research Institute (NERI)	Yes	Traffic-related air pollution prediction	http://www.dmu.dk/International/air/
DEGADIS	Dr. Spicer & Dr. Havens (Univ. of Arkansas)	No	Dense gas dispersion	http://www.epa.gov

DIPCOT	EREL – Demokritos Institute (Greece)	No	Dispersion over complex terrain	http://milos.ipta.demokritos.gr/
DISPERSE	P&I Design Ltd.	No	Short-term concentration predictions	http://www.pidesign.co.uk/disperse.htm
DREAM	NERI (Denmark)	No	Radioactive dispersion (wet and dry deposition)	http://www2.dmu.dk/AtmosphericEnvironment/WEPTEL/DREAM/
AirWare	ESS GmbH (Austria)	Yes	Urban & industrial air quality management	http://www.ess.co.at/AIRWARE/
EDMS	US FAA	Yes	Airport emissions assessment	http://www.faa.gov/about/office_org/headquarters_offices/aep/models/edms_model/
FLACS	Gexcon Consulting	Yes	3D gas dispersion and explosion modelling	http://www.gexcon.com/index.php?src=flacs/flacs.html
HGSYSTEM	Shell International	No	Gas dispersion modelling	http://www.hgsystem.com/hgweb.html
Airviro	SMHI (Sweden)	Yes	Emissions inventory + urban dispersion	http://www.indic-airviro.smhi.se/
ISC-AERMOD View.	Lakes Environmental Software	Yes	Regulatory dispersion tools	http://www.lakes-environmental.com/
MIDAS Models	ABS Consulting	Yes	Urban & accidental releases	http://www.absconsulting.com/midas/advantage.html
NAME	UK Met Office	Yes	Radioactive dispersion modelling	http://www.metoffice.gov.uk/research/nwp/publications/nwp_gazette/3rd96/name2.html
Oklahoma Dispersion Model	Dr. J.D. Carlson	No	Gases and particulates dispersion	http://agweather.mesonet.org/models/dispersion/default.html
OML	NERI (Denmark)	Yes	Pollution forecasting	http://www2.dmu.dk/1_viden/2_Miljoe-tilstand/3_luft/4_spredningsmodeller/5_oml/OMLlong_en.asp

WindRose PRO3, etc.	Enviroware s.r.l.	Yes	Flare sizing, road traffic emissions, dispersion plotting	http://enviroware.com/en/products_en.htm
PHAST	Det Norske Veritas (DNV)	Yes	Industrial risk, unified dispersion modelling	http://www.dnv.com/software/all/phast/productInfo.asp
PlantSafe	CSM Solutions, Inc.	Yes	Risk-based modelling for plant safety	http://www.geospheresystems.com/product/plantsafe.html
Polair	ODOTECH (Canada)	Yes	Odour and pollutant dispersion	http://www.odotech.qc.ca/en/
PROKAS	Lohmeyer Consulting Engineers	Yes	Environmental impact assessment	http://www.lohmeyer.de/air-eia/models/prokas.htm
HPAC	L-3 Communications Titan Corporation	Yes	Hazard prediction and assessment	http://www.titan.com/about/
SCRAM	US EPA – AQMG	Yes	Atmospheric dispersion model resources	http://www.epa.gov/scram001/
TRACE	SAFER Systems LLC	Yes	Dense and buoyant plume modelling	http://www.safersystem.com/trace.htm
Wölfel	Wölfel Engineering	Yes	Environmental noise and air modelling	http://www.woelfel.de/wms/noise/pollution/index.htm
A2C	Yamada Science & Art (YSA)	No	Airflow and pollutant transport in terrain	http://ysasoft.com/
COST728, COST732, COST ES0602	University of Hertfordshire	Yes	Urban flow modelling and integrated air quality	http://www.chemicalweather.eu/
DAM	JRC – Institute for Environment & Sustainability	Yes	Atmospheric modelling and database management	http://rem.jrc.ec.europa.eu/dam/

EURAD	University of Cologne	Yes	Urban and regional air quality forecasting	http://db.eurad.uni-koeln.de/index_e.html
Air4EU	NILU (Norway)	Yes	GIS-based air quality mapping	http://www.air4eumaps.info
SoundPLAN	SoundPLAN LLC	Yes	Noise and air pollution dispersion modelling	http://www.soundplan.com/
CMAQ	University of North Carolina	Yes	Tropospheric chemistry and regional air quality	http://www.cmaq-model.org/
ISC3, ADAM	US EPA	No	Regulatory dispersion and exposure estimation	http://www.epa.gov/
ADMS-3	CERC (UK)	Yes	Urban and regional air quality simulation	http://www.cerc.co.uk/
SIRANE	Laboratoire de Physique de l'Atmosphère (CNRS Lyon)	Yes	Urban air pollution modelling in street canyons using a street-network approach	https://sirane.cerema.fr
GRAL / GRAMM	ZAMG (Austrian Central Institute for Meteorology and Geodynamics)	Yes	3D CFD-based dispersion model for urban environments, coupled with meteorology	https://www.zamg.ac.at/cms/en/klima/klimamodellierung/GRAL

Despite advancements in air pollution modeling, several critical limitations persist, especially in complex urban environments. First, accurately simulating dispersion in dense cityscapes remains challenging due to the aerodynamic effects of street canyons, building geometries, and traffic-induced turbulence, which significantly alter flow patterns and pollutant concentrations (Peng Qin et al., 2023; Kubilay et al., 2017). Second, urban air pollution comprises both a local component dominated by near-road emissions and a regional background component, which vary in spatial and temporal characteristics and pollutant types (D'Elia et al., 2021; Silvana Di Sabatino, 2019). Third, reliable estimation of atmospheric deposition fluxes remains problematic.

Both wet scavenging and dry deposition depend heavily on particle size distribution, meteorological conditions, and surface types, yet current models often rely on oversimplified parameterizations (L. Zhang et al., 2001). A major source of uncertainty stems from model inputs such as emission inventories, meteorological data, and boundary conditions—uncertainties that can exceed 50%, particularly for emissions (Guoqiang Tang et al., 2023).

Additional uncertainty arises from the mathematical formulations used to represent complex physico-chemical processes. Chemical mechanisms often incorporate substantial simplifications, and urban turbulence is generally parameterized rather than explicitly resolved. Moreover, numerical factors such as time step selection, vertical and horizontal resolution, and solver approximations introduce further variability in output results (Russell & Dennis, 2000; Thunis et al., 2019). These limitations underscore the importance of rigorous model validation and sensitivity analyses when applying dispersion models in urban air quality management

IX. Conclusion

This first chapter has outlined a comprehensive review of current knowledge regarding atmospheric particulate matter, its sources, dispersion behavior, health impacts, and the modelling frameworks used to study it. The analysis began with a classification of atmospheric particles and a description of their physical and chemical characteristics, with particular attention to fine particles (PM_{10} and $PM_{2.5}$) emitted primarily by transport and energy-related combustion sources.

The chapter then examined the mechanisms through which atmospheric particles disperse and are removed from the environment, considering the effects of meteorological parameters, topography, and built environments. These processes are essential for understanding how pollutants behave in space and time. The public health consequences of vehicular emissions

were also discussed, with multiple studies showing clear associations between long-term exposure to fine particulates and respiratory, cardiovascular, and neurological disorders.

Existing air quality standards, regulations, and international recommendations were then reviewed, demonstrating both progress and disparity in enforcement across regions. Despite well-established legal frameworks in Europe and North America, regulatory implementation in many developing countries remains inconsistent. Tunisia, like many North African countries, faces challenges in enforcing emission standards, maintaining air quality monitoring infrastructure, and integrating data-driven decision-making.

The chapter further presented a typology of modelling approaches, including traffic models, emission estimators, and air quality dispersion models. These tools are critical for diagnosing pollution levels, understanding emission sources, and simulating future scenarios. Advanced models such as CMAQ, CHIMERE, GRAL, and SIRANE allow for high-resolution simulations that incorporate meteorology, emissions, and urban morphology—especially when enhanced with GIS technologies.

A global survey of recent studies has shown that while Europe, Asia, and North America have developed extensive modelling frameworks supported by robust data and interdisciplinary research, North African countries, including Tunisia, remain underrepresented in the scientific literature. The lack of high-resolution data, limited institutional capacity, and minimal integration of modern modelling tools are persistent obstacles. However, Tunisia has seen the emergence of localized research initiatives that reflect growing awareness of air quality concerns and the need for context-sensitive solutions.

In summary, this state-of-the-art review highlights the pressing need for context-specific, integrated modelling frameworks that respond to Tunisia's urban and environmental challenges. The identified gaps, ranging from insufficient emission data to limited application of advanced simulation tools, underscore the importance of designing robust methodologies tailored to local conditions. The next chapter will build upon these findings by presenting the materials, data sources, and modelling methods selected for this study.

CHAPTER 2

Materials and Method

I. Introduction

This chapter outlines the methodological framework adopted to evaluate and simulate the dispersion of particulate matter (PM_{10} and $PM_{2.5}$) in the urban environment of Sousse, Tunisia. The study integrates geospatial data, traffic characterization, emission estimation, and dispersion modeling to assess pollutant concentrations across different locations and time periods.

The chapter begins with a description of the study area, highlighting its geographic, urban, and road network characteristics. It then presents the overall research design, detailing the integration of traffic flow data with emission factor models and the deployment of virtual receptors for pollutant monitoring. Emphasis is placed on the selection and implementation of atmospheric dispersion models, namely COPERT, SIRANE, and GRAL/GRAMM, chosen for their ability to simulate urban pollution under varying spatial and temporal conditions.

Furthermore, the chapter details the experimental measurement campaign, including the configuration of PM sensors, validation protocol, and statistical indicators used to assess model performance. Together, these elements form a comprehensive methodological approach that ensures the robustness and reliability of the study's findings.

II. Description of the Study Area

II-1. Geographic and Urban Characteristics of Sousse

Sousse, a Mediterranean coastal city in northeastern Tunisia, is situated at an average altitude of 25 meters above sea level (fr-ca.topographic-map.com). Spanning over 4,516 hectares, the city had a population of 221,715 in 2023 (ins, 2023) and is renowned for its historical significance and vibrant tourism industry, making it a key economic center in Tunisia.

For this research, the traffic monitoring site was chosen based on several criteria, such as traffic density and composition, road classifications (including highways and residential streets), road layout, population exposure, and local atmospheric conditions (wind speed, direction, humidity, and temperature).

The dispersion of PM_{10} and $PM_{2.5}$ was simulated using the SIRANE model within a defined area of 9,580 x 4,060 square meters, aligned with the traffic counting contours. The results from SIRANE were then used to pinpoint intersections with the highest pollution concentrations, designated as air quality hotspots.

These hotspots were further analyzed at a microscopic level using the GRAL model. The accuracy of the findings for these hotspot areas was verified by comparing the modeled results with real-world measurements. Figure 11 delineates the boundaries and key features of the study area.

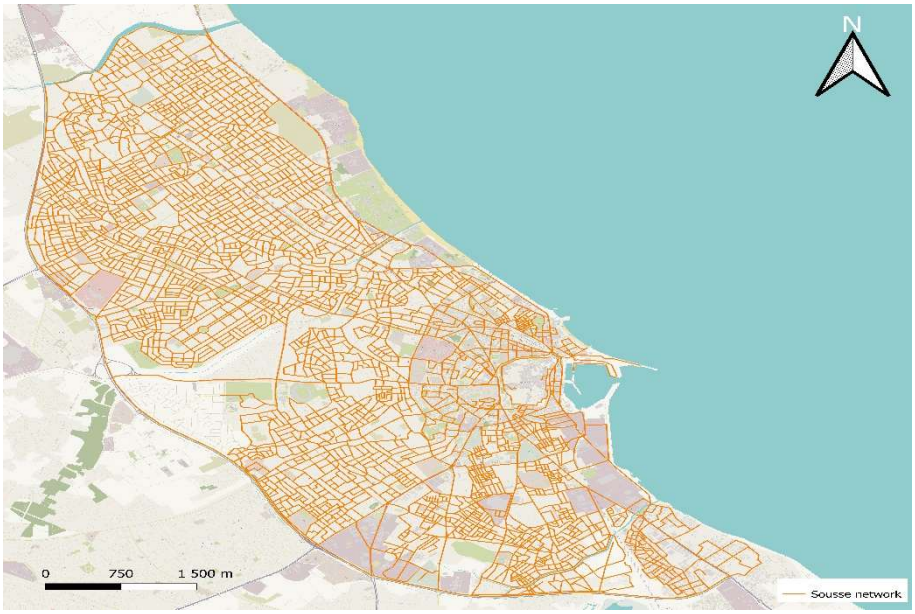

Figure 11 : Area of study

II-2. Land use patterns and road network typologies

The land use patterns of Sousse reflect its multifunctional urban character, combining residential, commercial, industrial, and recreational zones within a relatively compact geographic footprint. The historic city core, dominated by the medina, is surrounded by medium- to high-density residential neighborhoods, while modern commercial districts are concentrated along major transport corridors and in recently developed areas. Industrial activities are primarily located in peripheral zones, particularly toward the south and west, where manufacturing, logistics, and port-related operations generate significant freight traffic.

The road network typology is hierarchical, comprising national highways that connect Sousse to other major Tunisian cities, urban arterial roads that distribute traffic across districts, and a dense grid of local streets that serve residential and commercial areas. Several key intersections and roundabouts act as critical nodes, often experiencing congestion during peak travel periods. The proximity of high-traffic routes to sensitive land uses, such as schools, hospitals, and recreational spaces, creates potential exposure risks, particularly in densely built environments. This spatial configuration of land use and transport infrastructure plays a central role in shaping traffic flow patterns, emission hotspots, and pollutant dispersion characteristics across the city.

III. Description of the Methodological Approach

The methodological workflow for this study was designed as a sequential yet interconnected process that integrates data acquisition, emission estimation, dispersion modeling, and empirical validation to ensure robust and reproducible results. It begins with the spatial characterization of Sousse's urban environment, mapping its land use patterns, road network typology, and meteorological context within a GIS framework. This geospatial baseline serves as the foundation for selecting monitoring sites and positioning 19 virtual receptors to represent diverse urban settings, from high-traffic arterials to mixed-use residential corridors.

Traffic activity data comprising vehicle counts, classification by type, and speed profiles, were collected during both rush and non-rush periods and processed to match the temporal resolution of meteorological datasets. These inputs were integrated into the COPERT 5 model to generate location-specific emission factors and calculate PM_{10} and $PM_{2.5}$ emission rates for each road segment. Background concentrations were also quantified to differentiate between local traffic contributions and regional or natural sources such as Saharan dust intrusions.

Air quality monitoring was conducted using portable, pre-calibrated sensors co-located with selected virtual receptors. Field protocols emphasized standardized sampling durations, humidity corrections, and routine calibration checks to maintain measurement accuracy. These ground observations formed the reference dataset for validating model outputs.

As illustrated in Figure 12, our modeling framework (Lendvai-Emmert et al., 2020) follows a two-stage process utilizing both the SIRANE and GRAL models. Initially, a macroscopic-scale simulation was carried out using SIRANE to identify pollution hotspots. This step focused on modeling general airflow patterns and $PM_{2.5}$ and PM_{10} concentrations across the entire Sousse metropolitan area, with outputs visualized via QGIS (Duarte et al., 2023). The simulation framework combined multiple datasets to accurately represent the emission and dispersion processes influencing particulate matter (PM_{10} and $PM_{2.5}$) concentrations across the urban area of Sousse.

As depicted in Figure 13 (a), the first phase of the modeling framework employed the SIRANE model in combination with COPERT, aiming to simulate pollutant emissions and dispersion processes at the macroscopic scale. This stage provided a citywide overview of pollutant transport patterns and allowed the identification of emission hotspots requiring further detailed analysis.

The workflow began with the COPERT model, which quantifies traffic-related emissions based on hourly traffic volumes, vehicle composition, and driving behavior. Within this configuration, the hourly traffic volumes acted as a critical input variable, allowing COPERT to compute particulate matter (PM) emission factors under realistic operational conditions.

The emission factors generated by COPERT were subsequently used as inputs for the SIRANE model, a Gaussian-based street-network dispersion model designed to evaluate pollutant transport and accumulation across complex urban geometries. Within SIRANE, complementary spatial and environmental inputs, such as road network geometry, building configuration data, receptor locations, meteorological conditions, and background pollution levels, were pre-processed and harmonized within QGIS.

The coupling of emission factors derived from COPERT with SIRANE's Gaussian street-network algorithm provided a meso-urban scale overview of pollutant transport and accumulation, identifying key hotspots characterized high traffic density.

In the second phase, as illustrated in Figure 13 (b), a more refined analysis was conducted using the GRAMM/GRAL V22.09 modeling system. This phase focused on the microscale simulation of air pollutant dispersion in the specific hotspot areas identified during the SIRANE assessment. The GRAMM module was employed to compute the three-dimensional, non-hydrostatic wind field, which accounts for the influences of local topography and urban morphology. Importantly, GRAMM relied primarily on meteorological data (e.g., wind speed, direction, temperature profiles) and high-resolution building geometry data to simulate the flow field and the effects of turbulence and channeling within the urban canopy. The resulting wind field provided a physically realistic representation of microscale air movement patterns influenced by terrain and structural configurations.

Subsequently, the GRAL module (Graz Lagrangian Model) utilized the wind field output from GRAMM to simulate the transport, dispersion, and concentration of emitted pollutants. GRAL employs a Lagrangian particle tracking approach, in which virtual particles represent the trajectories of pollutant masses released from road traffic and other emission sources. The model incorporated almost the same input parameters as used in SIRANE but applied them at a significantly finer spatial resolution.

To ensure representativeness and comparability, site-specific field data were collected on January 15, 2024, covering two contrasting traffic conditions: the morning rush hour (07:30–08:30) and the non-rush period (10:30–11:30). These measurements supported the calibration

and validation of GRAL simulations, ensuring that the modeled results corresponded closely with real-world observations.

The combination of both models, SIRANE for citywide screening and GRAL for detailed hotspot analysis, provided a comprehensive multiscale understanding of pollutant behavior, capturing both regional dispersion dynamics and localized concentration peaks.

Overall, this integrated modeling approach, supported by QGIS-based preprocessing and visualization, ensured spatial accuracy, consistency between model inputs, and high-resolution insight into the air quality dynamics of Sousse's urban environment.

Finally, a model–measurement reconciliation stage aligned simulation outputs with observational data in both time and space. While statistical performance metrics such as $NMSE^{1/2}$, FB were predefined, their computation and interpretation are reported in the Results chapter. This integrated framework ensures that each methodological step from spatial analysis to modeling and validation is systematically linked, enabling the study to generate policy-relevant insights into urban particulate matter dynamics.

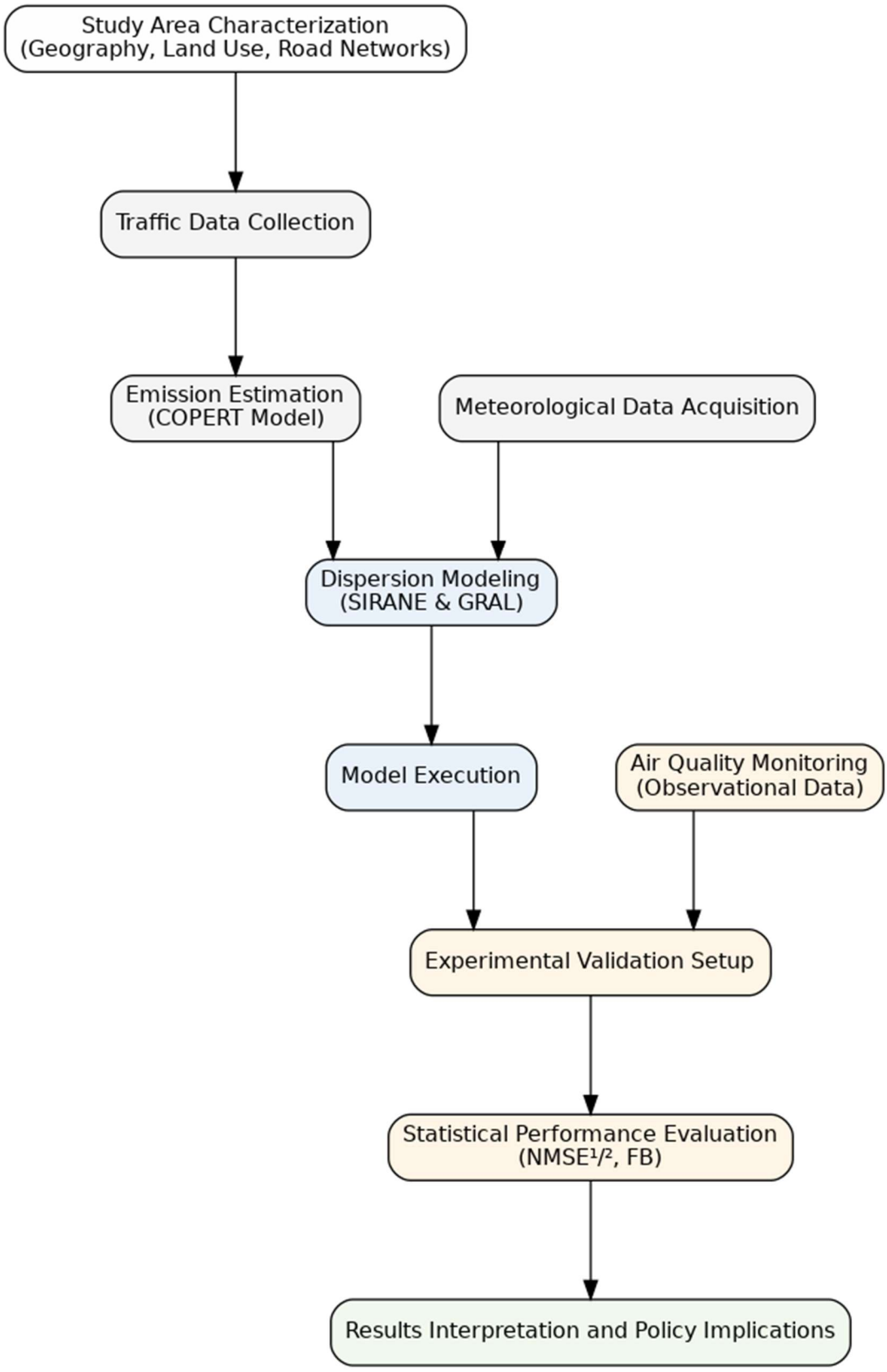

Figure 12 : Study Design and Workflow for PM_{10} and $PM_{2.5}$ Emission, Dispersion, and Validation

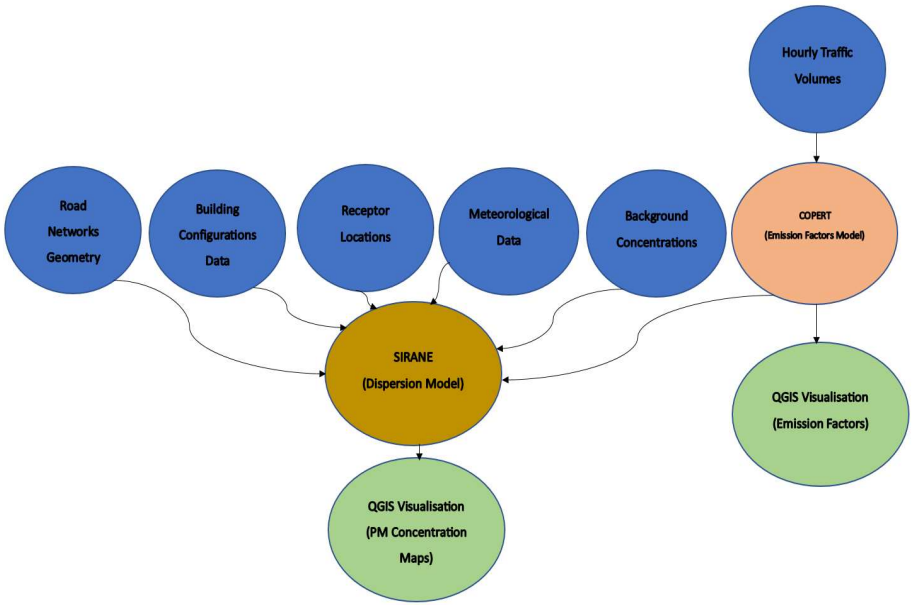

(a)

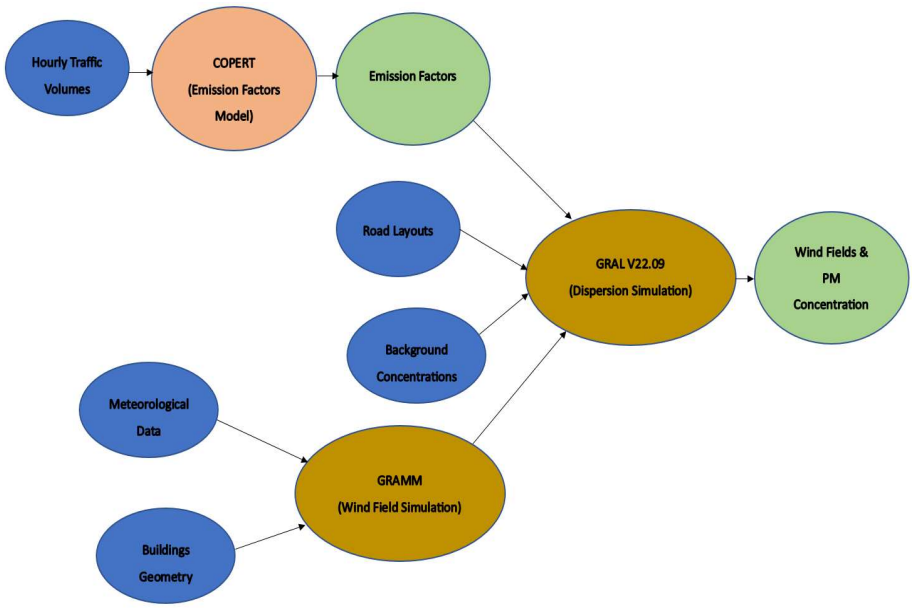

(b)

Figure 13 : Overall structure of (a) the SIRANE model and (b) the GRAMM/GRAL model

IV. Air Quality Monitoring and Virtual Receptors Deployment

Air quality monitoring in this study was conducted through a combination of ground-based field measurements and model-based virtual receptor placement to achieve a high-resolution spatial characterization of PM_{10} and $PM_{2.5}$ concentrations across the urban area of Sousse. A total of 19 virtual receptors were strategically positioned within the SIRANE modeling framework, selected based on traffic density maps, land use typologies, and proximity to sensitive land uses

such as residential neighborhoods, healthcare facilities, and schools. The deployment aimed to capture pollutant gradients across diverse microenvironments, including high-traffic intersections, commercial corridors, and mixed-use districts.

Field monitoring campaigns were conducted using portable, high-accuracy particulate matter sensors capable of measuring PM_{10} and $PM_{2.5}$ in real time. These sensors were specifically used to capture both background PM concentrations and total particulate levels during peak and off-peak periods at the three selected hotspots. The collected sensor data were then compared with outputs from virtual receptors located at the same hotspots within the GRAL modeling framework, enabling cross-verification of spatial pollution distributions and ensuring that the modeled outputs closely aligned with actual field observations.

IV-1. Design and placement of 19 virtual receptors

The deployment of the 19 virtual receptors was guided by a spatially representative strategy aimed at capturing the heterogeneity of traffic-related particulate matter concentrations within Sousse's urban environment. Receptor locations were determined through a combination of GIS-based spatial analysis, traffic flow mapping, and land use classification, with priority given to areas of high population density, significant traffic activity, and proximity to sensitive receptors such as residential districts, commercial hubs, schools, and healthcare facilities. The road network typology, including primary arterials, secondary roads, and local streets—was used to ensure balanced representation across different traffic intensities and street configurations.

Each receptor was assigned precise geographic coordinates in UTM projection to ensure compatibility with both SIRANE and GRAL dispersion models, and placement height was standardized at approximately 3 m above ground level to reflect the average breathing zone while minimizing ground-level turbulence effects. In locations where built morphology was expected to influence pollutant dispersion, such as semi-enclosed streets, open intersections, or roadside open spaces, receptors were positioned to capture both upwind and downwind variations.

Several virtual receptor positions corresponded to field measurement points during both peak and off-peak hours, enabling direct comparison for model calibration and validation. Figure 9 (a) illustrates the spatial distribution of the 19 virtual receptor locations across the study area and (b) the specific field measurement sites used for validation, highlighting the integration

between modeled and observed datasets for improved spatial and temporal resolution in air quality assessment.

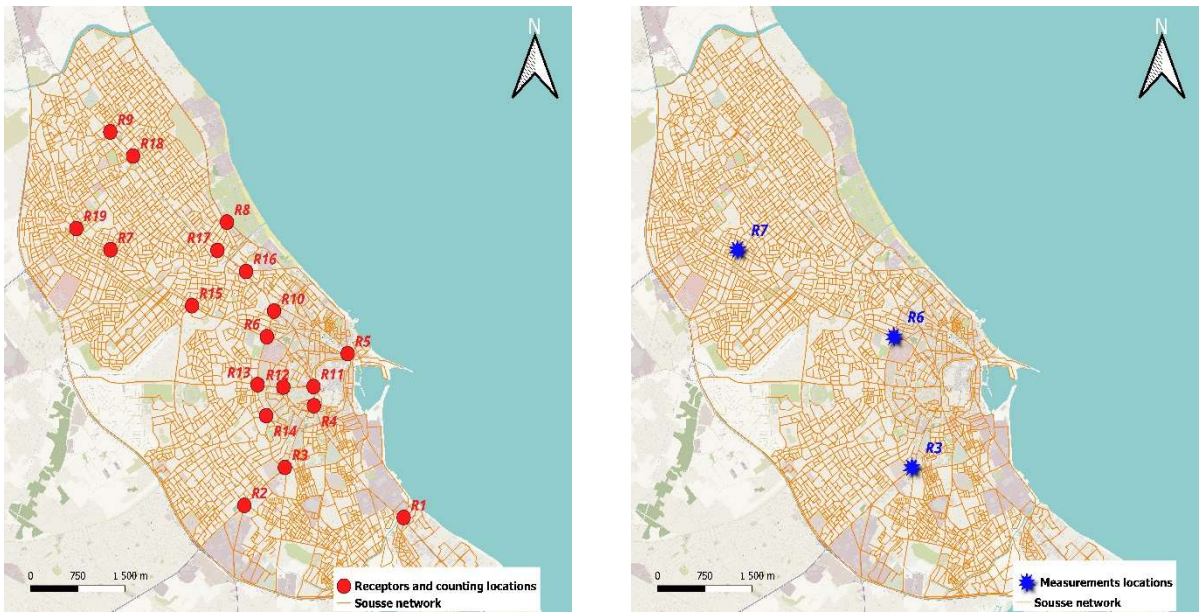

(a) (b)

Figure 14 : (a) Receptor's location and (b) measurements sites

IV-2. Temporal Monitoring Strategy and Sensor Deployment Scheduling

The temporal resolution of monitoring in this study was specifically structured to capture the variability in particulate matter concentrations resulting from changes in traffic intensity over the course of the day. Two main traffic-related conditions were targeted: peak traffic periods, characterized by high vehicle density, frequent acceleration and deceleration, and congestion-driven stop-and-go movement; and off-peak periods, defined by smoother, free-flowing traffic with significantly reduced emissions. This differentiation enables a more precise analysis of the diurnal variation of PM_{10} and $PM_{2.5}$ concentrations and their direct relationship with urban mobility patterns.

These two periods—peak and off-peak hours—were also essential for determining the optimal timing for sensor installation and measurement campaigns, ensuring that the captured data reflected the full contrast between peak congestion and baseline atmospheric conditions. For each receptor location, particulate measurements were conducted in continuous or short-interval modes, ensuring high temporal granularity. Data acquisition was synchronized with meteorological monitoring, including wind speed, wind direction, temperature, and atmospheric stability class, as these factors critically influence dispersion processes and the persistence of pollutants in the urban atmosphere.

As shown in Figure 11, the traffic flow profiles for five major roads in Sousse reveal a pronounced morning peak between approximately 07:30 and 08:30, corresponding to daily commuting activity and the opening of commercial establishments. A secondary lower-intensity peak was also observed in the late afternoon, associated with post-work traffic. By contrast, non-rush periods, characterized by relatively stable and low traffic volumes, were identified between 10:30 and 11:30, offering representative baseline conditions for air quality assessment.

Integrating these traffic flow patterns with synchronous air quality and meteorological measurements allows for robust calibration and validation of dispersion models, while also providing valuable insight into short-term population exposure during both typical and elevated pollution episodes.

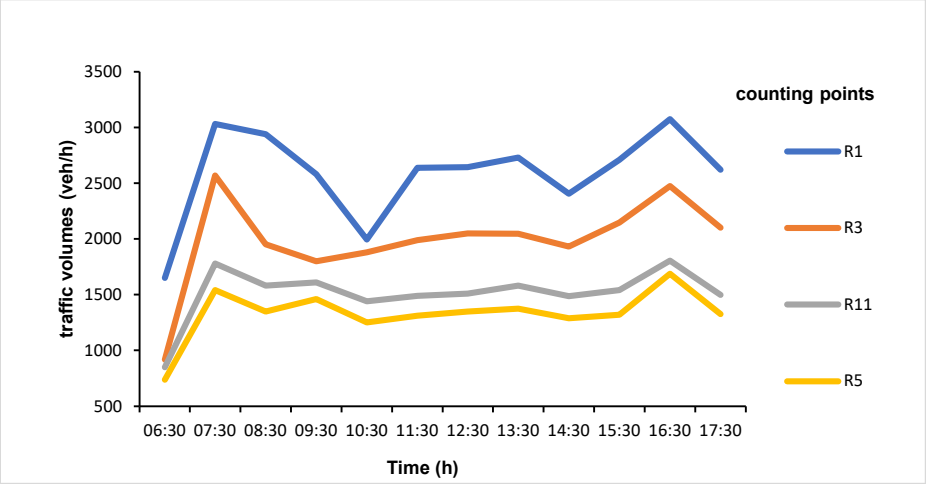

Figure 15 : Traffic volumes of certain key roadways (November 07, 2023)

V. Atmospheric Dispersion Modeling

The atmospheric dispersion modeling component of this study was designed to simulate the spatial and temporal distribution of PM_{10} and $PM_{2.5}$ within the urban environment of Sousse under realistic meteorological and traffic conditions. A multi-scale approach was adopted, combining the street-scale capabilities of the SIRANE model with the microscale, building-resolving resolution of the GRAL model.

SIRANE was used to provide citywide dispersion estimates based on an emission inventory generated through COPERT 5, allowing for the assessment of pollutant transport across the urban canopy without explicit 3D building effects.

GRAL was then applied to selected hotspot areas to incorporate detailed urban morphology, including building geometry, street canyon configurations, and turbulence patterns, enabling a refined simulation of localized pollutant accumulation and dispersion.

Model inputs included high-resolution traffic emissions data, hourly meteorological parameters, terrain elevation grids, and land-use datasets. The integration of these datasets within the modeling framework allowed for a comprehensive representation of pollutant dispersion dynamics, while subsequent calibration with field measurements ensured the reliability of predictions for both large-scale and microscale scenarios.

V-1. Models Selection

The selection of dispersion models for this study was guided by the need to address both meso-urban and microscale pollutant dynamics in the complex urban environment of Sousse. A dual-model strategy was adopted to leverage the complementary strengths of SIRANE and GRAL.

SIRANE was selected for its efficiency in simulating pollutant dispersion at the street-network scale, using a Gaussian-type street-canyon approach that can integrate traffic emissions, meteorological inputs, and street geometry in a computationally efficient manner. This made it well suited for producing citywide concentration fields based on the emission inventory generated via COPERT 5.

GRAL, on the other hand, was chosen for its capability to resolve microscale flow and dispersion patterns in areas with complex building geometries. Its Lagrangian particle tracking approach, combined with the diagnostic wind field module GRAMM, enables the explicit simulation of turbulence, wind–building interactions, and pollutant accumulation in street canyons—processes that are critical for identifying localized hotspots.

The combination of these two models ensured that the methodology captured both broad spatial patterns and localized effects, thereby improving the robustness and applicability of the results for urban air quality management.

V-2. COPERT Model

V-2-1. Description and Application

In this study, road-traffic emissions were quantified using the COPERT 5 (Computer Programme to Calculate Emissions from Road Transport) model, developed under the European Environment Agency (EEA) framework. The theoretical background and emission-

factor development principles of COPERT are presented in Chapter 1 (Section VII-2); this section therefore focuses exclusively on its practical implementation for the Sousse case study.

The model estimates pollutant emission factors (g km^{-1}) for each vehicle category as a function of fuel type, Euro standard, and average speed. Both cold-start and hot-running emissions were taken into account in the emission factor calculations using the COPERT model. This decision is justified by the advanced age of Tunisia's vehicle fleet, which lacks modern after-treatment technologies, making cold-start emissions, particularly hydrocarbons (HC) and carbon monoxide (CO)—a significant contributor, especially during winter morning rush hours. For instance, temperatures around 10 °C at 7:30 a.m. (e.g., January 15, 2024) can substantially increase cold-start emissions, which are also known precursors to secondary PM formation. Including both phases provides a more accurate representation of real-world urban emissions.

Using locally measured traffic flows and speed profiles, COPERT 5 generated hourly PM_{10} and $PM_{2.5}$ emission inventories for the main road network of Sousse. Terrain effects were neglected (flat-road assumption) to isolate traffic-activity influences. The outputs were exported in structured tabular format and directly coupled with the SIRANE and GRAL dispersion models used in subsequent simulations.

COPERT 5 was chosen for its regularly updated emission-factor database, compatibility with large traffic datasets, and alignment with European methodologies. Other models—such as HBEFA, MOVES, EMEP/EEA, or CIRCUL'AIR (ASPA; Strasbourg 2005); can serve specific regional applications, but COPERT 5 ensures methodological consistency with the Tunisian vehicle-fleet characteristics and available data. Its integration with high-resolution dispersion modeling therefore provides a robust basis for quantifying and managing transport-related emissions in urban areas.

V-2-2. Mathematics Formulations

Traffic emissions were estimated using COPERT, a standard methodology developed for European conditions. COPERT computes pollutant emissions based on vehicle activity data and category-specific emission factors.

The emission factors for $PM_{2.5}$ and PM_{10} particles were calculated using the COPERT 5 software package according to the formula (II.1).

$$EF_{i,j,k,l} = EF_{H,i,j,k,l} + EF_{T,i} + EF_{B,i} + EF_{R,i} \quad \text{(II.1)}$$

Where $EF_{i,j,k,l}$ denotes PM overall emission factor (g/km.veh); $EF_{H,i,j,k,l}$: emission factor for PM under high-temperature conditions (g/km.veh); $EF_{T,i}$: emission factor from tire-related sources (g/km.veh); $EF_{B,i}$: PM emission factor from brake systems (g/km.veh); $EF_{R,i}$: the emission factor of PM from road surface abrasion (g/km.veh).

The average particulate matter emission factor, EF_m (g/km.veh), was expressed for a heterogeneous vehicle fleet as follows:

$$EF_m = \sum_{i,j,k,l}\left(p_{i,j,k,l} \cdot EF_{i,j,k,l}\right) \quad \text{(II.2)}$$

Where, $p_{i,j,k,l}$ denotes the share of vehicles belonging to category i, complying with emission standard j, using fuel type k and having an engine cylinder or a maximum permissible laden weight l.

The emission rate of each road $\dot{m}_r(\ kg/h/km)$, considered as a linear emission source, was then:

$$\dot{m}_r = \frac{EF_m Q_r}{1000} \quad \text{(II.3)}$$

V-3. SIRANE Model

V-3-1. Description and Application

The SIRANE model was used to simulate the dispersion of traffic-related particulate matter (PM_{10} and $PM_{2.5}$) within the Sousse urban domain.

It represents the urban environment as a network of interconnected street segments, each treated as an emission line source, and computes pollutant exchanges between street canyons and the overlying atmosphere based on local meteorological and traffic conditions.

SIRANE was configured using COPERT 5 emission outputs as input sources, combined with hourly meteorological data—wind speed, wind direction, and stability class—provided by the National Meteorological Institute (Infoclimat.fr).

The street network was digitized in a GIS environment to ensure accurate spatial representation of roads, intersections, and receptor locations.

To ensure methodological robustness, a sensitivity analysis on grid resolution was carried out prior to the main simulation runs. The SIRANE model was configured with a series of grid refinements ranging from coarse meshes (5 × 6.05 m cells) to very fine meshes (2.5 × 3.02 m cells), with mesh dimensions increasing correspondingly up to 4000 × 4000 cells. For each

tested configuration, predicted concentrations of PM_{10} and $PM_{2.5}$ were compared across representative receptor points within the study domain. This step enabled the assessment of whether increasing grid refinement materially altered pollutant concentration fields or whether results stabilized, indicating grid independence.

The comparative results, summarized in Table 5, showed that deviations in simulated concentrations decreased progressively as the grid resolution increased. Once the cell size reached 2.5 × 3.02 m, variations between successive refinements fell below 0.5% (0.16% for PM_{10} and 0.41% for $PM_{2.5}$). Such small deviations demonstrate that the model had effectively reached a point of numerical stability, where additional grid refinement no longer produced significant changes in outcomes.

Table 5 : sensitivity to spatial resolution

		PM_{10}		**$PM_{2.5}$**	
Nx×Ny	**Δx×Δy**	**Maximum concentration**	**Relative deviations**	**Maximum concentration**	**Relative deviations**
2000×2000	5×6.05	43,851135	10,84%	25,2077	25,17%
2500×2500	4×4.84	48,508663	9,60%	28,678274	12,10%
3000×3000	3.3×4.03	50,338062	3,63%	30,039528	4,53%
3500×3500	2.85×3.45	48,75759	3,24%	28,804363	4,27%
4000×4000	2.5×3.02	48,836407	0,16%	28,921619	0,41%

Based on these findings, the 2.5 × 3.02 m resolution was adopted as the optimal configuration for subsequent simulations. This resolution provided a fine enough representation to capture microscale dispersion phenomena, such as localized pollutant build-up in densely built urban corridors, while avoiding unnecessary computational overhead. The methodological decision to select this resolution ensures a balance between accuracy, efficiency, and reproducibility, providing a reliable foundation for subsequent modeling and validation stages.

V-3-2. Mathematics Formulations

The SIRANE model, a specialized tool for urban air pollution analysis, was employed for dispersion modeling. This model uses parametric relationships to simulate how pollutants disperse within the urban boundary layer and build environments. It combines a Gaussian plume model for open areas with a street-network model to accurately represent road traffic emissions within the urban canopy.

- **Street Canyon Concentration Model**

In a street canyon, pollutant dispersion is restricted by the surrounding buildings, leading to a confined space where turbulence is intensified. The SIRANE model adopts a box model approach to calculate the average concentration within the street, simulating flow in the upper boundary layer based on the Monin-Obukhov similarity theory (Stiperski & Calaf, 2023). It treats urban areas as a network of interconnected street canyon segments. The model calculates two types of concentrations: spatially averaged concentrations within each street segment (C_{street}) and external flow concentrations (C_{ext}), while accounting for three primary mechanisms: turbulent transfer across the street boundary layer interface, advective fluxes along the street axes, and turbulent fluxes at street intersections, all of which are critical for understanding pollution behavior under the urban canopy. A basic concentration gradient method is used to model the turbulent flux at the street-boundary layer interface, as described by (Salizzoni et al., 2009):

$$Q_{H,turb} = U_d WL(C_{street} - C_{ext}) \tag{II.4}$$

where W denotes the roadway width and L the length accordingly, and U_d was defined as a mixing or transfer velocity identified as:

$$u_d = \frac{\sigma_w}{\sqrt{2\pi}} \tag{II.5}$$

σ_w was the vertical component of the turbulent velocity's standard deviation at street canyon intersections. Flow and pollution exchanges arise from the advection of pollutants along streets feeding into an intersection and their subsequent redistribution among the downwind streets.

The mean advective flow ($\bar{u}$) of pollutants at the downwind region of a street segment was calculated as follows:

$$\bar{u} = C_{street} U_{street} HW \tag{II.6}$$

The street's time- and space-averaged concentration was C_{street}; the time and space averaged wind velocity was U_{street}; the street height and breadth were H and W, respectively.

- **Gaussian Plume Model for Open Areas**

Outside the street canyon, contaminants are dispersed in an open atmosphere following a Gaussian plume formulation (Soulhac et al., 2001).

$$C(x,y,z) = \frac{Q}{\pi U \sigma_y \sigma_z} exp\ (-\frac{y^2}{2{\sigma_y}^2})[exp\ exp\ \left(-\frac{(Z-Hs)^2}{2{\sigma_Z}^2}\right) + exp\ exp\ \left(-\frac{(Z+Hs)^2}{2{\sigma_Z}^2}\right)] \tag{II.7}$$

σ_y and σ_z are the horizontal and vertical dispersion coefficients (m); H_s is the height of emission (m); (x,y,z) are spatial coordinates (m); U is the wind speed at emission height (m/s).

V-4. GRAL Model

V-4-1. Description and Application

The GRAL is a high-resolution microscale atmospheric dispersion model designed to simulate pollutant transport in urban environments with complex geometries. Unlike meso-urban Gaussian-based models such as SIRANE, which rely on simplified representations of airflow, GRAL employs a Lagrangian particle tracking approach driven by three-dimensional wind fields generated by its companion module, GRAMM (Graz Mesoscale Model). This modeling system explicitly accounts for the influence of buildings, street canyons, terrain irregularities, and surface roughness, allowing it to resolve detailed flow structures such as recirculation zones, leeward accumulation pockets, and localized stagnation areas, phenomena that strongly shape pollutant dispersion in dense urban settings.

In this study, GRAL was applied to simulate PM_{10} and $PM_{2.5}$ dispersion in the three identified hotspots of Sousse, serving as a microscale complement to the broader SIRANE simulations. Its high spatial resolution (meter-scale) enabled precise characterization of pedestrian-level exposure and revealed the fine-scale interactions between traffic emissions, local wind dynamics, and urban morphology. The GRAMM/GRAL system proved particularly effective for diagnosing pollution behavior in narrow or poorly ventilated corridors—critical information for designing targeted mitigation and urban planning strategies.

Therefore, GRAMM/GRAL remains one of the most advanced and reliable tools for urban air quality modeling. Its ability to represent microscale flow phenomena provides insights that cannot be achieved with traditional Gaussian models alone. In this research, GRAL's detailed treatment of geometry and turbulence significantly strengthened the assessment of pollution hotspots in Sousse and reinforced the robustness of the integrated emission–dispersion modeling framework.

V-4-2. Mathematics Formulations

The GRAL model is based on lagrangian particle dispersion, which was used to assess atmospheric pollution dispersion, forecasting particle dispersion in urban settings by combining a lagrangian method with a microscale flow field model, to obtain concentrations of pollutants considered in the study ($PM_{2.5}$ and PM_{10}).

Lagrangian models were fundamentally based on tracking many imaginary particles following paths inside a 3D wind field (Oettl, 2015). Combining a typical K-E turbulence model with the Reynolds-averaged Navier-Stokes equations, the microscale wind field model computes airflow around barriers as described below (Kajishima & Taira, 2017):

$$\left| \frac{\partial \bar{u}_i}{\partial x_i} = 0 \quad \frac{\partial \bar{u}_i}{\partial t} + \bar{u}_j \frac{\partial \bar{u}_i}{\partial x_j} = -\frac{1}{\rho}\frac{\partial \bar{p}}{\partial x_i} + \frac{\partial}{\partial x_j}\left[\mu_t\left(\frac{\partial \bar{u}_i}{\partial x_j} + \frac{\partial \bar{u}_j}{\partial x_i}\right) - \frac{2}{3}\delta_{ij}k\right] \right. \tag{II.8}$$

where $\bar{u}_i (i = 1,2,3)$ displayed the components of the mean wind speed, ρ the density of air, $\underline{p}$ stands for the mean pressure, μ_t was the turbulent viscosity and k indicated the turbulent kinetic energy. The associated turbulence model was the $K - E$ model as detailed below (Savicki et al., 2021):

$$\left| \frac{\partial k}{\partial t} + \frac{\partial(\bar{u}_j k)}{\partial x_j} = \frac{\partial}{\partial x_j}\left(\mu_t \frac{\partial k}{\partial x_j}\right) + P_m + P_b - E \quad \frac{\partial E}{\partial t} + \frac{\partial(\bar{u}_j \mathrm{E})}{\partial x_j} \right. \tag{II.9}$$
$$= \frac{\partial}{\partial x_j}\left(\mu_t \frac{\partial E}{\partial x_j}\right) + \frac{E}{k}(1.44(P_m + P_b) - 1.92E$$

Whereas E signified the dissipation rate of turbulent kinetic energy, P_m and P_b reflected the production terms for turbulent kinetic energy originating from shear stresses and buoyancy, respectively. The primary function of lagrangian models was to trace the motions of particles in three-dimensional flows. Based on this approach, the concentration of particles in the volume dV=dx1.dx2.dx3 was given as (Barone et al., 2023):

$$C = \sum_{i=1}^{R}\left(\frac{m_{p,i}}{dvt_a}dt\right) \tag{II.10}$$

$m_{p,i}$ represented the mass of a particle, R was the total number of integration steps, and t_a was the time used to calculate the average concentration.

V-5. Geographic Information Systems for Spatial Data Processing and Analysis

Geographic Information Systems (GIS) played a central role in this study by integrating, managing, and visualizing spatial datasets required for emission modeling, dispersion simulations, and validation. The main advantage of using GIS lies in its ability to handle heterogeneous geospatial information including road networks, land use classifications, receptor coordinates, and meteorological grids, within a unified and consistent spatial framework. This integration ensures that all spatial inputs align precisely with the computational domains of the SIRANE and GRAL models, minimizing georeferencing errors and improving the accuracy of spatial interpolation between emission sources and receptors.

From an analytical perspective, GIS provides several key benefits. First, it enables fine-scale spatial segmentation of urban road networks, allowing roads to be represented as discrete emission line sources with attributes such as traffic density, speed, and fleet composition. This is particularly useful in urban dispersion modeling, where pollutant concentration gradients are strongly influenced by local geometry and traffic flow variability. Second, GIS enhances visual interpretation and communication of model outputs, producing maps of PM_{10} and $PM_{2.5}$ concentration fields that reveal spatial trends, hotspots, and the interaction between built morphology and dispersion patterns. These spatial visualizations are invaluable for planners and policymakers in identifying priority intervention zones.

Furthermore, GIS was instrumental in post-processing and validation, allowing the overlay of modeled concentration fields with field measurement locations. This made it possible to extract modeled values directly at receptor points, thereby streamlining statistical validation using indices such as the Fractional Bias (FB) and Normalized Mean Square Error (NMSE).

However, several limitations accompany the use of GIS in this context. The accuracy of GIS-based modeling is highly dependent on the quality, completeness, and resolution of spatial data. In developing contexts such as Tunisia, urban GIS datasets—especially those related to dynamic traffic volumes or building geometries—may be outdated or incomplete, which can introduce uncertainty into emission estimates and dispersion simulations. Another limitation is that GIS, by itself, is primarily a static spatial tool; it does not simulate temporal variability or dynamic meteorological interactions. Therefore, GIS must be integrated with physically based models like GRAL or SIRANE to capture time-dependent processes such as wind field changes and diurnal traffic fluctuations.

Overall, GIS offers major advantages in spatial data integration, visualization, and model validation. However, its limitations notably the absence of temporal dynamics and reliance on high-quality input data, require its integration with physically based atmospheric models to capture real-world variability. In this study, GIS contributed at every stage of the workflow, from data preparation to post-model analysis, ensuring a coherent spatial representation of the Sousse urban environment and strengthening the reliability of simulation results from both the SIRANE and GRAL models.

V-6. Input Data

The preparation of input data for the SIRANE and GRAL models involved the integration of multiple datasets to ensure reliable simulation of pollutant dispersion. Traffic activity data,

including vehicle counts, fleet composition, and temporal distribution, were processed to generate line-source emissions using COPERT-derived factors. Meteorological inputs such as wind speed, wind direction, temperature, and atmospheric stability were collected from local monitoring stations and formatted for compatibility with both models. For GRAL, additional high-resolution urban morphology data, including building geometry and land use layers, were incorporated to resolve microscale airflow patterns, while SIRANE relied on aggregated street-scale representations.

V-6-1. Road Network Architecture

The open-source software QGIS was utilized to generate the road network file required for the SIRANE model (Duarte et al., 2023). This file contains detailed information on the spatial layout and geometry of the roads, such as road width (W) and the position and characteristics of surrounding buildings, particularly their height (H). These data were essential for classifying roads topographically, distinguishing between open terrain ($W/H > 3$) and street canyon environments ($W/H \leq 3$). Figure 14 illustrates the citywide road network, including 19 virtual receptors and traffic count stations (marked as red points), as well as the locations of PM_{10} and $PM_{2.5}$ sensors (blue stars).

Each road was subdivided into sections based on factors like the number of lanes, speed limits, and the presence or absence of traffic control devices such as stop signs, traffic lights, or intersections. In total, 829 road sections were identified, with lengths varying from 3 meters to 3.1 kilometers. For computational purposes, QGIS further segmented these into 5,778 smaller linear elements, with their lengths measured directly in the software. Among these, 1,472 segments were classified as open street types.

Data collection focused on 332 sections located within traffic counting zones, primarily covering major arteries that connect Sousse to neighboring regions and key institutions. In contrast, lower-capacity values were assigned to sections representing less-traveled rural roads or bypass routes, which are often preferred by residents or travelers avoiding highway tolls or seeking scenic alternatives.

For the GRAL model, the building layouts and road networks within each hotspot area were extracted from Google Earth (https://earth.google.com). This allowed for precise identification of road segments where traffic activity could be a significant source of pollutant emissions. The data gathered included details such as lane counts, widths, lengths, building footprints, heights, and names, all represented by graphic polygons.

Table 6 summarizes the parameters for the selected hotspots, which cover areas of 830 x 1370 m², 660 x 1059 m², and 829 x 1291 m² in zones 1, 2, and 3, respectively. The average elevation above sea level for these locations is approximately 31 meters in areas 1 and 3, and 26 meters in area 2.

Table 6 : Some parameters of the hotspot areas

Parameters	**Area 1**	**Area 2**	**Area 3**
Latitude	35°48'49"N	35°49'52"N	35°50'33"N
Longitude	10°37'45"E	10°37'34"E	10°35'55"E
Elevation (above sea level)	31 m	26 m	31 m
Domain dimensions	830 x 1370 m²	660 x 1059 m²	829 x 1291 m²
Building heights	3-35 m	3-35 m	3-35 m
Road widths	3.5-20 m	3.5-20 m	3.5-20 m
Building coverage ratio (BCR)	40%	40%	40%

V-6-2. Emission Factor and Traffic Volumes

We utilized the COPERT V methodology to calculate pollutant emissions (Horváth and Szemesová, 2023). The COPERT models, which rely on the carbon balance method, determine unit emission factors (measured in grams of pollutants per kilometer) for each vehicle category. These calculations consider several factors, including the distribution of vehicle types (percentage of trucks, buses, and cars), the fuel type used (petrol, diesel, Liquefied Petroleum Gas (LPG), or Compressed Natural Gas (CNG)), the vehicle's compliance with anti-pollution standards (Euro 1 through Euro 7), engine capacity or authorized weight for heavy vehicles, road infrastructure (such as slope and traffic conditions), vehicle speed, and the cold-start rate of vehicles.

i. Fleet composition

The Tunisian vehicle fleet was 72% private cars with 74% gasoline, 25.6% diesel, and 0.4% LPG, 1% trucks and vans with 2.94% gasoline and 97.05% diesel, 1% buses with 100% diesel,

1% motorcycles with 100% gasoline. The mean age of vehicles was 10-15 years (ANME, 2016). The fleet composition data is necessary for GRAL and SIRANE models.

ii. Traffic data

To meet the requirements of the SIRANE model, we concentrated on measuring traffic volumes during both morning peak and off-peak hours at specified traffic counting points (figure 14.a). These measurements indicated that the highest and lowest hourly traffic volumes recorded as 4,425 and 80, and 2,570 and 20, respectively. In this context, figure 15 illustrates the fluctuations in traffic flow along four key roads—R1, R3, R11, and R5—over a 12-hour span. On average, the data confirmed that peak traffic occurred between 7:30 and 8:30 AM, while off-peak traffic was observed between 10:30 and 11:30 AM. Additionally, the analysis showed a notable decline in traffic volume, with a reduction exceeding 40% between peak and off-peak periods.

For the GRAL model, manual traffic counts were conducted at three designated sites (Area 1, Area 2, and Area 3), all located along major urban roadways.

At Area 1, rush-hour volumes ranged between 160 and 4,380 vehicles per hour, while at Area 2 and Area 3, counts varied from 120 to 2,720 and 65 to 2,015 vehicles per hour, respectively. During non-rush periods, traffic volumes dropped markedly, ranging from 75 to 2,120 vehicles per hour at Area 1, 55 to 1,310 at Area 2, and 30 to 920 at Area 3, corresponding to a reduction of more than 50% compared to peak values. These traffic data were subsequently processed through the COPERT 5 model to estimate emission rates of PM_{10} and $PM_{2.5}$, which were then used as inputs for GRAL simulations.

V-6-3. Meteorological Data

Meteorological data played a key role in ensuring the reliability and accuracy of the dispersion simulations across both modeling phases. For the SIRANE simulations, weather data were retrieved from the Infoclimat Association website (Infoclimat, 2023), including wind speed and direction, temperature, cloud cover, and precipitation.

During both peak and non-peak periods, precipitation and cloud cover were recorded at 0 mm and 0/8 oktas, respectively. The mean temperatures were 19.1 °C during rush hour and 23.6 °C during non-rush hour, with relative humidity levels of 74% and 49%, respectively. Wind conditions during the rush hour were recorded at 360° with a speed of 2.5 m/s, shifting to 340° at 4.7 m/s during non-peak hours. These conditions were suitable for conducting a macro-scale

simulation to assess air quality and identify pollution hotspots across the entire study area using the SIRANE model.

After identifying the pollution hotspots, GRAL simulations were performed to model pollutant dispersion at a finer spatial resolution. This phase relied on the associated meteorological data, with the corresponding parameters presented in Table 7.

Table 7 : Meteorological conditions at the three hotspot locations for GRAL/GRAMM simulations

Parameters	**Hotspot Locations** (15/01/2024)	
	Rush hour	Non-rush
Wind velocity	4,1 m/s	2.2 m/s
Wind direction	240°	190°
Temperature	10 °C	15,9 °C
Atmospheric pressure	1012,2 hPa	1013,1 hPa
Relative humidity	68 %	47 %
Cloud cover	0/8 oktas	0/8 oktas
Precipitation	0 mm	0 mm
stability class	B	B

V-6-4. Background Concentrations

Assuming no contribution from pollutant emissions outside the study boundaries, both the SIRANE and GRAL models calculate air pollutant concentrations exclusively from emission sources located within the modeled domain. This modeling assumption makes it essential to explicitly include background pollution, since omitting it would underestimate total exposure.

For the SIRANE model, background concentrations were incorporated as uniform hourly values, set at approximately 15 µg/m³ for PM_{10} and 7.5 µg/m³ for $PM_{2.5}$. These values, adopted from earlier studies (Kaminski et al., 2013; Su et al., 2013), provide a pragmatic approximation given the large spatial extent of the Sousse region and the limited availability of continuous monitoring data. In practice, SIRANE applies the same background levels across the entire

study area. While this approach simplifies computation and ensures consistency, it does not reflect small-scale variations in background pollution that can arise from differences in meteorological conditions, local land use, or nearby sources not explicitly modeled.

By contrast, the GRAL model relied on real-time, site-specific background measurements to capture more dynamic and localized conditions. During traffic-counting campaigns, PM_{10} and $PM_{2.5}$ were monitored using sensors positioned about 300 meters from each hotspot at a height of 2 meters. This setup reduced direct interference from immediate traffic emissions while still characterizing the local urban background. The results revealed marked spatial and temporal differences:

- **PM_{10}**: During rush hours, background levels reached 61, 40, and 19 μg/m³ in Areas 1, 2, and 3, respectively, decreasing to 42, 20, and 9 μg/m³ in non-rush periods.
- **$PM_{2.5}$**: Corresponding values were 35, 21, and 11 μg/m³ during rush hours, falling to 20, 9, and 5 μg/m³ during off-peak times.

In the SIRANE model, a uniform background concentration of 15 μg/m³ for PM_{10} was applied consistently across the simulation domain. In contrast, the GRAL model relied on real-time measurement data, which produced variable background concentrations reaching as high as 61 μg/m³. This methodological divergence is critical, as the background level directly affects pollutant concentration estimates and overall model outputs. The significantly elevated background observed in GRAL suggests the influence of regional-scale pollution sources, potentially including Saharan dust intrusions, which are common in Tunisia, particularly during autumn and winter. Although Chapter 1 acknowledges the relevance of such events, the two dates selected for simulation—November 7, 2023, and January 15, 2024—must be specifically assessed for dust transport episodes. If confirmed, such events would explain the elevated background values and indicate that a considerable portion of the measured PM_{10} may originate from long-range atmospheric transport rather than local traffic emissions. This distinction is essential to ensure accurate source attribution and avoid overestimating the impact of vehicular activity. The variability and uncertainty associated with background values underscore the need for further refinement. Future work will focus on integrating satellite-based aerosol data and meteorological diagnostics to verify dust episodes and improve spatial and temporal calibration of background concentrations, thus enhancing the consistency between meso-scale and micro-scale dispersion models.

These observations highlight two important points. First, background pollution is highly variable, fluctuating with traffic activity, time of day, and local dispersion conditions. Second, the contrast between SIRANE's static assumptions and GRAL's dynamic measurements illustrates the implications of background treatment in exposure assessment. While SIRANE offers a practical, large-scale estimate suitable for regional urban planning, GRAL provides a more detailed representation of near-road and hotspot dynamics—critical for health impact evaluations and traffic-related air quality management.

VI. Experimental Framework

VI-1. Experimental Setup

The experimental validation setup was designed to ensure that field measurements accurately represented the atmospheric and traffic conditions simulated in the dispersion models. Validation sites were selected based on multiple criteria, emphasizing their proximity to major traffic corridors, where vehicular emissions are the dominant source of particulate pollution—and their location within densely populated areas where exposure risks are elevated. To enable direct comparison with modeled outputs, these monitoring locations were intentionally matched with receptor points defined in the SIRANE and GRAL modeling frameworks, particularly within the three identified pollution hotspots.

The selected monitoring points reflect the diverse urban typologies of Sousse, ranging from high-intensity arterial roads to mixed-use environments combining residential, commercial, and institutional functions. This diversity ensured that the validation framework captured the variability in emission levels and dispersion conditions arising from differences in road geometry, building configuration, and local microclimates. Sites situated immediately adjacent to non-traffic emission sources such as construction zones or industrial activities were deliberately avoided to prevent contamination of the measurements and ensure that recorded concentrations predominantly reflected traffic-related contributions.

The monitoring campaign was scheduled to capture the diurnal dynamics of particulate pollution by conducting measurements during both rush-hour periods, characterized by congestion and increased emission intensity—and non-rush-hour periods with lighter traffic flow. Aligning the field measurements with the temporal windows used in the model simulations ensured coherence and comparability between observed and simulated datasets. Additionally, background concentrations were measured at each hotspot to differentiate regional background pollution from locally generated traffic emissions. This combined

approach strengthened the reliability of the validation process by enabling a rigorous assessment of the models under varying emission and meteorological conditions.

VI-2. Experimental Protocol

The experimental protocol was designed to provide reliable field data for validating GRAL model outputs and for determining the background concentrations required as input to the dispersion simulations. The measurement campaign was conducted on 15 January 2024, selected as a representative winter day marked by stable meteorological conditions and sustained traffic activity across Sousse, ensuring that the collected data reflected typical urban pollution dynamics.

Particulate matter levels were measured using a Modbus-based $PM_{2.5}/PM_{10}$ air quality sensor, a widely adopted device in urban air pollution studies. The instrument operates on the laser scattering principle, which enables real-time detection of airborne particles by quantifying light scattered as they pass through a laser beam. Its technical specifications include a measurement range of 0–1000 $\mu g/m^3$ and a resolution of 1 $\mu g/m^3$, ensuring sufficient sensitivity for detecting short-term fluctuations in both coarse (PM_{10}) and fine ($PM_{2.5}$) particulate fractions. The sensor is also equipped with a highly sensitive gas detection unit, allowing it to function in a wide range of monitoring environments, from roadside corridors to residential and commercial areas.

For field deployment, the devices were installed at a height of 2 meters above ground level (approximating the breathing zone) and positioned at the intersections of major streets in each hotspot, as illustrated in Figure 16. A subset of sensors was dedicated to capturing background concentrations by being placed in less trafficked peripheral zones to establish baseline conditions. All units were powered by a portable generator and connected via the RS485 interface using the Modbus RTU communication protocol. Data were continuously logged and visualized in real time through the QMOD MASTER software, ensuring seamless monitoring throughout the campaign.

(a)

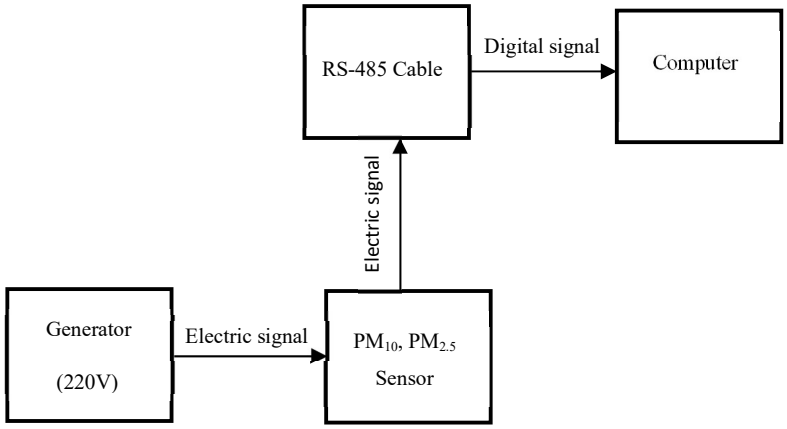

(b)

Figure 16 : Measurement apparatus and (b) description of the working principle of the PM_{10} and $PM_{2.5}$ sensors

By collecting both hotspot concentrations and background values simultaneously, the methodology not only supplied the baseline input required for GRAL simulations but also established a solid empirical foundation for validating its dispersion outputs. This combined approach enhanced the robustness and credibility of the model evaluation under actual traffic and meteorological conditions.

VII. Model Performance Evaluation and Statistical Metrics

The performance of the GRAL model was rigorously evaluated using statistical metrics, specifically fractional bias (FB) and normalized mean square error (NMSE), which are widely recognized indicators in atmospheric dispersion modeling (Irankunda et al., 2022). The FB metric provides insight into the direction of systematic deviation between modeled and observed values, as described by Equation II.11. A negative FB indicates that the model tends to overestimate pollutant concentrations, while a positive FB suggests underestimation. This distinction is particularly important in urban air quality studies, as systematic biases may arise from inaccurate emission inventories (e.g., under or overestimation of traffic activity), inappropriate emission factors, or insufficient representation of urban morphology effects. For instance, if diurnal variations in traffic intensity or meteorological fluctuations such as wind direction shifts are not properly accounted for, the model may consistently skew results in one direction.

In contrast, NMSE is a broader measure of model reliability, as it incorporates both systematic and random errors. As defined in Equation II.12, where $\overline{C}_c$ and $\overline{C}_m$ denote the mean modeled and measured concentrations, respectively, NMSE quantifies the overall magnitude of discrepancy between modeled and observed concentrations, regardless of whether the model over- or underestimates. Elevated NMSE values typically point to issues such as insufficient spatial resolution, temporal mismatches in measurement scheduling, or an incomplete representation of urban turbulence and local meteorological conditions. Low NMSE values, however, suggest that the model reproduces the observed variability in pollutant levels with strong consistency.

$$FB = \frac{2(\overline{C}_m - \overline{C}_c)}{(\overline{C}_m + \overline{C}_c)} \tag{II.11}$$

$$NMSE = \frac{\overline{(C_m - C_c)^2}}{\overline{C_m}\,\overline{C_c}} \tag{II.12}$$

Together, FB and NMSE provide a comprehensive framework for evaluating dispersion model performance. While FB highlights the direction of deviation, NMSE captures the overall scale of disagreement. The use of both metrics allows for the detection of not only systematic biases but also the extent to which random variability affects model accuracy. In the context of this study, these metrics were particularly valuable, as they allowed the validation of GRAL under complex urban conditions where traffic emissions, meteorology, and built environment interact. Their combined use ensured that the model evaluation extended beyond simple concentration

comparisons, offering a more nuanced understanding of its predictive robustness and its capacity to support reliable decision-making in urban air quality management.

VIII. Conclusion

This chapter presented the comprehensive methodological framework developed to assess the spatial and temporal variability of particulate matter (PM_{10} and $PM_{2.5}$) concentrations in the urban area of Sousse, Tunisia. The approach integrated emission estimation, atmospheric dispersion modeling, and experimental validation within a coherent structure that ensured both scientific rigor and local applicability.

The study area was characterized in detail, highlighting its complex urban morphology, traffic intensity, and coastal meteorological influences, all of which play critical roles in shaping air quality dynamics. The methodological design combined traffic data collection, emission quantification using COPERT 5, and pollutant dispersion simulations via two complementary models, SIRANE for meso-urban scale analysis and GRAMM/GRAL for high-resolution microscale representation. These models were supported by GIS-based spatial analysis, ensuring accurate spatial integration of road networks, receptor placements, and emission grids.

The deployment of 19 virtual receptors, coupled with on-site PM measurements and background concentration monitoring, provided both calibration and validation datasets for model evaluation. Statistical performance indicators such as FB and NMSE were employed to quantify model accuracy, while sensitivity analyses ensured the robustness of spatial resolution and input parameterization.

Each tool; COPERT, SIRANE, GRAL, and GIS played a distinct yet interdependent role, contributing to a multi-scale understanding of pollutant behavior across Sousse's diverse urban typologies. While acknowledging inherent limitations such as simplified meteorological assumptions and data availability constraints, the methodology establishes a strong foundation for reliable air quality modeling and policy-relevant assessments.

Overall, this chapter lays the groundwork for the results and discussion that follow, where the validated models are applied to identify pollution hotspots, analyze PM concentration patterns, and evaluate the implications for urban air quality management and public health in Sousse.

CHAPTER 3

Results and Discussions

I. Introduction

This chapter presents and discusses the results obtained from the integrated modeling framework developed to assess particulate matter (PM_{10} and $PM_{2.5}$) pollution in the urban area of Sousse, Tunisia. It brings together findings from emission estimation, dispersion simulations, and model validation to provide a coherent understanding of the spatial and temporal dynamics of urban air quality.

The results are structured to follow the methodological sequence established in the previous chapter. First, emission patterns derived from the COPERT 5 model are analyzed to quantify and characterize traffic-related PM emissions during rush and non-rush periods of the day. Next, the SIRANE model is used to evaluate pollutant dispersion across the urban domain, identifying key hotspots and spatial gradients in pollutant concentrations. These outputs are then refined through a microscale analysis using the GRAMM/GRAL system, which incorporates detailed information on wind fields, building geometry, and local turbulence to better capture near-road exposure and localized accumulation.

The chapter also presents the experimental validation of model outputs using field measurements of PM_{10} and $PM_{2.5}$ concentrations. Statistical performance indicators, including the Fractional Bias (FB) and Normalized Mean Square Error (NMSE), are applied to assess model accuracy and reliability. Finally, the discussion integrates the diagnostic interpretation of results, including the $PM_{2.5}/PM_{10}$ ratio, to identify dominant emission sources and evaluate the influence of urban structure, meteorology, and traffic activity on air pollution levels.

Beyond scientific interpretation, this chapter emphasizes the practical and policy relevance of the findings. The results provide actionable insights for urban planning, traffic management, and environmental health protection in Sousse.

In summary, this chapter bridges scientific analysis with policy-oriented implications, demonstrating how the integration of emission modeling, dispersion simulation, and empirical validation can support evidence-based decision-making for sustainable urban air quality management.

II. Emission Factors Evaluation and Analysis Using COPERT

II-1. Characterization of Traffic Flow and Vehicular Composition

Traffic-related emissions represent the primary source of particulate matter in Sousse’s urban environment.

To quantify these emissions with precision, traffic activity data were compiled along the city's main corridors and intersections, covering both peak and off-peak periods.

The vehicular fleet was classified according to COPERT categories; light-duty vehicles, heavy-duty trucks, buses, and two-wheelers—each associated with specific fuel types and emission factors.

These datasets, described in greater detail in Chapter 2, Section V-6-2, were integrated within the COPERT 5 framework to calculate pollutant loads at a fine spatial resolution, expressed as emission rates per kilometer of roadway. This characterization provided a realistic representation of urban traffic dynamics and served as the foundational input for both the SIRANE and GRAL dispersion models.

II-2. Evaluation of PM_{10} and $PM_{2.5}$ Emissions Factors

Pollutant emissions were estimated using the COPERT methodology to generate emission rates for PM_{10} and $PM_{2.5}$ under varying traffic conditions. The results, illustrated in Figure 17, reveal the spatial distribution of PM emissions within Sousse's residential and central urban areas. During rush-hour periods (Figure 5a and 5b), emission rates peaked along the main road corridors and intersections, reaching 0.269 kg/h/km for PM_{10} and 0.201 kg/h/km for $PM_{2.5}$. These elevated levels correspond to periods of dense traffic flow, frequent acceleration-deceleration cycles, and congestion-induced idling—conditions that intensify particulate release from exhaust and non-exhaust sources.

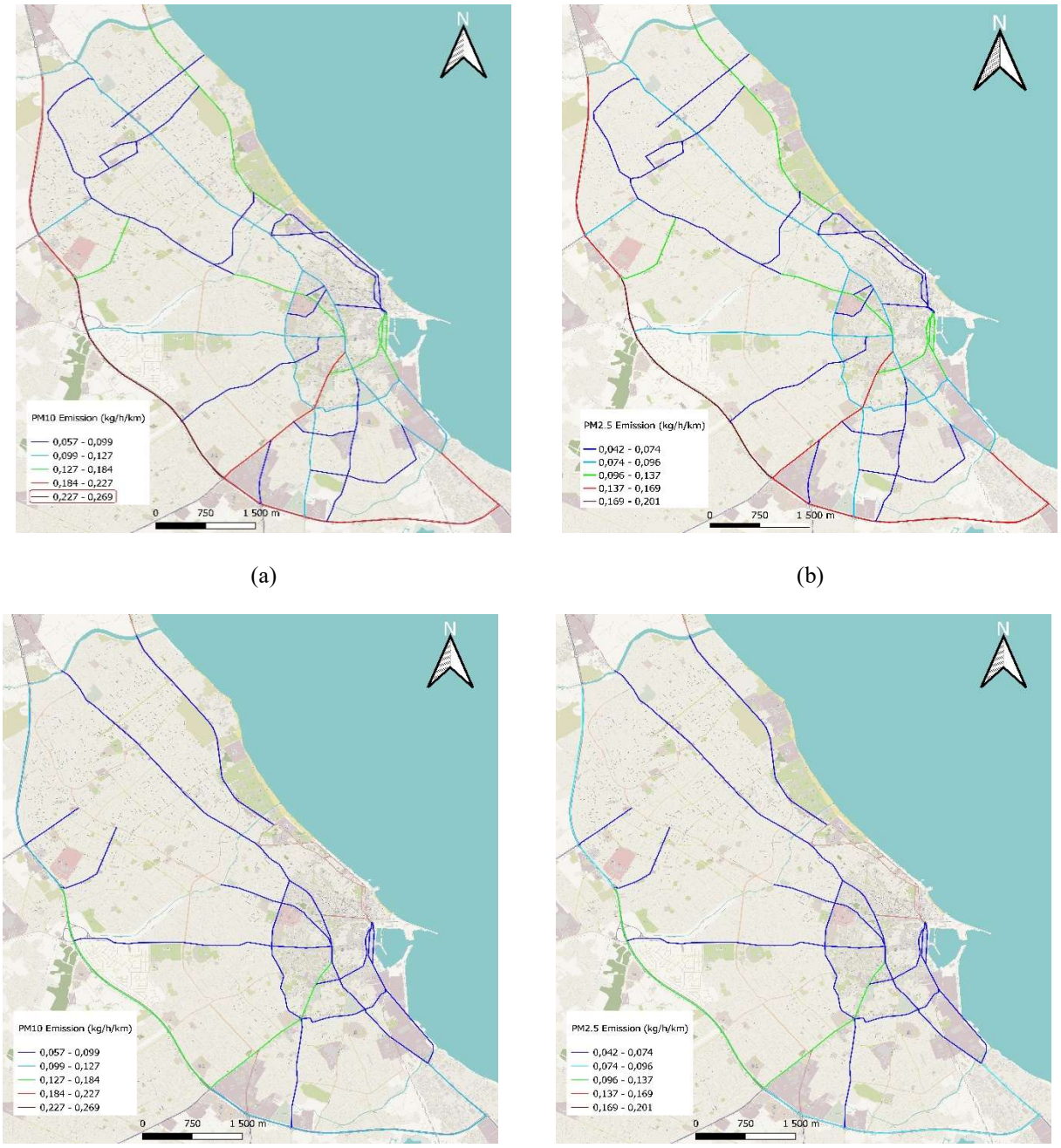

Figure 17 : Hourly emissions of PM_{10} (a) and $PM_{2.5}$ (b) during rush hour and hourly emissions of PM_{10} (c) and $PM_{2.5}$ (d) during non-rush hour

The SIRANE model utilized these emission rates to simulate citywide pollutant dispersion, while the GRAL model applied localized emission inputs for detailed microscale simulations at three identified hotspots. As presented in Table 8, the GRAL configuration confirmed emission rates within a similar range, with peak values of 0.2667 kg/h/km for PM_{10} and 0.1986 kg/h/km for $PM_{2.5}$, further validating the robustness of the emission inventory. The consistency

between the two models underscores the accuracy of the emission estimates and the reliability of the applied traffic and fleet characterization methods.

Table 8 : Configuration parameters for GRAMM/GRAL simulations

	Value					
Parameter	**Area 1**		**Area 2**		**Area 3**	
Road's emission rates ranges	Rush hour	Non-rush	Rush hour	Non-rush	Rush hour	Non-rush
PM_{10} (kg/h/km)	0.0097-0.2667	0.0045-0.1291	0.0073-0.1656	0.0033-0.0797	0.0039-0.1227	0.0018-0.0560
$PM_{2.5}$ (kg/h/km)	0.0072-0.1986	0.0034-0.0961	0.0054-0.1233	0.0024-0.0594	0.0029-0.0913	0.0013-0.0417
Horizontal concentration grid	2 m x 2m					
Vertical concentration grid	4 layers, 1 m per layer					
Dispersion time	3600 s					
Maximum iterations	2000 iterations					
Surface roughness	0.8 m					

II-3. Temporal and Spatial Variability of Emissions Factors (Rush vs. Non-Rush Hours)

Temporal analysis revealed a marked contrast between peak and non-peak traffic conditions. During rush hours, particulate emissions were significantly higher due to intense vehicle activity and recurrent stop-and-go driving. In contrast, non-rush hours (Figure 17c and 17d) exhibited smoother traffic flow and a corresponding reduction of nearly 40% in total emissions. This variation highlights the strong dependence of PM emissions on traffic volume and operational patterns.

Comparable findings were reported by (Biswal et al., 2023) in Delhi, where the authors demonstrated that reduced vehicle speeds and congestion peaks during rush hours lead to pronounced increases in PM_{10} and $PM_{2.5}$ emissions. The alignment between these international observations and the present results reinforces the conclusion that traffic intensity is the dominant driver of urban particulate pollution.

Furthermore, the spatial distribution of emissions identified consistent high-intensity corridors, particularly in central Sousse, where narrow roadways, limited ventilation, and high traffic convergence amplify emissions and potential exposure risks.

III. Urban Dispersion Modeling Using SIRANE

III-1. Model Input Parameterization

The SIRANE model was driven by combined inputs—including traffic emissions, meteorological parameters, background concentrations, and simplified urban geometry—compiled for a representative weekday (detailed in Chapter 2, Section V-6). These data were used to compute hourly mean concentrations at 19 virtual receptors strategically distributed across the city, ensuring that the simulations captured typical urban dispersion behavior in Sousse.

The resulting concentration maps are presented in Figure 18, which illustrates the simulated spatial distribution of PM_{10} and $PM_{2.5}$ across the urban area. Figure 18.a and 18.b show that the highest PM_{10} and $PM_{2.5}$ concentrations occur along the primary traffic corridors connecting the city center with the main arterial routes. These zones correspond to the most congested road segments, where heavy-duty vehicles and buses operate at low speeds, intensifying mechanical emissions and resuspension of road dust. The modeled concentration field forms continuous plumes that extend outward from these corridors, reflecting the advection of pollutants under dominant wind directions.

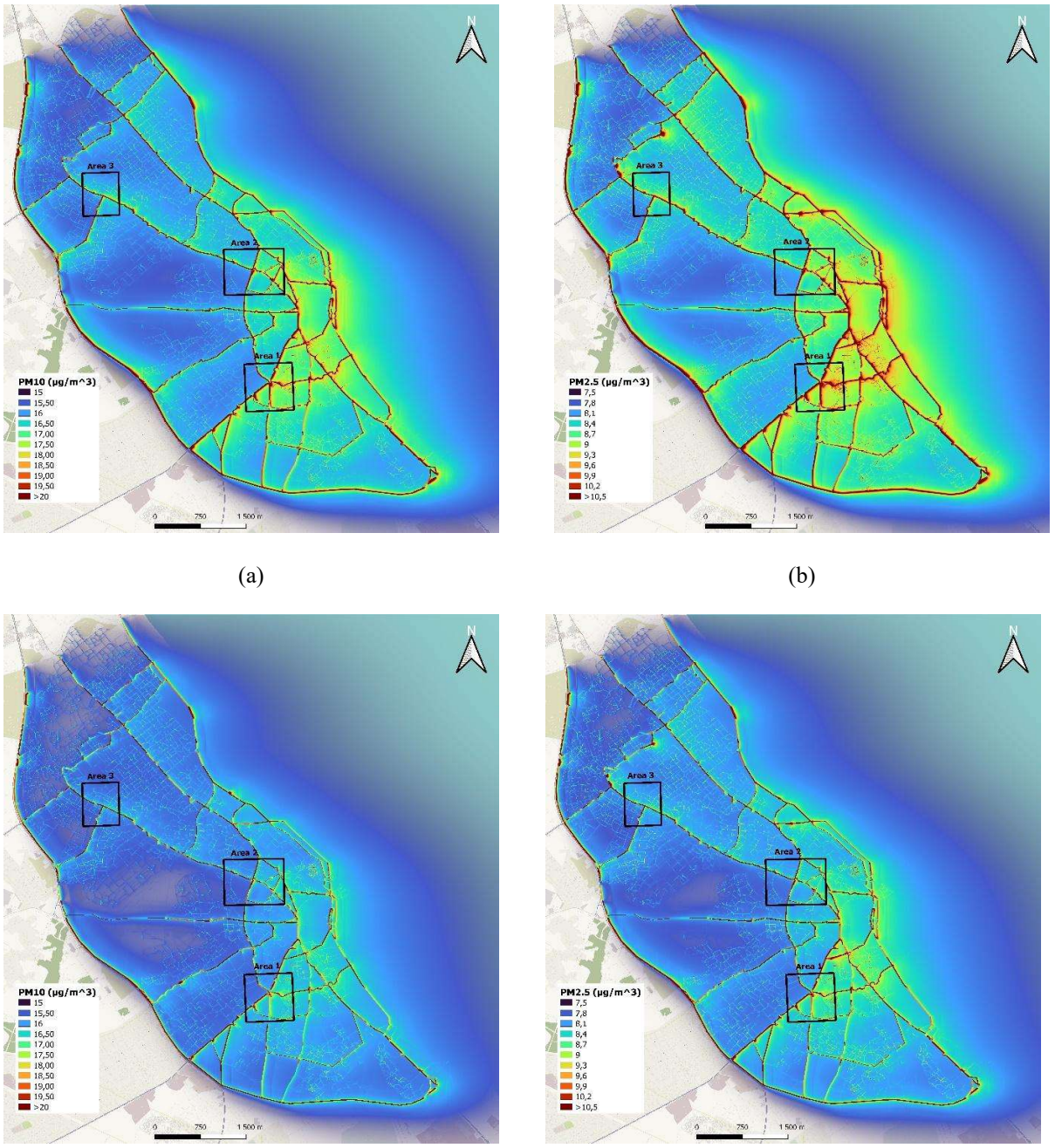

(a) (b)

(c) (d)

Figure 18 : Rush hour concentration of PM_{10} (a) and $PM_{2.5}$ (b) and non-rush hour concentration of PM_{10} (c) and $PM_{2.5}$ (d)

By contrast, peripheral residential areas display considerably lower concentrations, indicating the rapid dilution of pollutants in less dense neighborhoods with wider streets and higher ventilation potential. The model also highlights localized accumulation zones near intersections and enclosed streets, where limited airflow restricts horizontal dispersion. These findings are consistent with field observations of stagnant air pockets and traffic-related emission peaks during morning rush hours.

The agreement between simulated concentration gradients and known traffic patterns validates the coupling of COPERT-derived emissions with SIRANE's dispersion framework. The concentration range in Figure 18 (approximately 20–55 µg/m³ for PM_{10} and 10–30 µg/m³ for $PM_{2.5}$) aligns with empirical measurements reported in similar Mediterranean urban environments (Annesi-Maesano et al., 2007; Belarbi et al., 2020). The figure therefore serves not only as a visual confirmation of model accuracy but also as an analytical tool for identifying critical exposure zones.

These outputs were essential for guiding the subsequent microscale analysis with the GRAMM/GRAL model, where the three most impacted zones (Areas 1–3) were selected for detailed investigation.

Overall, Figure 18 provides a clear depiction of how particulate pollution is spatially structured within the Sousse urban canopy. It confirms that traffic emissions are the predominant contributors to PM concentration hotspots and highlights the model's effectiveness in reproducing realistic pollutant dispersion patterns across a heterogeneous urban landscape.

III-2. Spatial Distribution Mapping of Particulate Matter and Detection of Pollution Hotspots

The spatial output of the SIRANE model revealed marked heterogeneity in pollutant concentrations across the Sousse metropolitan area. Among the 19 receptors, R3, R6, and R7—corresponding to Areas 1, 2, and 3 were consistently identified as pollution hotspots (Figure 19). These receptors exhibited the highest concentrations of both PM_{10} and $PM_{2.5}$ during rush-hour periods.

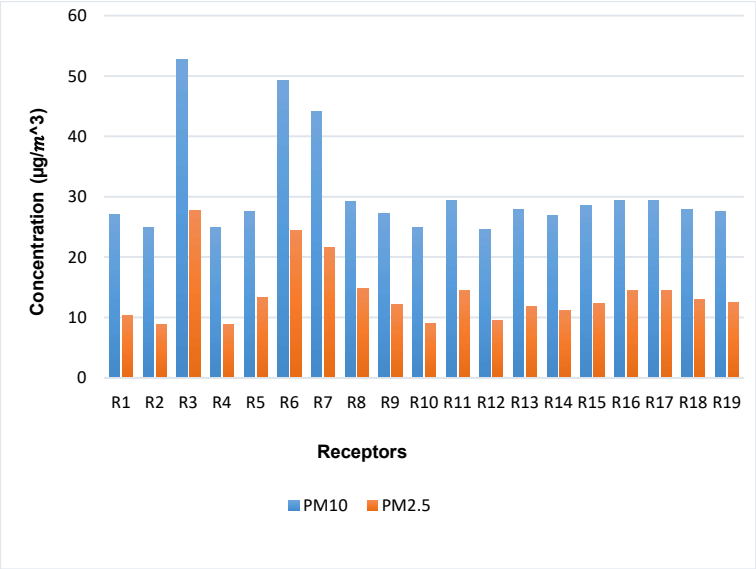

(a)

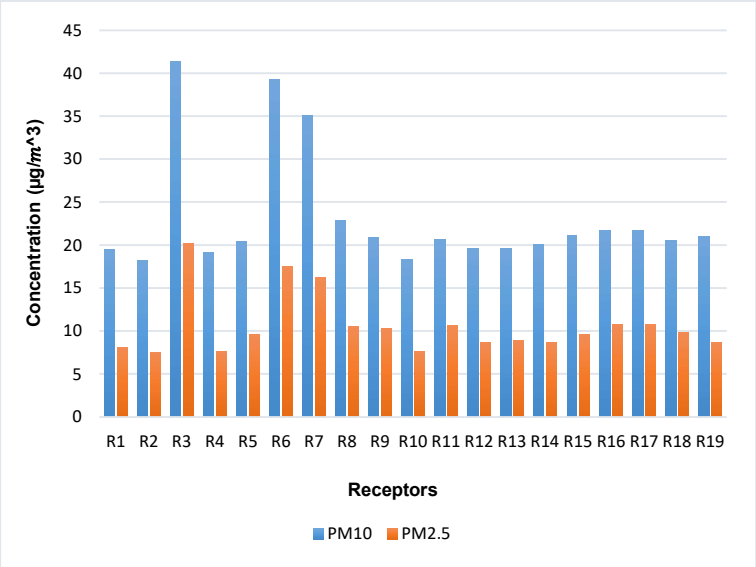

(b)

Figure 19 : Histograms of PM_{10}, $PM_{2.5}$ concentration levels at 19 receptors during (a) rush and (b) non-rush hour

During rush hours, modeled PM_{10} concentrations reached 52.83 µg/m³, 49.33 µg/m³, and 44.08 µg/m³, while $PM_{2.5}$ levels were 27.69 µg/m³, 24.46 µg/m³, and 21.58 µg/m³ in Areas 1, 2, and 3, respectively. These values exceed the EU regulatory limits of 40 µg/m³ for PM_{10} and 25 µg/m³ for $PM_{2.5}$ (Suter, 2008), underscoring the urgency of implementing emission-reduction measures. The spatial concentration patterns followed the city's primary traffic axes, highlighting the strong correlation between road density, traffic volume, and pollutant accumulation.

Each of the three identified hotspots exhibits unique urban characteristics influencing pollutant dispersion.

Area 1 is situated at a major traffic ingress point into the city, where constant vehicular inflow and high proportions of heavy-duty vehicles contribute to sustained PM emissions. The combination of combustion exhaust, tire and brake wear, and road-dust resuspension amplifies local pollution levels, especially under dry climatic conditions.

Area 2 represents a mixed-use institutional corridor encompassing hospitals, educational facilities, and administrative centers. This area experiences continuous traffic and high pedestrian activity throughout the day, exposing sensitive populations such as patients and children to elevated $PM_{2.5}$ levels. The steady movement of service and emergency vehicles further increases local emissions and prolongs pollutant residence times.

Area 3 functions as a critical traffic convergence zone where multiple arterial roads intersect. Prolonged idling and low vehicle speeds during congestion reduce combustion efficiency, leading to enhanced particulate formation. This area also experiences relatively poor ventilation due to the alignment of built structures, which restricts horizontal air exchange and favors pollutant accumulation.

Collectively, the three zones represent distinct yet complementary cases illustrating the interaction between traffic intensity, land use, and urban form in determining local air quality degradation.

III-3. Limitations of the SIRANE Model and Transition to Microscale Analysis

While SIRANE provides a robust framework for simulating pollutant dispersion at the meso-urban scale, its assumptions limit its accuracy in complex urban geometries. The model treats wind fields as horizontally homogeneous above roof level and assumes uniform mixing within each street segment, which restricts its capacity to resolve fine-scale airflow variability. Additionally, SIRANE does not differentiate between street types, such as one-sided versus open corridors, nor does it explicitly model recirculation zones and corner vortices commonly found near intersections (Soulhac et al., 2011).

These simplifications can lead to an underestimation of pollutant retention in densely built environments or in narrow street canyons where turbulence and flow separation dominate. To overcome these limitations, the GRAMM/GRAL modeling system was employed in the subsequent phase of this study to simulate microscale dispersion in the three identified hotspots.

GRAL's three-dimensional turbulence-resolving approach provides a more detailed understanding of pollutant behavior under real urban flow conditions, complementing the broader insights obtained from SIRANE.

IV. Microscale Analysis Using GRAMM/GRAL

IV-1. Model Input Parameterization

The GRAMM/GRAL modeling system (version 22.09) was used to perform high-resolution microscale simulations of PM_{10} and $PM_{2.5}$ dispersion within the three major hotspot areas of Sousse. The coupled system combines the meteorological pre-processing capability of GRAMM with the Lagrangian particle dispersion scheme of GRAL, enabling detailed representation of pollutant transport in complex urban environments.

The simulation inputs combined meteorological observations, traffic-based emission rates, and background concentration data, harmonized to maintain consistency across model domains. The background concentrations used as boundary inputs are presented in Chapter 2, Section V-6-4, while the overall configuration parameters—such as grid structure, dispersion duration, emission rate ranges, and turbulence settings—are summarized in Table 8.

Each hotspot domain included a surrounding buffer area to minimize boundary interference. A horizontal grid spacing of 2 × 2 m and a vertical extension up to 4 m, divided into four layers, were adopted to capture fine-scale concentration gradients in the exposure zone. The simulation period was set to one hour (3600 s) to align with the field measurement intervals on 15 January 2024, ensuring consistent temporal comparison. A surface roughness length (z_0 = 0.8 m) was assigned, representative of the aerodynamic properties of Sousse's dense urban texture.

Traffic emissions derived from COPERT 5 were introduced as hourly line sources along major roads, reflecting both rush-hour and non-rush-hour conditions. The meteorological parameters—wind speed, direction, temperature, and relative humidity—were processed through GRAMM to produce steady-state flow and turbulence fields for GRAL's dispersion runs.

This configuration provided a robust and spatially explicit framework for reproducing particulate transport and accumulation patterns across Sousse's urban corridors. The adopted setup ensured stable model convergence and accurate representation of pollutant gradients.

IV-2. Simulated Dispersion of PM_{10} and $PM_{2.5}$

The GRAL model simulations provided a detailed representation of how particulate matter (PM_{10} and $PM_{2.5}$) is dispersed within the complex urban canopy of Sousse. The results, illustrated in Figure 20, highlight clear spatial and temporal variations in pollutant concentrations across the three hotspot areas, each characterized by different traffic intensities, building configurations, and land-use functions. These variations emphasize the close interdependence between emission sources, meteorological conditions, and urban morphology in shaping air quality at the microscale.

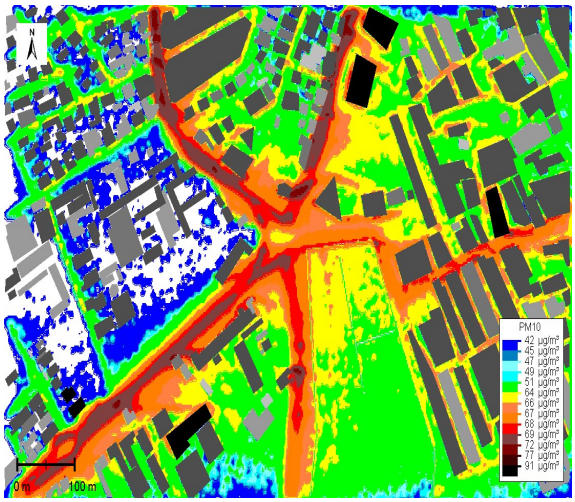

(a)

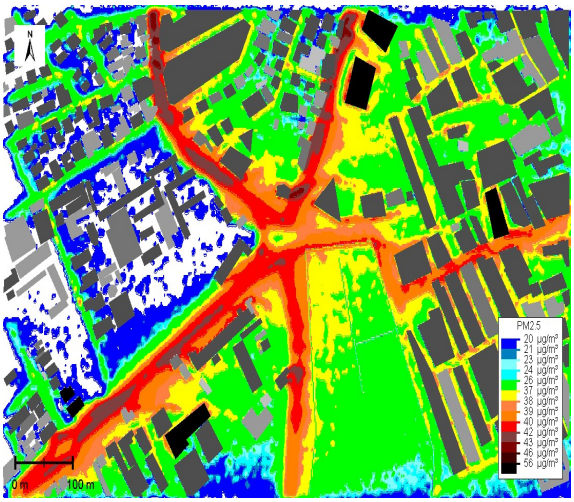

(b)

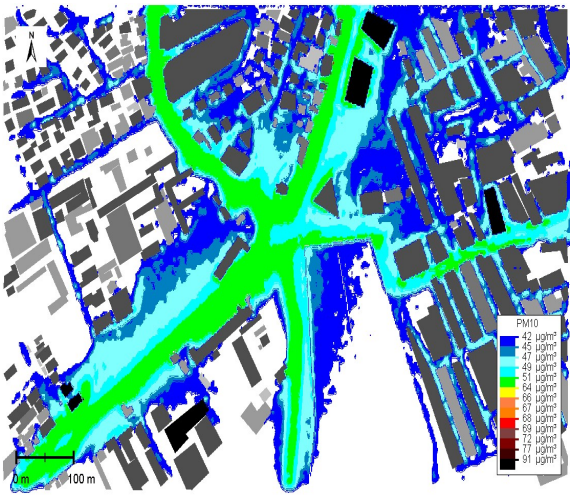

(c)

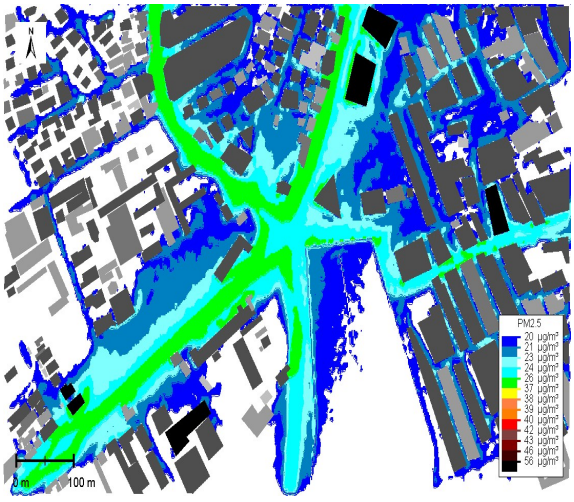

(d)

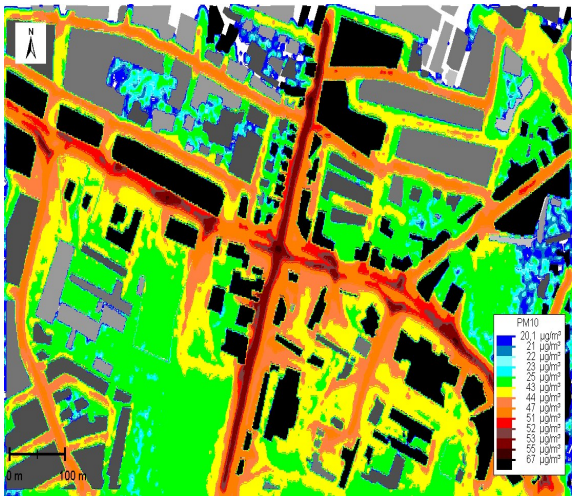
N
PM10
0 m
100 m

(e)

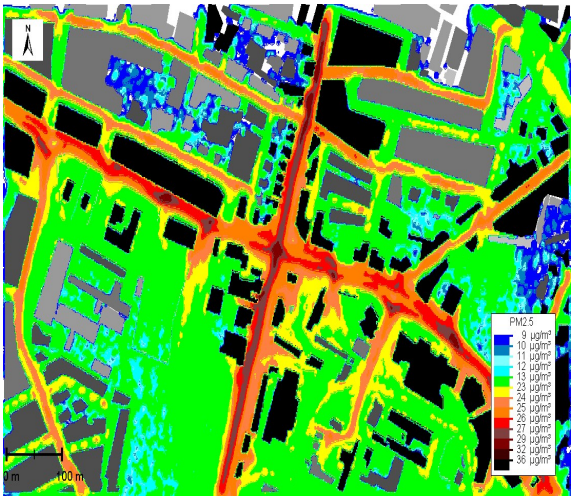
N
PM2.5
0 m
100 m

(f)

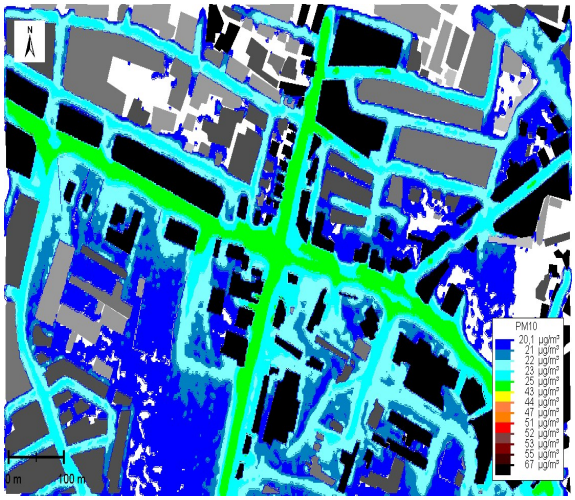
N
PM10
0 m
100 m

(g)

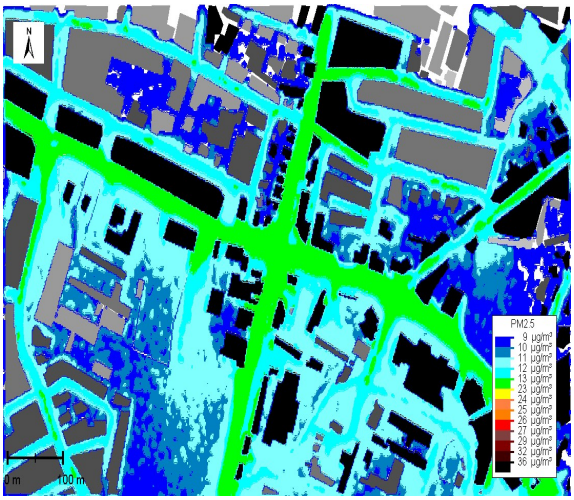
N
PM2.5
0 m
100 m

(h)

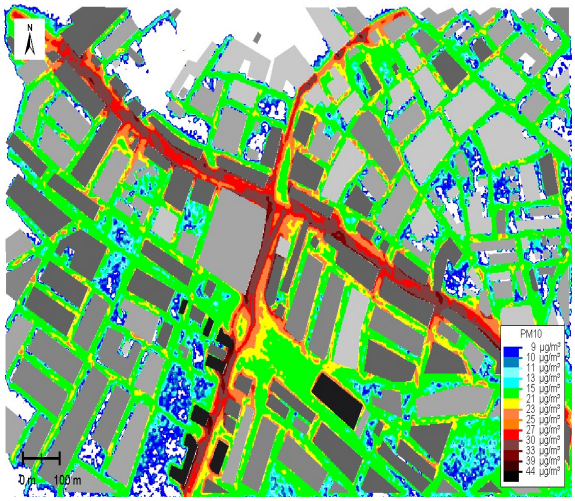
N
PM10
0 m
100 m

(i)

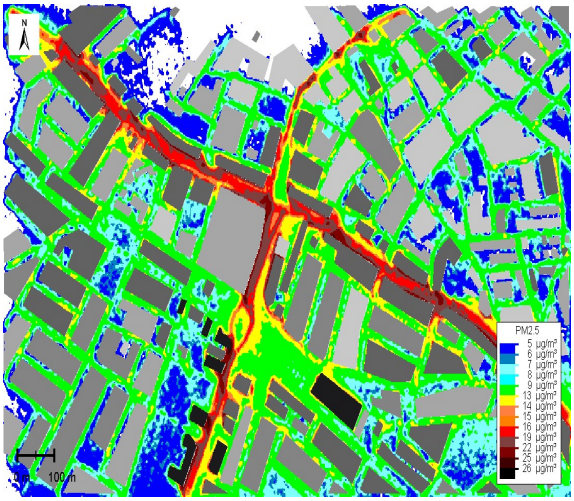
N
PM2.5
0 m
100 m

(j)

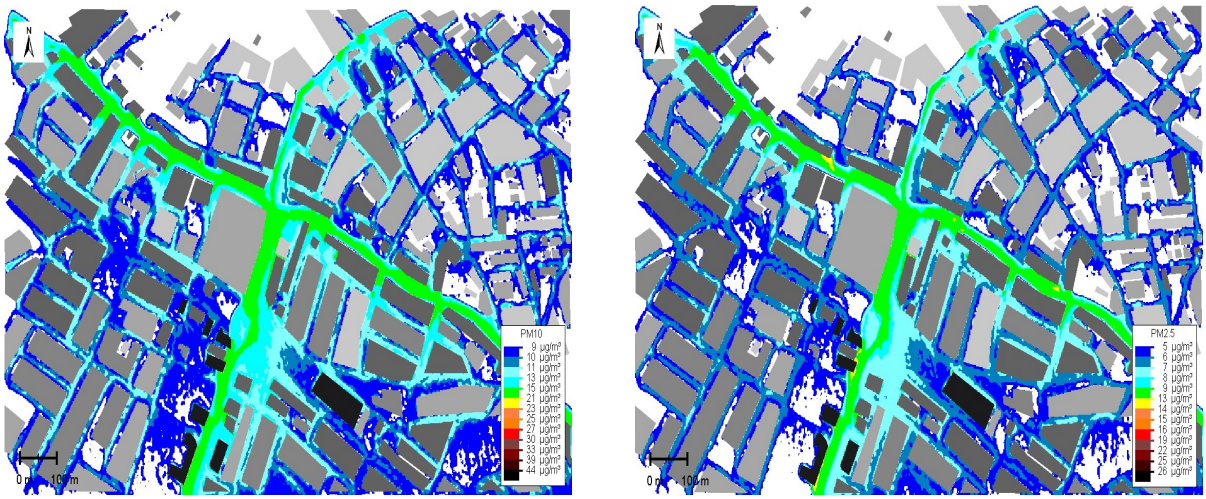

(k) (l)

Figure 20 : Simulated average concentrations of PM_{10} and $PM_{2.5}$ in the three study areas during rush and non-rush periods: (a–d) Area 1, (e–h) Area 2, and (i–l) Area 3. Panels (a, e, i) show PM_{10} during rush hours, (b, f, j) show $PM_{2.5}$ during rush hours, (c, g, k)

During rush-hour periods (07:30–08:30), PM levels reached their highest values across all modeled areas. Area 1 exhibited the most severe pollution, with simulated hourly averages of 91 µg/m³ for PM_{10} and 56 µg/m³ for $PM_{2.5}$, far exceeding the EU hourly guideline limits of 40 µg/m³ and 25 µg/m³, respectively. This area functions as a major urban ingress point, dominated by heavy-duty vehicles and high traffic turnover. The intense stop-and-go movement and frequent acceleration events enhance exhaust and non-exhaust emissions, while the surrounding narrow streets and moderate building heights restrict lateral and vertical air exchange. These conditions lead to pollutant accumulation near the ground, producing persistent high concentration zones, a phenomenon consistent with observations in dense Mediterranean cities (Riccardo Buccolieri et al., 2021).

In Area 2, PM concentrations also exceeded regulatory limits but were comparatively lower, reaching 67 µg/m³ for PM_{10} and 36 µg/m³ for $PM_{2.5}$. The area's mixed institutional land use (including hospitals, offices, and educational buildings) contributes to continuous traffic activity, though vehicle flow tends to be more distributed and slower. While the urban canyon effect is less pronounced than in Area 1, the moderate building density and limited vegetation still prevent effective pollutant dispersion. Furthermore, the presence of high pedestrian and patient populations makes this zone particularly sensitive from a public health perspective, reinforcing the importance of exposure-based mitigation planning.

Area 3 presented the lowest pollutant concentrations among the three hotspots, averaging 44 µg/m³ for PM_{10} and 26 µg/m³ for $PM_{2.5}$ during rush hour. Despite high traffic volumes, its open road layout with wider intersections and reduced building density enhances mechanical ventilation. The model's output shows smoother horizontal concentration gradients and smaller stagnation zones, indicating that urban form and street orientation can significantly improve air exchange rates, a finding supported by recent studies in Seoul and Singapore (Daeun Lee et al., 2025).

Under non-rush-hour conditions (10:30–11:30), PM levels decreased markedly, with average reductions of 35–40% relative to rush-hour peaks across all sites. This decline reflects both lower emission rates and improved dilution as traffic turbulence subsides and meteorological dispersion becomes more effective. Nevertheless, residual particulate levels remained elevated compared to the background concentrations measured in nearby non-urbanized areas, confirming that even during off-peak hours, the city's atmospheric environment retains a substantial pollution load due to slow dispersion and re-suspension of deposited particles.

From an applied perspective, these findings underscore the critical role of urban morphology in shaping air quality outcomes. The results suggest that traffic management measures alone are insufficient if not accompanied by urban design interventions that enhance natural ventilation, such as optimizing building spacing, reducing canyon aspect ratios, or introducing vegetative corridors. In the context of Sousse, such interventions would not only mitigate pollutant accumulation in confined areas like Area 1 but also reduce exposure for vulnerable populations in institutional districts like Area 2.

In summary, the GRAL simulations demonstrate that particulate pollution in Sousse exhibits strong spatial heterogeneity and temporal dependency on traffic dynamics. The results confirm that the most polluted areas coincide with the city's densest and least ventilated corridors, highlighting the necessity for integrated urban air quality management strategies.

IV-3. Vertical Concentration Gradients

The vertical concentration profiles of PM_{10} and $PM_{2.5}$ presented in Figure 21 illustrate the decline of particulate matter concentrations with increasing height across the three hotspot areas of Sousse. The results confirm that pollutant accumulation is most intense near ground level, particularly within the first few meters where vehicular emissions, resuspension of road dust, and limited air circulation combine to produce maximum exposure levels.

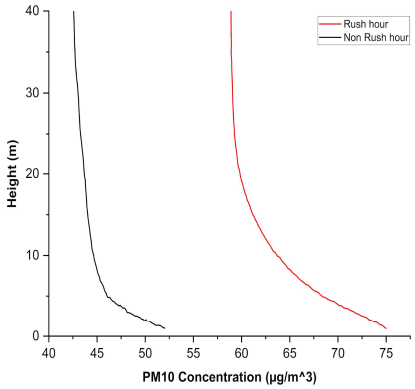

(a)

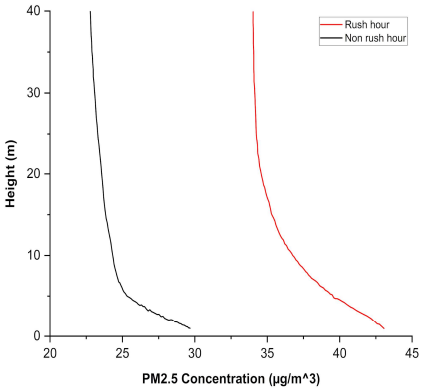

(d)

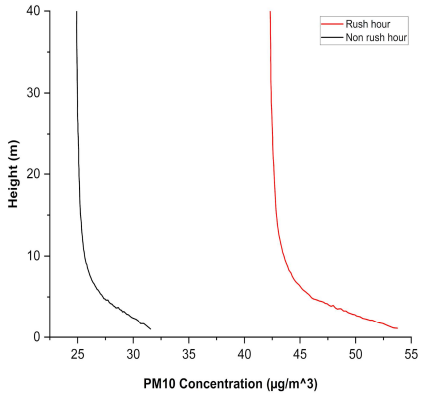

(b)

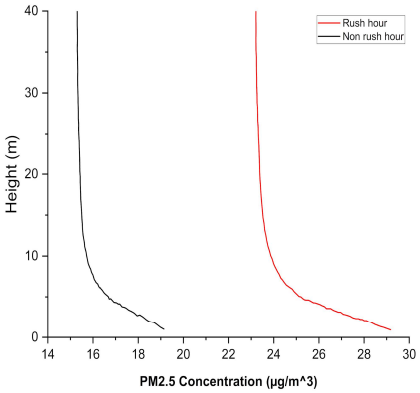

(e)

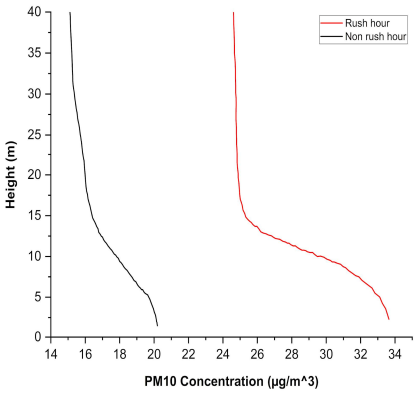

(c)

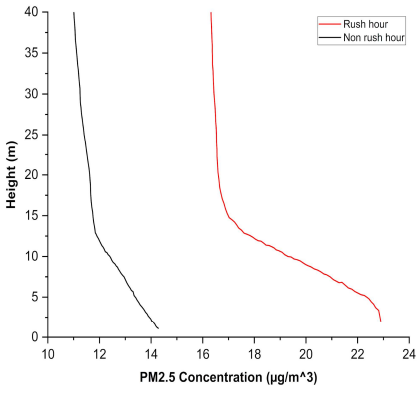

(f)

Figure 21 : Vertical concentration profile of PM_{10} and $PM_{2.5}$ during rush hour. (a), (b), (c) are the PM_{10} concentration profile respectively for Area 1, Area 2 and Area 3; (d), (e), (f) are the $PM_{2.5}$ concentration profile of the same community

During the rush-hour period, the model shows that particulate concentrations decrease progressively with height, although the rate of decline varies among the three areas according to their morphological and traffic characteristics. In Areas 1 and 2, both PM_{10} and $PM_{2.5}$ concentrations at 40 m fall to approximately 80 % and 83 % of the values measured at 2 m, respectively. This gentle vertical attenuation reflects the persistence of fine and coarse particles in the lower atmospheric layer due to weak vertical turbulence and limited ventilation caused by surrounding buildings. In Area 3, the gradient is more pronounced, with PM_{10} and $PM_{2.5}$ concentrations reduced to 73 % and 75 %, respectively, at the same height—evidence of improved air mixing resulting from a more open street configuration and lower building density.

These results align with numerous empirical and modeling studies (Gao et al., 2017; García et al., 2019; H.-T. Liao et al., 2023; Roostaei et al., 2024; Wu et al., 2002) that have shown how particulate concentrations diminish with altitude, particularly under stable meteorological conditions. The observed patterns are governed by a combination of atmospheric and mechanical processes. Wind speed and direction influence advection and mixing: higher velocities enhance dispersion at upper layers, while thermal inversions and calm conditions suppress turbulence, confining pollutants near the surface. The aerodynamic diameter of particles further dictates their behavior, PM_{10} tends to settle rapidly due to gravitational forces, whereas $PM_{2.5}$ remains suspended for longer periods, allowing it to disperse farther both vertically and horizontally.

Urban geometry exerts an equally critical influence. The height-to-width ratio of streets, building orientation, and density control the extent of vertical air exchange. Narrow street canyons with tall or closely spaced structures, such as those characteristics of Area 1—inhibit upward transport and promote pollutant entrapment, while broader avenues or open intersections typical of Area 3 facilitate upward motion and dilution. Studies by (Ezhilkumar et al., 2022; H. Liao et al., 2021; V. Kokkonen et al., 2021) corroborate these findings, emphasizing that variations in built morphology can either amplify or mitigate vertical pollution gradients by altering local turbulence intensity.

The comparison between rush and non-rush hours in Figure 21 underscores the temporal dependence of vertical dispersion. During rush hours, enhanced emissions coincide with relatively weak mixing, producing steep concentration profiles and pronounced surface accumulation. By contrast, during non-rush periods, reduced emissions and slightly stronger convective mixing flatten the vertical curves, indicating more efficient dilution throughout the lower boundary layer.

Collectively, these results demonstrate that particulate matter in Sousse is highly stratified, with maximum exposure occurring within the first 10 m above ground level, the breathing zone for pedestrians and residents of lower-floor buildings. This finding reinforces the necessity of considering vertical pollutant distribution when assessing population exposure and developing mitigation strategies.

V. Model Validation with Experimental Data

V-1. Validation Metrics

The comparison between modeled and observed particulate concentrations serves as a key step in validating the predictive capacity of the GRAL model under real urban conditions. The evaluation was conducted using fractional bias (FB) and normalized mean square error (NMSE) metrics, which had been previously introduced to quantify systematic and random deviations between simulated and measured data. Figures 22 and 23 display the comparative trends for PM_{10} and $PM_{2.5}$ concentrations at the three hotspot locations, demonstrating a high degree of correlation between model outputs and field measurements.

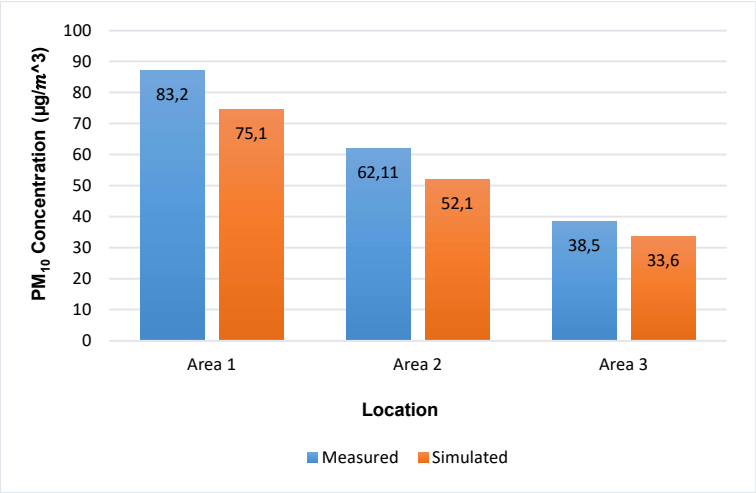

(a)

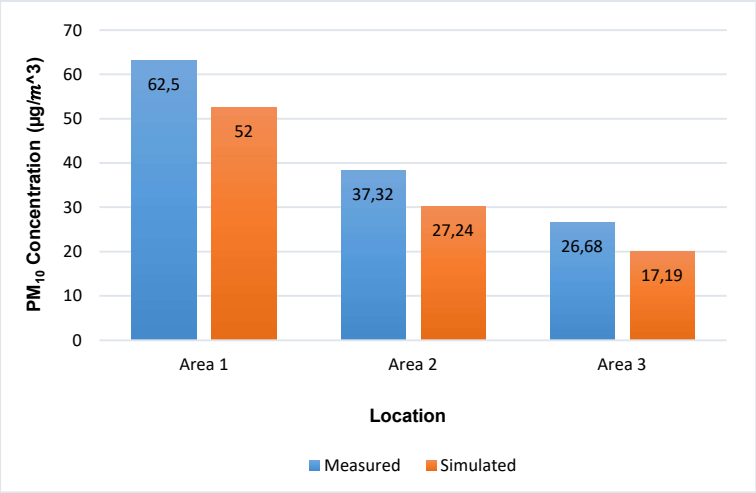

(b)

Figure 22 : Comparison between PM_{10} values and modeled values during (a) rush and (b) non-rush hour

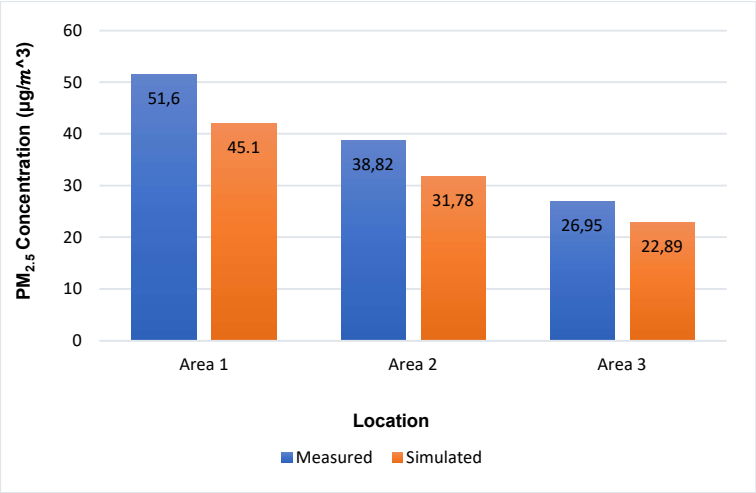

(a)

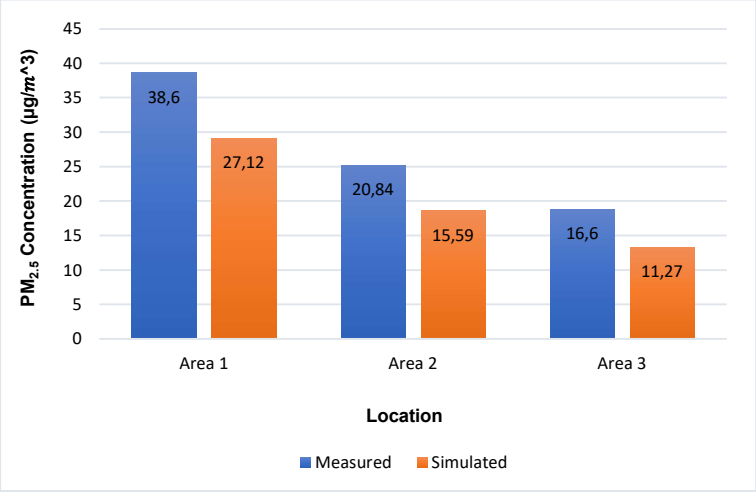

(b)

Figure 23 : Comparison between $PM_{2.5}$ values and modeled values during (a) rush and (b) non-rush hour

Across all validation sites, the results showed that the GRAL simulations accurately reproduced both the magnitude and temporal variation of PM_{10} and $PM_{2.5}$. The computed FB values: 0.14 for PM_{10} and 0.18 for $PM_{2.5}$, indicate a slight underestimation of observed values, while remaining well within the acceptable range of ±0.3 defined for urban dispersion models (Hanna & Chang, 2012). Similarly, the $NMSE^{1/2}$ values of 0.14 and 0.16 for PM_{10} and $PM_{2.5}$, respectively, confirm that the discrepancies between measured and modeled data are minimal.

These low bias and error scores collectively demonstrate that the model maintains high statistical reliability and performs within internationally accepted accuracy standards for mesoscale urban applications.

The consistency between simulated and measured data further validates the robustness of the emission inputs derived from the COPERT model, which provided the spatially and temporally resolved PM emission inventory used in GRAL. The strong agreement between model and observation suggests that the emission estimates successfully captured the real traffic-induced variability in Sousse. Moreover, the use of local meteorological data collected simultaneously during the January 2024 validation campaign, ensured that transient atmospheric conditions, such as low wind speed and directional shifts, were well represented in the model's dispersion behavior.

Spatially, the GRAL model successfully replicated the observed pollution ranking among the three hotspots. Area 1 consistently exhibited the highest PM_{10} and $PM_{2.5}$ concentrations, followed by Area 2, while Area 3 showed the lowest levels. This pattern demonstrates the model's ability to capture the spatial gradients resulting from variations in traffic volume, built geometry, and air exchange potential. The model's predictive accuracy across distinct urban typologies, ranging from dense arterial corridors to more ventilated intersections, highlights its versatility in handling heterogeneous microenvironments.

The minor differences observed between modeled and measured data can be attributed to short-term fluctuations in traffic flow, unmolded local turbulence, and micro-scale emission sources such as roadside dust resuspension or nearby construction activities, which are difficult to represent explicitly in dispersion models. Nevertheless, these deviations remained within the error margins typically encountered in field-based model validation exercises (Craig et al., 2020; Ilarri et al., 2022).

Overall, the statistical outcomes confirm that the GRAL model reliably simulates PM_{10} and $PM_{2.5}$ dispersion under the conditions of Sousse's urban environment. The low FB and NMSE values indicate that the model can effectively reproduce measured concentrations both spatially and temporally, validating its application for microscale air quality assessments. This strong correspondence between modeled and empirical data strengthens confidence in the methodology adopted in this study and supports the use of GRAL as a predictive and diagnostic tool for urban air pollution management in North African coastal cities.

V-2. Discussion of Validation Results

The recorded PM_{10} and $PM_{2.5}$ concentrations across the three identified hotspots in Sousse reveal substantial exceedances relative to the U.S. Environmental Protection Agency (EPA) recommended limits of 40 $\mu g/m^3$ for PM_{10} and 25 $\mu g/m^3$ for $PM_{2.5}$ (Suter, 2008). These findings

emphasize the critical air quality challenges faced in densely trafficked urban zones and underline the urgent necessity for targeted mitigation measures to control particulate emissions. The spatial and temporal variations observed in the measured data clearly reflect the combined effects of vehicular dynamics, local micro-meteorology, and urban morphology on pollutant accumulation and dispersion.

In Area 1, the highest particulate concentrations were recorded, reaching 83 μg/m³ for PM_{10} and 51 μg/m³ for $PM_{2.5}$ during rush-hour periods. These results align closely with the findings of Cheerfree & Singh (2024), who reported comparable values of 104.28 μg/m³ for PM_{10} and 61.57 μg/m³ for $PM_{2.5}$ at roadside monitoring stations in Imphal, Manipur, India, during intense traffic congestion. Similarly, Robert Cichowicz et al. (2019) in Poland observed that hourly PM_{10} concentrations in metropolitan environments typically ranged between 28.76 and 75.87 μg/m³, highlighting that vehicular activity and emission density are dominant drivers of fine and coarse particulate accumulation in urban air. The particularly elevated levels observed in Area 1 can be attributed to continuous, high-intensity traffic flow and limited interruption intervals, which, as Chen et al. (2020) noted, can maintain sustained emission rates throughout the day. The cumulative effect of frequent acceleration, braking, and mechanical dust resuspension further enhances particulate concentrations near road surfaces, especially under stagnant wind conditions that restrict vertical mixing.

In Area 2, average rush-hour concentrations were comparatively lower, 62 μg/m³ for PM_{10} and 39 μg/m³ for $PM_{2.5}$, yet still substantially exceeded the EPA thresholds. These values are consistent with the empirical measurements reported by Bizualem et al. (2023) in Megenagna, Addis Ababa, Ethiopia, where PM_{10} and $PM_{2.5}$ concentrations varied between 58.6 ± 3.1 μg/m³ and 30.3 ± 2.2 μg/m³, depending on local traffic density and road conditions. Similar magnitudes were observed in Portugal by Vicente et al. (2018), who recorded 33.0 μg/m³ for $PM_{2.5}$ during morning peak traffic. The relatively high concentrations in Area 2 can be partially attributed to its urban morphology, an institutional corridor with medium-rise buildings and limited open spaces. The surrounding built structures create aerodynamic obstructions that hinder horizontal airflow and reduce pollutant dilution, leading to localized pollutant retention. Studie by Huang et al. (2021) has shown that such physical barriers can significantly alter flow fields, creating stagnation zones that amplify near-surface particulate accumulation, even when emission rates are moderate.

Conversely, Area 3 exhibited the lowest rush-hour concentrations, with measured averages of 38 μg/m³ for PM_{10} and 26 μg/m³ for $PM_{2.5}$. These findings are in close agreement with the

results reported by D. Mecca et al. (2024), who observed 36 µg/m³ for PM_{10} and 24 µg/m³ for $PM_{2.5}$ in the urban area of Turin. The reduced pollutant levels in Area 3 are largely due to its more open street geometry and lower building density, which collectively enhance ventilation efficiency and pollutant dispersion. Open street configurations allow for greater wind penetration and vertical mixing, effectively diluting particulate concentrations near ground level. As Daeun Lee et al. (2025) demonstrated in Seoul, urban designs that maximize air permeability through broader intersections, lower aspect ratios, and reduced physical obstructions, significantly improve pollutant removal processes and lower human exposure levels.

Taken together, these spatial and temporal patterns confirm that vehicular emissions are the dominant source of particulate pollution in Sousse, with traffic intensity and street design acting as key modulators of concentration variability. Rush-hour periods consistently produced the highest levels of PM_{10} and $PM_{2.5}$ due to compounded emissions from combustion and non-exhaust sources, whereas lower levels during off-peak hours reflected both reduced emission rates and improved atmospheric dispersion. However, even during non-rush periods, residual particulate concentrations remained well above background levels, indicating that pollutant resuspension and limited urban ventilation continue to degrade local air quality.

Overall, the measured data reveal that air pollution in Sousse exhibits strong spatiotemporal heterogeneity governed by the interplay between emission dynamics, built form, and meteorological factors. The consistent alignment between the observed results and those documented internationally (Cheerfree & Singh, 2024; Cichowicz et al., 2019; Bizualem et al., 2023; Vicente et al., 2018; D. Mecca et al., 2024) validates the robustness of the field measurements and underscores the universal influence of traffic-induced emissions on urban particulate pollution.

VI. Diagnostic Analysis Using $PM_{2.5}/PM_{10}$ Ratios

The diagnostic evaluation of the $PM_{2.5}/PM_{10}$ ratio offers a deeper understanding of particulate matter composition, emission sources, and atmospheric behavior across the three monitored hotspot areas. As shown in Table 9, both measured and modeled ratios fall within a consistent range of 0.53 to 0.70, demonstrating strong agreement between empirical data and simulated outputs. This consistency underscores the reliability of the emission inventory and the GRAL model's capacity to accurately capture the size distribution and temporal variability of particulate matter under varying traffic and meteorological conditions.

Table 9: Measurements and modeled $PM_{2.5}/PM_{10}$ ratios in hotspots locations during rush and non-rush hour

	Measurements $PM_{2.5}/PM_{10}$ ratio		**Modeled $PM_{2.5}/PM_{10}$ ratio**	
Location	Rush hour	Non-rush hour	Rush hour	Non-rush hour
Area 1	0.62	0.61	0.60	0.54
Area 2	0.62	0.55	0.60	0.53
Area 3	0.70	0.62	0.68	0.60

In Areas 1 and 2, the ratios during rush-hour periods were 0.62 (measured) and 0.60 (modeled), indicate a significant presence of fine particulate matter ($PM_{2.5}$). Such elevated ratios are typically associated with vehicular emissions, particularly diesel exhaust, as well as non-exhaust sources such as brake and tire wear. The dominance of $PM_{2.5}$ within total particulate matter reflects the strong contribution of combustion-related emissions, which generate finer particles with aerodynamic diameters small enough to remain airborne for extended durations. According to Evangelia Diapouli et al. (2022), fine particles tend to persist in the atmosphere, especially under meteorological conditions that inhibit dispersion, such as weak wind speeds, atmospheric stability, or temperature inversions. These conditions are frequent in Sousse during early morning and late afternoon rush hours, leading to the accumulation of $PM_{2.5}$ and the consequent elevation of the ratio.

In contrast, the lower $PM_{2.5}/PM_{10}$ ratios observed in Area 2 during non-rush hours were 0.55 (measured) and 0.53 (modeled), suggest a relative shift toward coarse particulate dominance. This shift can be attributed to the reduced intensity of vehicle emissions coupled with an increased influence of mechanical processes, including road dust resuspension, soil particle entrainment, and minor construction activity. These coarser particles are typically heavier, settle more rapidly, and are less likely to remain suspended in the air for extended periods, resulting in a lower proportion of $PM_{2.5}$ within the total particulate mass. Such findings are consistent with the results of Yago Alonso Cipoli et al (2024), who demonstrated that PM_{10} contributions become more pronounced in low-traffic conditions due to mechanical and surface-related sources dominating over combustion emissions.

The highest $PM_{2.5}/PM_{10}$ ratios were found in Area 3, reaching 0.70 (measured) and 0.68 (modeled) during rush hours. This elevated ratio indicates a more intense generation of fine

particulate matter relative to coarse particles, likely resulting from repeated acceleration and deceleration cycles at major intersections. These traffic dynamics promote incomplete combustion, generating large amounts of submicron particles that substantially raise $PM_{2.5}$ concentrations. The spatial configuration of Area 3, characterized by open intersections and wider roadways, may also allow finer particles to disperse more evenly, resulting in broader but lower-intensity plumes of $PM_{2.5}$ across the modeled domain.

From a diagnostic perspective, the $PM_{2.5}/PM_{10}$ ratio serves as an effective indicator for distinguishing between fine and coarse particle sources and for interpreting the interactions between emission strength, atmospheric dispersion, and urban morphology. Elevated ratios in densely trafficked corridors point to the predominance of combustion-related fine particles, whereas lower ratios in less congested or mechanically influenced zones reflect a stronger contribution from coarse resuspended materials. Moreover, the temporal evolution of the ratio between rush and non-rush hours provides an indirect measure of emission dynamics and atmospheric cleansing efficiency.

Overall, this analysis confirms that the particulate pollution in Sousse is heavily influenced by vehicular emissions, with fine particles ($PM_{2.5}$) representing a substantial portion of total suspended matter during peak traffic periods. The ratio-based findings complement the concentration-based results presented earlier, offering a more nuanced understanding of emission mechanisms and their temporal variability. These insights can support targeted air quality management strategies, emphasizing the reduction of combustion-related emissions during high-traffic periods and the control of road dust and coarse particle sources during off-peak hours.

VII. Practical and Policy Implications

The results of this study carry critical implications for both urban planning and air quality policy, emphasizing that the management of particulate pollution in cities like Sousse requires an integrated, multi-sectoral approach that bridges environmental science, public health, and urban design. A key conclusion derived from the dispersion modeling and field validation is that urban morphology is a decisive factor in shaping local air quality. In compact districts such as Area 2, where buildings are densely arranged and street widths are limited, restricted air circulation promotes pollutant stagnation, particularly for fine particulates such as $PM_{2.5}$. This structural confinement amplifies exposure levels and prolongs pollutant residence time. Therefore, urban planners and municipal authorities must consider air quality as a central

parameter in development decisions by encouraging more open urban configurations, designing wider street canyons, and establishing ventilation corridors that enhance natural airflow and pollutant dispersion.

The persistent exceedance of EU regulatory thresholds for PM_{10} (40 μg/m³) and $PM_{2.5}$ (25 μg/m³), especially evident in Areas 1 and 2—demonstrates a pattern of chronic exposure to particulate matter. Long-term inhalation of elevated concentrations is scientifically associated with increased incidences of respiratory and cardiovascular diseases, as well as reduced life expectancy in urban populations. This underscores the urgent need for proactive health-focused policies, including early warning systems, continuous environmental surveillance, and public awareness campaigns. Local health authorities should coordinate with environmental agencies to establish permanent air monitoring stations within critical exposure zones, ensuring that citizens are promptly informed of pollution episodes and that mitigation actions can be triggered in real time.

The diagnostic analysis of $PM_{2.5}/PM_{10}$ ratios adds further depth to policy formulation by identifying the dominant emission sources in different urban contexts. Ratios between 0.6 and 0.7—as found in Areas 1 and 3—indicate a dominance of fine particulates from combustion-related emissions, particularly diesel engines, while lower ratios, such as those in Area 2 during non-rush periods, point to the prominence of coarse particles arising from mechanical processes like road dust resuspension and construction activity. These distinctions imply that mitigation strategies must be area-specific and source-oriented.

For Area 1, where fine particles predominate due to heavy traffic and exhaust emissions, policies such as establishing Low-Emission Zones (LEZs), restricting access to high-emission diesel vehicles, and promoting electric and hybrid transport systems would be particularly effective. Complementary measures could include optimizing traffic flow through smart signaling systems, encouraging public transport use, and implementing congestion pricing during peak hours.

In contrast, Area 2, where coarse particulate matter (PM_{10}) plays a more prominent role—especially during non-rush hours—requires dust-control policies. These may involve enforcing strict construction site regulations, increasing street cleaning frequency, and using water suppression techniques to minimize resuspension. Given that this area hosts sensitive facilities such as hospitals and educational institutions, the introduction of buffer zones, green belts, and

filtration barriers can further reduce near-ground particulate concentrations and protect vulnerable populations.

From a public health perspective, protective measures should include installing indoor air purification systems in schools, hospitals, and residential complexes within high-exposure zones. Authorities should also promote public awareness campaigns about exposure reduction practices, such as limiting outdoor activity during peak traffic times and adopting cleaner home heating alternatives.

Furthermore, the results underscore the importance of institutionalizing continuous air quality monitoring networks that integrate fixed and mobile sensors, enabling both real-time data collection and adaptive policy responses. Such systems can enhance transparency, support compliance enforcement, and strengthen community engagement in air quality management.

On a broader policy level, incentivizing cleaner technologies and revising Environmental Impact Assessment (EIA) frameworks to explicitly consider urban geometry and pollutant dispersion dynamics are vital. Urban development projects should undergo air quality audits that evaluate their potential to alter ventilation pathways or amplify pollutant retention. Similarly, building retrofits that improve indoor air circulation, the integration of vegetative infrastructure (green roofs and roadside trees), and the promotion of renewable transport energy systems represent crucial long-term investments.

In conclusion, the findings of this study advocate for a multidimensional policy strategy that integrates three interlinked pillars:

- Source-specific emission control; through transport and industrial regulation.
- Urban design optimization; to enhance ventilation and reduce pollutant buildup.
- Health-centered interventions; to protect at-risk populations and strengthen monitoring systems.

Without such integrated and adaptive policies, urban environments like Sousse will continue to experience critical air quality degradation, leading to substantial health and socio-economic burdens despite compliance with nominal environmental standards. Hence, the translation of modeling insights into actionable, evidence-based urban policy is both a scientific and civic imperative for sustainable city development in North Africa.

VIII. Conclusion

This chapter presented an integrated analysis of vehicular emissions, dispersion dynamics, and measured particulate concentrations in the urban area of Sousse, combining modeling and empirical observations to assess air quality patterns at both regional and microscale levels. Using the COPERT model for emission estimation and the SIRANE and GRAL models for dispersion analysis, the study successfully identified three pollution hotspots characterized by persistent exceedances of international air quality standards. The results demonstrated that traffic intensity, urban geometry, and meteorological conditions jointly govern the spatial and temporal variability of PM_{10} and $PM_{2.5}$ concentrations.

Model validation using field measurements confirmed the robustness of the GRAL simulations, with low fractional bias and normalized mean square error values indicating strong agreement between modeled and observed data. The diagnostic analysis based on $PM_{2.5}/PM_{10}$ ratios further clarified the relative contribution of fine and coarse particles, revealing that fine particulates originating from combustion and vehicle emissions dominate during rush hours, while coarse particles from mechanical sources prevail during off-peak periods.

Overall, the findings underline that vehicular traffic is the principal contributor to particulate pollution in Sousse, particularly in densely built and poorly ventilated zones. The integration of modeling tools and experimental validation proved essential for understanding how emissions interact with urban form and meteorology to shape local air quality. The final section of this chapter translated these scientific insights into practical and policy recommendations, emphasizing the need for low-emission transport strategies, improved street ventilation, continuous air quality monitoring, and health-oriented urban planning.

In summary, Chapter 3 establishes a comprehensive evidence base linking urban morphology and mobility patterns to particulate matter dynamics, providing both diagnostic clarity and actionable guidance for sustainable air quality management in Sousse-Tunisian citiy.

General conclusion

This thesis provides a comprehensive and multidisciplinary assessment of urban air pollution in the city of Sousse, Tunisia, with a specific focus on particulate matter (PM_{10} and $PM_{2.5}$) originating from vehicular emissions. By integrating emission modeling, atmospheric dispersion simulation, and field validation, this research establishes a methodological framework capable of quantifying, analyzing, and interpreting the dynamics of traffic-related air pollution at both meso-urban and microscale levels.

The first chapter laid the conceptual and scientific groundwork for the study by exploring the nature, classification, and behavior of atmospheric particles, their physical and chemical properties, and the mechanisms governing their formation, dispersion, and removal from the atmosphere. It highlighted that fine and coarse particles $PM_{2.5}$ and PM_{10}, derive largely from anthropogenic activities, particularly from internal combustion engines and non-exhaust sources such as tire and brake wear. The review of the literature also underlined the serious health impacts of particulate pollution, which include respiratory, cardiovascular, and neurological disorders. Furthermore, it presented a critical evaluation of modeling techniques, including traffic flow models, emission estimation tools such as COPERT, and dispersion models like SIRANE and GRAL, emphasizing their respective advantages, limitations, and applicability to urban contexts. The chapter concluded by identifying a clear research gap in North Africa, especially in Tunisia, where high-resolution modeling and integrated environmental assessment frameworks remain limited.

Building on this foundation, the second chapter developed a rigorous methodological design tailored to the complex urban environment of Sousse. It described the geographic, meteorological, and infrastructural characteristics of the study area, highlighting its dense road network, mixed land use, and high vehicular activity; all of which contribute to sustained particulate emissions. The methodological framework integrated multiple modeling tools: COPERT 5 was used to estimate PM_{10} and $PM_{2.5}$ emissions based on locally measured traffic flows and vehicle fleet composition; the SIRANE model simulated dispersion patterns at the city scale, while GRAL/GRAMM provided a microscale perspective for detailed assessment of three pollution hotspots. Nineteen virtual receptors were strategically distributed across the study area to capture spatial variability, and meteorological data; such as wind speed, direction, temperature, and atmospheric stability; were incorporated to represent realistic dispersion conditions. The chapter also detailed the experimental validation procedure, where particulate

sensors were deployed at hotspot locations to measure background and ambient concentrations, ensuring model accuracy. Statistical metrics such as fractional bias (FB) and normalized mean square error (NMSE) were used to quantitatively evaluate the reliability of simulation results.

The third chapter presented and discussed the core findings of the study. Emission analysis using COPERT revealed significant spatial and temporal variability in PM_{10} and $PM_{2.5}$ output, with rush-hour emissions up to 40% higher than off-peak periods. When integrated into the SIRANE dispersion model, these emissions produced concentration maps that identified three major hotspots with PM levels exceeding EU and WHO regulatory thresholds. GRAL microscale simulations further refined these results, capturing the influence of building geometry, road alignment, and localized turbulence on pollutant dispersion. Area 1; an urban entry corridor with high vehicular density; showed the highest pollutant concentrations due to limited ventilation and road dust resuspension. Area 2; an institutional district with hospitals and schools also exhibited high PM levels, aggravated by moderate building density and constant traffic flow. Area 3, by contrast, had lower concentrations owing to its wider streets and open intersections that favor natural ventilation. The model validation confirmed excellent performance, with FB and NMSE values within accepted ranges, and demonstrated strong consistency between measured and simulated concentrations. The diagnostic use of $PM_{2.5}/PM_{10}$ ratios (0.53–0.70) indicated the predominance of fine, combustion-related particulates during peak traffic hours and coarse mechanical particles during non-rush periods, reinforcing the link between traffic behavior and particulate composition.

From a policy and planning perspective, the findings underscore that vehicular emissions remain the dominant source of particulate pollution in Sousse and that urban form; specifically building density, street width, and the presence of ventilation corridors; plays a critical role in modulating air quality. Effective mitigation therefore requires a multidimensional approach combining emission control, sustainable traffic management, and urban design interventions. The establishment of Low-Emission Zones (LEZs), promotion of electric vehicles, regulation of construction dust, and integration of green infrastructure could substantially reduce particulate accumulation. Furthermore, continuous air quality monitoring and public health measures such as buffer zones around sensitive sites and air filtration in public institutions are essential to minimize exposure risks.

In conclusion, this thesis contributes both scientifically and practically to the understanding and management of urban air pollution in North Africa. Methodologically, it demonstrates the value of coupling emission models with multi-scale dispersion tools and ground-based validation to

achieve a realistic representation of pollutant behavior in complex urban environments. Scientifically, it advances the regional knowledge base by providing the first integrated emission–dispersion–validation framework applied to a Tunisian city. Practically, it offers actionable insights for policymakers, urban planners, and public health authorities, supporting evidence-based strategies for improving air quality and urban resilience. The overall findings highlight that addressing urban air pollution requires not only technological solutions but also structural urban reforms that prioritize ventilation, mobility sustainability, and human health protection.

References

Bibliographic References

Adeyanju, A., & Manohar, K. (2017). Effects of VehicularEmissions on Environmental Pollution in Lagos. Science Afric Journal of Scientific Issues, Research and Essays(5), 34-51.

Afton Chemical to Present at 2024 Responsible Care® and Sustainability Conference. (s. d.). Afton. Consulté 20 décembre 2025, à l'adresse https://www.aftonchemical.com/resources-events/events/afton-chemical-to-present-at-2024-responsible-care-and-sustainability-conference/

Ambient (outdoor) air pollution. (s. d.). Consulté 21 juillet 2025, à l'adresse https://www.who.int/news-room/fact-sheets/detail/ambient-%28outdoor%29-air-quality-and-health?utm_source=chatgpt.com

Annesi-Maesano, I., Forastiere, F., Kunzli, N., & Brunekref, B. (2007). Particulate matter, science and EU policy. In *European Respiratory Journal* (Vol. 29, Numéro 3, p. 428-431). Eur Respiratory Soc. https://erj.ersjournals.com/content/29/3/428.short

Antoaneta Ene et al.,. (2024). Major and Trace Element Accumulation in Soils and Crops (Wheat, Corn, Sunflower) around Steel Industry in the Lower Danube Basin and Associated Ecological and Health Risks. *Applied Sciences*, *14*(13), 5616-5616. https://doi.org/10.3390/app14135616

Barone, P. W., Keumurian, F. J., Neufeld, C., Koenigsberg, A., Kiss, R., Leung, J., Wiebe, M., Ait-Belkacem, R., Tabrizi, C. A., & Barbirato, C. (2023). Historical evaluation of the in vivo adventitious virus test and its potential for replacement with next generation sequencing (NGS). *Biologicals*, *81*, 101661.

Basic Information about Carbon Monoxide (CO) Outdoor Air Pollution | US EPA. (s. d.). Consulté 21 juillet 2025, à l'adresse https://www.epa.gov/co-pollution/basic-information-about-carbon-monoxide-co-outdoor-air-pollution?utm_source=chatgpt.com

Belarbi, N., Belamri, M., Dahmani, B., & Benamar, M. A. (2020). Road Traffic and PM10, PM2.5 Emission at an Urban Area in Algeria : Identification and Statistical Analysis. *Pollution*, *6*(3), 651-660. https://doi.org/10.22059/poll.2020.294710.730

References

Belis, C. A., Djatkov, D., Toceva, M., Knezevic, J., Djukanovic, G., Stefanovska, A., Golubov, N., Jovic, B., & Gavros, A. (2025). Analysis of COVID-19 Lockdown to Understand Air Pollution Processes and Their Impacts on Health : A Case Study in the Western Balkans. *Atmosphere*, *16*(1), Article 1. https://doi.org/10.3390/atmos16010090

Benson, P. E. (1984). *CALINE4–a Dispersion Model for Predicting Air Pollution Concentrations Near Roadways*. State of California, Department of Transportation, Division of Engineering ….

Berchet, A., Zink, K., Muller, C., Oettl, D., Brunner, J., Emmenegger, L., & Brunner, D. (2017). A cost-effective method for simulating city-wide air flow and pollutant dispersion at building resolving scale. *Atmospheric Environment*, *158*, 181-196. https://doi.org/10.1016/j.atmosenv.2017.03.030

Berchet, A., Zink, K., Oettl, D., Brunner, J., Emmenegger, L., & Brunner, D. (2017). Evaluation of high-resolution gramm–gral (v15. 12/v14. 8) no x simulations over the city of zürich, switzerland. *Geoscientific Model Development*, *10*(9), 3441-3459.

Bergmann, M. L., Andersen, Z. J., Amini, H., Khan, J., Lim, Y. H., Loft, S., Mehta, A., Westendorp, R. G., & Cole-Hunter, T. (2022). Ultrafine particle exposure for bicycle commutes in rush and non-rush hour traffic : A repeated measures study in Copenhagen, Denmark. *Environmental Pollution*, *294*, 118631. https://doi.org/10.1016/j.envpol.2021.118631

Bin Zhao. (2024). *Global variability in atmospheric new particle formation mechanisms | Nature*. https://www.nature.com/articles/s41586-024-07547-1?utm_source=chatgpt.com

Biswal, A., Singh, V., Malik, L., Tiwari, G., Ravindra, K., & Mor, S. (2023). Spatially resolved hourly traffic emission over megacity Delhi using advanced traffic flow data. *Earth System Science Data*, *15*(2), 661-680. https://doi.org/10.5194/essd-15-661-2023

Bizualem, B., Tefera, N., Angassa, K., & Feyisa, G. L. (2023). Spatial and Temporal Analysis of Particulate Matter and Gaseous Pollutants at Six Heavily Used Traffic Junctions in Megenagna, Addis Ababa, Ethiopia. *Aerosol Science and Engineering*, *7*(1), 118-130. https://doi.org/10.1007/s41810-022-00167-0

References

Bochenina, K., Agriesti, S., Roncoli, C., & Ruotsalainen, L. (2025). From Urban Data to City-Scale Models : A Review of Traffic Simulation Case Studies. *IET Intelligent Transport Systems*, *19*. https://doi.org/10.1049/itr2.70021

Bouchlaghem, K., & Nsom, B. (2012). Effect of Atmospheric Pollutants on the Air Quality in Tunisia. *The Scientific World Journal*, *2012*, 863528. https://doi.org/10.1100/2012/863528

Brauer, M., Freedman, G., Frostad, J., van Donkelaar, A., Martin, R. V., Dentener, F., Dingenen, R. van, Estep, K., Amini, H., Apte, J. S., Balakrishnan, K., Barregard, L., Broday, D., Feigin, V., Ghosh, S., Hopke, P. K., Knibbs, L. D., Kokubo, Y., Liu, Y., … Cohen, A. (2016). Ambient Air Pollution Exposure Estimation for the Global Burden of Disease 2013. *Environmental Science & Technology*, *50*(1), 79-88. https://doi.org/10.1021/acs.est.5b03709

Bruckmann, P., Hiester, E., Klees, M., & Zetzsch, C. (2013). Trends of PCDD/F and PCB concentrations and depositions in ambient air in Northwestern Germany. *Chemosphere*, *93*(8), 1471-1478. https://doi.org/10.1016/j.chemosphere.2013.07.029

Bulatovic, I., Igel, A. L., Leck, C., Heintzenberg, J., Riipinen, I., & Ekman, A. M. L. (2021). The importance of Aitken mode aerosol particles for cloud sustenance in the summertime high Arctic – a simulation study supported by observational data. *Atmospheric Chemistry and Physics*, *21*(5), 3871-3897. https://doi.org/10.5194/acp-21-3871-2021

Capitanio, L., Ratte, S., Gautier, S., & Josseran, L. (2024). Impact of air pollution on mortality : Geo-epidemiological study in French-speaking Africa. *Heliyon*, *10*(20). https://doi.org/10.1016/j.heliyon.2024.e39473

Cheberli, M., Jabberi, M., Ayari, S., Nasr, J. B., Chouchane, H., Cherif, A., Ouzari, H.-I., Sghaier, H., Cheberli, M., Jabberi, M., Ayari, S., Nasr, J. B., Chouchane, H., Cherif, A., Ouzari, H.-I., & Sghaier, H. (2025). Assessment of indoor air quality in Tunisian childcare establishments. *AIMS Environmental Science*, *12*(2), Article Environ-12-02-016. https://doi.org/10.3934/environsci.2025016

References

Cheerfree, K. T., & Singh, N. P. (2024). *Assessment of PM2.5 and PM10 Exposure and Health Risks : A Study of Pedestrian and Two-Wheeler Transport During Peak-Traffic in Imphal, Manipur*. Research Square. https://doi.org/10.21203/rs.3.rs-5217315/v1

Chen, M., Guo, S., Hu, M., & Zhang, X. (2020). The spatiotemporal evolution of population exposure to PM2.5 within the Beijing-Tianjin-Hebei urban agglomeration, China. *Journal of Cleaner Production*, *265*, 121708. https://doi.org/10.1016/j.jclepro.2020.121708

Christel Bouet et al.,2019. (s. d.). *Impact of Desert Dust on Air Quality : What is the Meaningfulness of Daily PM Standards in Regions Close to the Sources ? The Example of Southern Tunisia*. Consulté 22 janvier 2025, à l'adresse https://www.mdpi.com/2073-4433/10/8/452

Christine. (2023, novembre 28). Air pollution levels still too high across Europe. *NILU*. https://nilu.com/2023/11/air-pollution-levels-still-too-high-across-europe/

Cochard, M. (2022). Toxicité des particules atmosphériques issues de zones urbano-industrielles et portuaires et impact sur la transition épithélio-mésenchymateuse des cellules pulmonaires [Doctoral dissertation, Université du Littoral Côte d'Opale]. HAL Open Science. https://theses.hal.science/tel-03971037

COPERT | Calculations of Emissions from Road Transport. (s. d.). Consulté 29 juillet 2025, à l'adresse https://copert.emisia.com/

Craig, K. J., Baringer, L. M., Chang, S.-Y., McCarthy, M. C., Bai, S., Seagram, A. F., Ravi, V., Landsberg, K., & Eisinger, D. S. (2020). Modeled and measured near-road PM2. 5 concentrations : Indianapolis and Providence cases. Atmospheric Environment, 240, 117775.

Csanady et al. (1973). Turbulent Diffusion in the Envi*ronment* | *SpringerLink*. https://link.springer.com/book/10.1007/978-94-010-2527-0?utm_source=chatgpt.com

D. Mecca et al. (2024). *Spatial variation, temporal evolution, and source direction apportionment of PM1, PM2.5, and PM10 : 3-year assessment in Turin (Po Valley) | Environmental Monitoring and Assessment*. https://link.springer.com/article/10.1007/s10661-024-13446-9

Dada, L., Brem, B. T., Amarandi-Netedu, L.-M., Collaud Coen, M., Evangeliou, N., Hueglin, C., Nowak, N., Modini, R., Steinbacher, M., & Gysel-Beer, M. (2025). Sources of ultrafine particles

References

at a rural midland site in Switzerland. *Aerosol Research*, *3*(1), 315-336. https://doi.org/10.5194/ar-3-315-2025

Daeun Lee et al. (2025). *Analyzing Dispersion Characteristics of Fine Particulate Matter in High-Density Urban Areas : A Study Using CFD Simulation and Machine Learning*. https://www.mdpi.com/2073-445X/14/3/632

Daganzo, C. F. (1994). The cell transmission model : A dynamic representation of highway traffic consistent with the hydrodynamic theory. *Transportation Research Part B: Methodological*, *28*(4), 269-287.

De Nunzio, G., Laraki, M., & Thibault, L. (2020). Road traffic dynamic pollutant emissions estimation : From macroscopic road information to microscopic environmental impact. *Atmosphere*, *12*(1), 53.

Deabji, N., Fomba, K. W., dos Santos Souza, E. J., Mellouki, A., & Herrmann, H. (2024). Influence of anthropogenic activities on metals, sugars and PAHs in PM10 in the city of Fez, Morocco : Implications on air quality. *Environmental Science and Pollution Research International*, *31*(17), 25238-25257. https://doi.org/10.1007/s11356-024-32740-0

Diakaki, C., Papageorgiou, M., & Aboudolas, K. (2000). Traffic-responsive urban network control using multivariable regulators. *Archives of Transport*, *12*(4), Article 4.

Duarte, L., Godinho, S., Gomes, A., Rodrigues, S., & Teodoro, A. C. (2023). A GIS open source application for cost distance modelling for site catchment analysis of prehistoric sites. *Earth Resources and Environmental Remote Sensing/GIS Applications XIV*, *12734*, 346-353. https://www.spiedigitallibrary.org/conference-proceedings-of-spie/12734/1273412/A-GIS-open-source-application-for-cost-distance-modelling-for/10.1117/12.2678993.short

Eclipse SUMO - Simulation of Urban MObility. (s. d.). Eclipse SUMO - Simulation of Urban MObility. Consulté 24 juillet 2025, à l'adresse https://eclipse.dev/sumo/

Elhaddaj, H., Chkara, L., Rangognio, J., Yahyaoui, A., Hanoune, B., & Maimouni, L. E. (2019). SIRANE modeling of oxides nitrogen (NOx) and ozone (O3) in the area of Agadir city,

References

southwestern Morocco. *Moroccan Journal of Chemistry*, *7*(4), Article 4. https://doi.org/10.48317/IMIST.PRSM/morjchem-v7i4.18116

El-Harbawi, M. (2013). Air quality modelling, simulation, and computational methods : A review. *Environmental Reviews*, *21*, 149-179. https://doi.org/10.1139/er-2012-0056

EPA, U. (2004). *User's guide for the AMS/EPA regulatory model (AERMOD)*. Office of Air Quality Planning and Standards, Research Triangle Park, US ….

Essamlali, I., Nhaila, H., & Khaili, M. E. (2025). Impact of urban block shape on traffic and air quality : A SUMO-based comparative study of rectangular, radial, and triangular forms. *Transportation Research Interdisciplinary Perspectives*, *31*, 101413. https://doi.org/10.1016/j.trip.2025.101413

Euchi, H., & Dahech, S. (2019). Temps, pollution aux particules fines (PM10) et morbidité respiratoire à Sfax (Tunisie). *Pollution atmosphérique. Climat, santé, société*, *239*. https://doi.org/10.4267/pollution-atmospherique.6809

Europe's air quality status 2023. (s. d.). [Briefing]. European Environment Agency. Consulté 21 juillet 2025, à l'adresse https://www.eea.europa.eu/publications/europes-air-quality-status-2023/europes-air-quality-status2023

Evangelia Diapouli et al. (2022). *PM2.5 Source Apportionment and Implications for Particle Hygroscopicity at an Urban Background Site in Athens, Greece*. https://www.mdpi.com/2073-4433/13/10/1685

Ewa Anioł et al. (2023, mai 15). *New insights into submicron particles impact on visibility*. SciSpace - Paper. https://doi.org/10.5194/egusphere-egu23-5289

Ezhilkumar, M. R., Karthikeyan, S., Aswini, A. R., & Hegde, P. (2022). Seasonal and vertical characteristics of particulate and elemental concentrations along diverse street canyons in South India. *Environmental Science and Pollution Research*, *29*(57), 85883-85903. https://doi.org/10.1007/s11356-021-15272-9

Fabbi, S., Asaro, S., Bigi, A., Teggi, S., & Ghermandi, G. (2019). Impact of vehicular emissions in an urban area of the Po valley by microscale simulation with the GRAL dispersion model. *IOP*

References

Conference Series: Earth and Environmental Science, *296*(1), 012006. https://doi.org/10.1088/1755-1315/296/1/012006

Fabien Leurent et al. (2023). *On Heterogenous Sampling Rates in Origin–Destination Matrix Estimation Based on Trajectory Data and Link Counts—Fabien Leurent, Danyang Sun, Xiaoyan Xie, 2023*. https://journals.sagepub.com/doi/abs/10.1177/03611981221103589

Fadel, M., Ledoux, F., Farhat, M., Kfoury, A., Courcot, D., & Afif, C. (2021). PM2.5 characterization of primary and secondary organic aerosols in two urban-industrial areas in the East Mediterranean. *Journal of Environmental Sciences*, *101*, 98-116. https://doi.org/10.1016/j.jes.2020.07.030

Faridi, S., Krzyzanowski, M., Cohen, A. J., Malkawi, M., Moh'd Safi, H. A., Yousefian, F., Azimi, F., Naddafi, K., Momeniha, F., Niazi, S., Amini, H., Künzli, N., Shamsipour, M., Mokammel, A., Roostaei, V., & Hassanvand, M. S. (2023). Ambient Air Quality Standards and Policies in Eastern Mediterranean Countries : A Review. *International Journal of Public Health*, *68*, 1605352. https://doi.org/10.3389/ijph.2023.1605352

Fellendorf, M., & Vortisch, P. (2000). *Integrated Modeling of Transport Demand, Route Choice, Traffic Flow and Traffic Emissions*.

Fellendorf, M., & Vortisch, P. (2010). Microscopic Traffic Flow Simulator VISSIM. *International Series in Operations Research & Management Science*, 63-93.

Gao, Y., Wang, Z., Lu, Q.-C., Liu, C., Peng, Z.-R., & Yu, Y. (2017). Prediction of vertical PM2.5 concentrations alongside an elevated expressway by using the neural network hybrid model and generalized additive model. *Frontiers of Earth Science*, *11*(2), 347-360. https://doi.org/10.1007/s11707-016-0593-0

García, M. Á., Sánchez, M. L., De Los Ríos, A., Pérez, I. A., Pardo, N., & Fernández-Duque, B. (2019). Analysis of PM10 and PM2.5 Concentrations in an Urban Atmosphere in Northern Spain. *Archives of Environmental Contamination and Toxicology*, *76*(2), 331-345. https://doi.org/10.1007/s00244-018-0581-3

References

Geroliminis, N., & Daganzo, C. F. (2008). Existence of urban-scale macroscopic fundamental diagrams : Some experimental findings. *Transportation Research Part B: Methodological*, *42*(9), 759-770. https://doi.org/10.1016/j.trb.2008.02.002

Geroliminis, N., & Sun, J. (2011). Properties of a well-defined macroscopic fundamental diagram for urban traffic. *Transportation Research Part B: Methodological*, *45*(3), 605-617. https://doi.org/10.1016/j.trb.2010.11.004

Global Leader in Petroleum Additives. (s. d.). Afton. Consulté 22 juillet 2025, à l'adresse https://www.aftonchemical.com/

Gousseau, P., Blocken, B., Stathopoulos, T., & van Heijst, G. (s. d.). *Large-Eddy Simulation of Pollutant Dispersion in Downtown Montreal : Evaluation of the Convective and Turbulent Mass Fluxes*.

H. Estuardo-Moreno et al.,. (2022). Application of Organic Particle Analysis in Inhalable Particulate Matter by TEM-EDS and GC-MS to Air Quality Studies. *Microscopy and Microanalysis*, *28*, 3212-3213. https://doi.org/10.1017/S1431927622011941

Habert, R., Muczynski, V., Lehraiki, A., Lambrot, R., Lécureuil, C., Levacher, C., Coffigny, H., Pairault, C., Moison, D., Frydman, R., & Rouiller-Fabre, V. (2009). Adverse effects of endocrine disruptors on the foetal testis development : Focus on the phthalates. *Folia Histochemica Et Cytobiologica*, *47*(5), S67-74. https://doi.org/10.2478/v10042-009-0056-5

Hamza Abderrahim et al. (2016). *Forecasting PM10 in Algiers : Efficacy of multilayer perceptron networks | Environmental Science and Pollution Research*. https://link.springer.com/article/10.1007/s11356-015-5406-6?utm_source=chatgpt.com

Hanna, S., & Chang, J. (2012). Acceptance criteria for urban dispersion model evaluation. *Meteorology and Atmospheric Physics*, *116*(3-4), 133-146. https://doi.org/10.1007/s00703-011-0177-1

HBEFA - Handbook Emission Factors for Road Transport. (s. d.). Consulté 29 juillet 2025, à l'adresse https://www.hbefa.net/?utm_source=chatgpt.com

Hernández-Ramírez, G., Martínez-Rojas, R., Pérez-García, L., Fernández-Santiesteban, E., Garcell-Puyáns, L., Álvarez-de-Prado, L., Menéndez, J., Fernández-Ordás, J., & Bernardo Sánchez, A. (2024). *Temperature : An Influencing Factor on the Rheological and Energetic Parameters of*

References

Acid Pressure Technology Operations. MDPI AG. https://doi.org/10.20944/preprints202411.1604.v1

H.M. ten Brink et al.,2008. (2008, janvier 1). *Carbon in Atmospheric Particulate Matter*. SciSpace - Paper; ECN. https://typeset.io/papers/carbon-in-atmospheric-particulate-matter-2dtm1nocb7

Huang, Y., Lei, C., Liu, C.-H., Perez, P., Forehead, H., Kong, S., & Zhou, J. L. (2021). A review of strategies for mitigating roadside air pollution in urban street canyons. *Environmental Pollution*, *280*, 116971. https://doi.org/10.1016/j.envpol.2021.116971

Huzzat, A., Anpalagan, A., Khwaja, A. S., Woungang, I., Alnoman, A. A., & Pillai, A. S. (2025). A comprehensive review of Digital Twin technologies in smart cities. *Digital Engineering*, *4*, 100040. https://doi.org/10.1016/j.dte.2025.100040

Ilarri, S., Trillo-Lado, R., & Marrodán, L. (2022). Traffic and Pollution Modelling for Air Quality Awareness : An Experience in the City of Zaragoza. *SN Computer Science*, *3*(4), 281. https://doi.org/10.1007/s42979-022-01105-0

Imad Khraibet Rashid Al-Khuwaylidee et al. (2024). *Distribution of Atmospheric Stability Classes in Baghdad Province and Its Relationship with Surface Wind Speed Rates | Iraqi Journal of Science*. https://www.ijs.uobaghdad.edu.iq/index.php/eijs/article/view/9456

Irankunda, E., Török, Z., Mereuță, A., Gasore, J., Kalisa, E., Akimpaye, B., Habineza, T., Shyaka, O., Munyampundu, G., & Ozunu, A. (2022). The comparison between in-situ monitored data and modelled results of nitrogen dioxide (NO2) : Case-study, road networks of Kigali city, Rwanda. *Heliyon*, *8*(12). https://www.cell.com/heliyon/fulltext/S2405-8440(22)03678-7

J. Cobiac Linda et al.,2022. (2022). Identification of Wind-Induced Particle Resuspension in Urban Environment Using CFD Modelling. *Atmosphere*, *14*(1), 57-57. https://doi.org/10.3390/atmos14010057

Jacobson, M. (2002). Fundamentals of Atmospheric Modeling. In *Fundamentals of Atmospheric Modeling Second Edition*. https://doi.org/10.1017/CBO9781139165389

Jephcote, C., & Gulliver, J. (2025). Development and evaluation of rapid, national-scale outdoor air pollution modelling and exposure assessment : Hybrid Air Dispersion Exposure System

References

(HADES). *Environment International*, *197*, 109304. https://doi.org/10.1016/j.envint.2025.109304

Kajishima, T., & Taira, K. (2017). Reynolds-Averaged Navier–Stokes Equations. In T. Kajishima & K. Taira, *Computational Fluid Dynamics* (p. 237-268). Springer International Publishing. https://doi.org/10.1007/978-3-319-45304-0_7

Kakosimos, K. E., Hertel, O., Ketzel, M., & Berkowicz, R. (2010). Operational Street Pollution Model (OSPM) – a review of performed application and validation studies, and future prospects. *Environmental Chemistry*, *7*(6), 485-503. https://doi.org/10.1071/EN10070

Kaminski, U., Fricker, M., & Dietze, V. (2013). The PM2. 5 Fine Particle Background Network of the German Meteorological Service-First Results. *Meteorologische Zeitschrift*, *22*(2), 187-194.

Karamchandani, P., Lohman, K., & Seigneur, C. (2009). Using a sub-grid scale modeling approach to simulate the transport and fate of toxic air pollutants. *Environmental Fluid Mechanics*, *9*, 59-71. https://doi.org/10.1007/s10652-008-9097-0

Khammassi, E., Rehimi, F., Halawani, A. T., & Kalboussi, A. (2024). Energy transition policy via electric vehicles adoption in the developing world : Tunisia as a case study. *Energy Policy*, *185*, 113927.

Kim, S., Mcgaughey, R., Andersen, H.-E., & Schreuder, G. (2009). Tree species differentiation using intensity data derived from leaf-on and leaf-off airborne laser scanner data. *Remote Sensing of Environment*, *113*, 1575-1586. https://doi.org/10.1016/j.rse.2009.03.017

Kim, Y., Seigneur, C., & Duclaux, O. (2014). Development of a plume-in-grid model for industrial point and volume sources : Application to power plant and refinery sources in the Paris region. *Geoscientific Model Development*, *7*(2), 569-585. https://doi.org/10.5194/gmd-7-569-2014

Kutlar Joss, M., Eeftens, M., Gintowt, E., Kappeler, R., & Künzli, N. (2017). Time to harmonize national ambient air quality standards. *International Journal of Public Health*, *62*(4), 453-462. https://doi.org/10.1007/s00038-017-0952-y

References

Lendvai-Emmert, D., Emmert, V., Fusz, K., Prémusz, V., Boncz, I., & Tóth, G. P. (2020). PAM10 SIGNIFICANCE OF STOOL TESTS IN CHILDREN WITH COW'S MILK PROTEIN ALLERGY. *Value in Health*, *23*, S12. https://doi.org/10.1016/j.jval.2020.04.062

Li, J., Deqing, Z., Liang, J., Guo, T., Yao, J., & Liu, W. (2025). Combustion aerosols and suspended dust with controlled processes in Lhasa : Elemental analysis and size distribution characteristics. *Journal of Environmental Sciences*, *148*, 591-601. https://doi.org/10.1016/j.jes.2023.09.026

Liao, H., Lee, C., Tsai, W., Yu, J. Z., Tsai, S., Chou, C. C. K., & Wu, C. (2021). Source apportionment of urban PM2.5 using positive matrix factorization with vertically distributed measurements of trace elements and nonpolar organic compounds. *Atmospheric Pollution Research*, *12*(4), 200-207. https://doi.org/10.1016/j.apr.2021.03.007

Liao, H.-T., Lai, Y.-C., Chao, H. J., & Wu, C.-F. (2023). Vertical Characteristics of Potential PM2.5 Sources in the Urban Environment. *Aerosol and Air Quality Research*, *23*(3), 220361. https://doi.org/10.4209/aaqr.220361

Lixin Zheng et al.,. (2024). Chemical Profiles of Particulate Matter Emitted from Anthropogenic Sources in Selected Regions of China. *Scientific Data*, *11*(1). https://doi.org/10.1038/s41597-024-04058-6

Luca Ferrero et al.,2019. (2019). Chemical Composition of Aerosol over the Arctic Ocean from Summer ARctic EXpedition (AREX) 2011–2012 Cruises : Ions, Amines, Elemental Carbon, Organic Matter, Polycyclic Aromatic Hydrocarbons, n-Alkanes, Metals, and Rare Earth Elements. *Atmosphere*, *10*(2), 54. https://doi.org/10.3390/ATMOS10020054

Mahmassani, H., Fei, X., Eisenman, S., Zhou, X. S., & Qin, X. (2005). *DYNASMART-X EVALUATION FOR REAL-TIME TMC APPLICATION : CHART TEST BED*.

May, M., Wald, S., Suter, I., Brunner, D., & Vardag, S. N. (2024). Evaluation of the GRAMM/GRAL model for high-resolution wind fields in Heidelberg, Germany. *Atmospheric Research*, *300*, 107207. https://doi.org/10.1016/j.atmosres.2023.107207

Morawska, L., Wierzbicka, A., Buonanno, G., Cyrys, J., Schnelle-Kreis, J., Kowalski, M., Riediker, M., Birmili, W., Querol, X., Cassee, F. R., Yildirim, A. Ö., Elder, A., Yu, I. J., Øvrevik, J.,

References

Hougaard, K. S., Loft, S., Schmid, O., Schwarze, P. E., Stoeger, T., … Lucht, S. (2019). *Ambient ultrafine particles : Evidence for policy makers. White paper*. https://nfa.elsevierpure.com/en/publications/ambient-ultrafine-particles-evidence-for-policy-makers-white-pape

Mulualem Abera Waza et al. (2025). *Shifting Patterns of Ethiopian MAM Rainfall : Effects of Sea Surface Temperature and Atmospheric Circulation (1981–2022)—Waza—2025—International Journal of Climatology—Wiley Online Library*. https://rmets.onlinelibrary.wiley.com/doi/full/10.1002/joc.8743

Mustafa, A. A., Shokr, M. S., Alharbi, T., Abdelsamie, E. A., El-Sorogy, A. S., & Meroño de Larriva, J. E. (2025). Integration of Google Earth Engine and Aggregated Air Quality Index for Monitoring and Mapping the Spatio-Temporal Air Quality to Improve Environmental Sustainability in Arid Regions. *Sustainability*, *17*(8), Article 8. https://doi.org/10.3390/su17083450

Naré, H., & Kamakaté, F. (s. d.). *Developing a roadmap for the adoption of clean fuel and vehicle standards in Southern and Western Africa*.

Neelesh Agrawal et al.,2021. (s. d.). *(Open Access) A review on contamination of heavy metal in road dust collected from heavy traffic areas (2021) | Neelesh Agrawal*. Consulté 25 décembre 2024, à l'adresse https://typeset.io/papers/a-review-on-contamination-of-heavy-metal-in-road-dust-rl56fcx1fl

Nikolaos Tsanakas et al. (2020). *Estimating Emissions from Static Traffic Models : Problems and Solutions—Tsanakas—2020—Journal of Advanced Transportation—Wiley Online Library*. https://onlinelibrary.wiley.com/doi/10.1155/2020/5401792?utm_source=chatgpt.com

Non-Exhaust Emissions. (2018). https://shop.elsevier.com/books/non-exhaust-emissions/amato/978-0-12-811770-5

Nora Kováts et al.,2020. (2020, septembre 1). *Seasonal Differences in Rural Particulate Matter Ecotoxicity*. SciSpace - Paper; Springer Singapore. https://doi.org/10.1007/S41810-020-00063-5

References

Nur Amanina Ramli et al.,2020. (2020). Chemical and Biological Compositions Associated with Ambient Respirable Particulate Matter : A Review. *Water Air and Soil Pollution*, *231*(3), 1-14. https://doi.org/10.1007/S11270-020-04490-5

Oettl, D. (2015). Quality assurance of the prognostic, microscale wind-field model GRAL 14.8 using wind-tunnel data provided by the German VDI guideline 3783-9. *Journal of Wind Engineering and Industrial Aerodynamics*, *142*, 104-110. https://doi.org/10.1016/j.jweia.2015.03.014

Oettl, D., & Uhrner, U. (2011). Development and evaluation of GRAL-C dispersion model, a hybrid Eulerian–Lagrangian approach capturing NO–NO2–O3 chemistry. *Atmospheric Environment*, *45*(4), 839-847.

Ohlwein, S., Kappeler, R., Kutlar Joss, M., Künzli, N., & Hoffmann, B. (2019). Health effects of ultrafine particles : A systematic literature review update of epidemiological evidence. *International Journal of Public Health*, *64*(4), 547-559. https://doi.org/10.1007/s00038-019-01202-7

Ouyang, H., Tang, X., Kumar, R., Zhang, R., Brasseur, G., Churchill, B., Alam, M., Kan, H., Liao, H., Zhu, T., Chan, E. Y. Y., Sokhi, R., Yuan, J., Baklanov, A., Chen, J., & Patdu, M. K. (2022). *Toward Better and Healthier Air Quality : Implementation of WHO 2021 Global Air Quality Guidelines in Asia*. https://doi.org/10.1175/BAMS-D-22-0040.1

Patnaik, G., Boris, J., & Grinstein, F. (2006). *LARGE SCALE URBAN SIMULATIONS WITH MILES*.

Pavanaditya Badida et al. (2022). Meta analysis of health effects of ambient air pollution exposure in low- and middle-income countries. *Environmental Research*, *216*, 114604-114604. https://doi.org/10.1016/j.envres.2022.114604

Payne, S. D., Johnson, T. J., & Symonds, J. P. R. (2023). Characterisation of the Aerodynamic Aerosol Classifier Transfer Function for Particle Sizes up to 5 Micrometres. *Aerosol and Air Quality Research*, *23*(6), 230008. https://doi.org/10.4209/aaqr.230008

Peng, L., Li, L., Zhang, G., Du, X., Wang, X., Peng, P., Sheng, G., & Bi, X. (2021). Technical note : Measurement of chemically resolved volume equivalent diameter and effective density of

References

particles by AAC-SPAMS. *Atmospheric Chemistry and Physics*, *21*(7), 5605-5613. https://doi.org/10.5194/acp-21-5605-2021

Penkała, M., Bihałowicz, J. S., Rogula-Kozłowska, W., Rogula-Kopiec, P., Klik, B., Bihałowicz, J., Lewicka, S., Olszowski, T., & Majewski, G. (2024). Sciendo. *Chemistry-Didactics-Ecology-Metrology*, *28*(1-2), 79-92. https://doi.org/10.2478/cdem-2023-0005

Pratiwi, Y. E., Taufik, F. F., Habibi, J., & Wibowo, A. (2023). The Impact of Particulate Matter on the Respiratory System. *Jurnal Respirasi (JR)*, *9*(3). https://e-journal.unair.ac.id/JR/article/download/43962/26329

Przemysław Furman et al.,2021. (2021). Seasonal Variability of PM10 Chemical Composition Including 1,3,5-triphenylbenzene, Marker of Plastic Combustion and Toxicity in Wadowice, South Poland. *Aerosol and Air Quality Research*, *21*(3), 200223. https://doi.org/10.4209/AAQR.2020.05.0223

Qiao, X., Zhang, Q., Wang, D., Hao, J., & Jiang, J. (2021). Improving data reliability : A quality control practice for low-cost PM2.5 sensor network. *Science of The Total Environment*, *779*, 146381. https://doi.org/10.1016/j.scitotenv.2021.146381

Rebaï, N., Desbonnet, J., & Rebei, H. (2023). Mutations récentes, dynamiques actuelles et perspectives de transition des territoires ruraux périurbains en Tunisie. Une analyse depuis Mahrès dans la périphérie de Sfax. *EchoGéo*. https://journals.openedition.org/echogeo/26122

Regina M.B.O. Duarte et al.,2020. (s. d.). *(Open Access) Urban Atmospheric Aerosols : Sources, Analysis, and Effects (2020) | Regina M.B.O. Duarte | 4 Citations*. Consulté 14 décembre 2024, à l'adresse https://typeset.io/papers/urban-atmospheric-aerosols-sources-analysis-and-effects-5e988uh9cy

Riccardo Buccolieri et al. (2021). *Urban Obstacles Influence on Street Canyon Ventilation : A Brief Review*. https://www.mdpi.com/2673-4931/8/1/11

Robert Cichowicz et al. (2019). *Average Hourly Concentrations of Air Contaminants in Selected Urban, Town, and Rural Sites | Archives of Environmental Contamination and Toxicology*. https://link.springer.com/article/10.1007/s00244-019-00627-8

References

Robert Oleniacz et al. (2023). *Air Quality Improvement in Urban Street Canyons : An Assessment of the Effects of Selected Traffic Management Strategies Using OSPM Model*. https://www.mdpi.com/2076-3417/13/11/6431?utm_source=chatgpt.com

Roostaei, V., Abbasi, A., Gharibzadeh, F., Faridi, S., Naddafi, K., Yunesian, M., & Hassanvand, M. S. (2024). Vertical Distribution of Air Particulate Matter (PM1, PM2.5, and PM10) in Different Regions of Tehran. *Aerosol and Air Quality Research*, *24*(10), 240036. https://doi.org/10.4209/aaqr.240036

Ru-Jin Huang et al.,. (2022). Chemical signature and fractionation of trace elements in fine particles from anthropogenic and natural sources. *Journal of Environmental Science (Print)*, *114*, 365-375. https://doi.org/10.1016/j.jes.2021.09.015

Salizzoni, P., Soulhac, L., & Mejean, P. (2009). Street canyon ventilation and atmospheric turbulence. *Atmospheric Environment*, *43*(32), 5056-5067.

Savicki, D. L., Goulart, A., & Becker, G. Z. (2021). A simplified $$k-\epsilon$$ turbulence model. *Journal of the Brazilian Society of Mechanical Sciences and Engineering*, *43*(8), 384. https://doi.org/10.1007/s40430-021-03084-4

Shaw, D. R., Carter, T. J., Davies, H. L., Harding-Smith, E., Crocker, E. C., Beel, G., Wang, Z., & Carslaw, N. (2023). INCHEM-Py v1.2 : A community box model for indoor air chemistry. *Geoscientific Model Development*, *16*(24), 7411-7431. https://doi.org/10.5194/gmd-16-7411-2023

Soulhac, L., Mejean, P., & Perkins, R. J. (2001). Modelling vehicle-generated atmospheric pollution in a quarter of Lyon using the model SIRANE. *Seventh International Conference on Harmo. within Atmos. Disp. Modell. for Regul. Purposes, Belgirate, Italy*.

Soulhac, L., Salizzoni, P., Cierco, F.-X., & Perkins, R. (2011). The model SIRANE for atmospheric urban pollutant dispersion; part I, presentation of the model. *Atmospheric Environment*, *45*(39), 7379-7395. https://doi.org/10.1016/j.atmosenv.2011.07.008

References

Soulhac, L., Salizzoni, P., Mejean, P., Didier, D., & Rios, I. (2012). The model SIRANE for atmospheric urban pollutant dispersion; PART II, validation of the model on a real case study. *Atmospheric Environment*, *49*, 320-337. https://doi.org/10.1016/j.atmosenv.2011.11.031

Squarcioni, A., Roustan, Y., Valari, M., Kim, Y., Sartelet, K., Lugon, L., Dugay, F., & Voitot, R. (2025). To what extent is the description of streets important in estimating local air quality : A case study over Paris. *Atmospheric Chemistry and Physics*, *25*(1), 93-117. https://doi.org/10.5194/acp-25-93-2025

Stewart, B. W. (2021). Enhanced communication of IARC Monograph findings to better achieve public health outcomes. *Carcinogenesis*, *42*(2), 159-168. https://doi.org/10.1093/carcin/bgaa129

Stiperski, I., & Calaf, M. (2023). Generalizing Monin-Obukhov Similarity Theory (1954) for Complex Atmospheric Turbulence. *Physical Review Letters*, *130*(12), 124001. https://doi.org/10.1103/PhysRevLett.130.124001

Su, B.-B., Liu, X.-D., & Tao, J. (2013). Characteristics of PM10 and PM2. 5 concentrations in mountain background region of east China. *Huan Jing ke Xue= Huanjing Kexue*, *34*(2), 455-461.

Suter, G. W. (2008). Ecological risk assessment in the United States environmental protection agency : A historical overview. *Integrated Environmental Assessment and Management*, *4*(3), 285-289. https://doi.org/10.1897/IEAM_2007-062.1

Tareq Hussein et al.,2022. (2022). Organic and Elemental Carbon in the Urban Background in an Eastern Mediterranean City. *Atmosphere*, *13*(2), 197-197. https://doi.org/10.3390/atmos13020197

Taylor, N. (2003). The CONTRAM dynamic traffic assignment model. *Networks and Spatial Economics*, *3*, 297-322. https://doi.org/10.1023/A:1025394201651

The Lancet Commission on pollution and health. (s. d.). Consulté 21 juillet 2025, à l'adresse https://repository.gheli.harvard.edu/repository/11822/?utm_source=chatgpt.com

The standard for calculating emissions in road transport—INFRAS. (s. d.). Consulté 29 juillet 2025, à l'adresse https://www.infras.ch/en/projects/handbook-emission-factors-for-road-transport-hbefa-the-standard-for-calculating-emissions-in-road-transport/?utm_source=chatgpt.com

References

Tian, X., Gao, J., Liu, L., Zhao, Z., Hang, J., Zheng, Y., & Wang, X. (2024). Mathematical models for traffic-source PM2.5 dispersion in an urban street canyon considering the capture capability of roadside trees. *Science of The Total Environment*, *951*, 175513. https://doi.org/10.1016/j.scitotenv.2024.175513

Timothy, Z. (2003). How does an internal combustion Engine Work? Consulté le November 27, 2021, sur www.carid.com: https://www.carid.com/articles/how-does-internal-combustion-engine-work.html

US EPA. (2021). *Overview of Particulate Matter (PM) Air Quality in the United States*.

US EPA, O. (2016, juillet 13). *Support Center for Regulatory Atmospheric Modeling (SCRAM)* [Data and Tools]. https://www.epa.gov/scram

Valentina Gluščićv et al. (2024, mars 11). *Insights into air pollution sources in urban enviroments during winter * SciSpace - Paper. https://doi.org/10.5194/egusphere-egu24-19928

Veratti, G., Bigi, A., Teggi, S., & Ghermandi, G. (2024). Description and validation of Vehicular Emissions from Road Traffic (VERT) 1.0, an R-based framework for estimating road transport emissions from traffic flows. *Geoscientific Model Development*, *17*(16), 6465-6487. https://doi.org/10.5194/gmd-17-6465-2024

Vicente, B., Rafael, S., Rodrigues, V., Relvas, H., Vilaça, M., Teixeira, J., Bandeira, J., Coelho, M., & Borrego, C. (2018). Influence of different complexity levels of road traffic models on air quality modelling at street scale. *Air Quality, Atmosphere & Health*, *11*(10), 1217-1232. https://doi.org/10.1007/s11869-018-0621-1

Vinay Kumar et al. (2025). *Environmental Pollutants as Emerging Concerns for Cardiac Diseases : A Review on Their Impacts on Cardiac Health*. https://www.mdpi.com/2227-9059/13/1/241

V. Kokkonen, T., Xie, Y., Paasonen, P., Gani, S., Jiang, L., Wang, B., Zhou, D., Qin, W., Nie, W., Kerminen, V.-M., Petäjä, T., Sun, J., Kulmala, M., & Ding, A. (2021). The effect of urban morphological characteristics on the spatial variation of PM 2.5 air quality in downtown Nanjing. *Environmental Science: Atmospheres*, *1*(7), 481-497. https://doi.org/10.1039/D1EA00035G

World Bank Group. (2023). *Tunisia Country Climate and Development Report*. Washington, DC: World Bank. https://doi.org/10.1596/40658

References

Wu, Y., Hao, J., Fu, L., Wang, Z., & Tang, U. (2002). Vertical and horizontal profiles of airborne particulate matter near major roads in Macao, China. *Atmospheric Environment*, *36*(31), 4907-4918. https://doi.org/10.1016/S1352-2310(02)00467-3

Xausa, F., Paasonen, P., Makkonen, R., Arshinov, M., Ding, A., Denier Van Der Gon, H., Kerminen, V.-M., & Kulmala, M. (2018). Advancing global aerosol simulations with size-segregated anthropogenic particle number emissions. *Atmospheric Chemistry and Physics*, *18*(13), 10039-10054. https://doi.org/10.5194/acp-18-10039-2018

Yadav, S. K., Mishra, R. K., & Gurjar, B. R. (2019). Ultrafine Particles in Concern of Vehicular Exhaust—An Overview. In A. K. Agarwal, A. Dhar, N. Sharma, & P. C. Shukla (Éds.), *Engine Exhaust Particulates* (p. 7-38). Springer. https://doi.org/10.1007/978-981-13-3299-9_2

Yago Alonso Cipoli et al.,. (2024). Emission Factors, Chemical Composition and Ecotoxicity of PM10 from Road Dust Resuspension in a Small Inland City. *Water Air and Soil Pollution*, *235*(11). https://doi.org/10.1007/s11270-024-07564-w

Yago Alonso Cipoli et al. (2024). *Emission Factors, Chemical Composition and Ecotoxicity of PM10 from Road Dust Resuspension in a Small Inland City | Water, Air, & Soil Pollution*. https://link.springer.com/article/10.1007/s11270-024-07564-w

Yevgen Nazarenko et al.,2021. (s. d.). *(Open Access) Air quality standards for the concentration of particulate matter 2.5, global descriptive analysis. (2021) | Yevgen Nazarenko | 32 Citations*. Consulté 13 décembre 2024, à l'adresse https://typeset.io/papers/air-quality-standards-for-the-concentration-of-particulate-2gsid8dfc1

Yu, I. J. (2022). Health and Environmental Effect of Advanced Materials and Fine Particles. *Biomolecules*, *12*(11), Article 11. https://doi.org/10.3390/biom12111579

Yuki Okazaki et al.,2024. (2024). Projections of non-exhaust emissions from brake wear across Japan for 2020–2050. *Science of The Total Environment*, *954*, 176508-176508. https://doi.org/10.1016/j.scitotenv.2024.176508

References

Zallinger, M., Tate, J., & Hausberger, S. (2008). *An instantaneous emission model for the passenger car fleet*. 16th International Transport and Air Pollution CongressTechnical University Graz. https://trid.trb.org/View/1084477

Zeb, B., Alam, K., Ditta, A., Ullah, S., Ali, H. M., Ibrahim, M., & Salem, M. Z. M. (2022). Variation in Coarse Particulate Matter (PM10) and Its Characterization at Multiple Locations in the Semiarid Region. *Frontiers in Environmental Science*, *10*. https://doi.org/10.3389/fenvs.2022.843582

Zhang, J., Chen, Z., Shan, D., Wu, Y., Zhao, Y., Li, C., Shu, Y., Linghu, X., & Wang, B. (2024). Adverse effects of exposure to fine particles and ultrafine particles in the environment on different organs of organisms. *Journal of Environmental Sciences*, *135*, 449-473. https://doi.org/10.1016/j.jes.2022.08.013

Zhong, J., Harrison, R. M., James Bloss, W., Visschedijk, A., & Denier van der Gon, H. (2023). Modelling the dispersion of particle number concentrations in the West Midlands, UK using the ADMS-Urban model. *Environment International*, *181*, 108273. https://doi.org/10.1016/j.envint.2023.108273